CARBIDE PRECIPITATION IN AUSTENITIC Fe-Mn-V-C ALLOYS

M. H. Ainsley
B.App.Sc., Hons.

Department of
Chemical Engineering
(Materials Engineering Group)

Ph.D. Thesis
March, 1980

TABLE OF CONTENTS

SUMMARY

Carbide precipitation in austenitic Fe-Mn-V-C alloys has been studied using transmission electron microscopy of carbon extraction replicas and thin foils. Particular attention has been focussed on a discontinuous reaction involving the formation of very fine vanadium carbide precipitates, the principle objective being to delineate the conditions leading to the observed precipitate morphologies and distributions. In order to achieve this objective, it was necessary to relate these microstructural features to the nature of the advancing grain boundary at which precipitation occurs. Accordingly, detailed crystallographic analyses of a number of grain boundaries of interest were undertaken, the results of which were then interpreted in terms of the Coincidence Site Lattice Model of grain boundary structure.

The precipitates which form at the advancing boundary during this discontinuous reaction were found to be present as either discrete particles (particulate precipitates) resulting from repeated nucleation or as long, thin fibres (fibrous precipitates). Whereas particulate precipitation occurs at boundaries which, according to the CSL model, contain a low density of atoms shared by both neighbouring grains, i.e. low coincidence boundaries, fibrous precipitation was found to take place at comparatively high coincidence boundaries. This correlation is believed to be due to the effect of grain boundary structure on the ease of precipitate nucleation, with nucleation being more difficult at the high coincidence boundaries due either to their lower energy or because solute diffusivity is lower at these sites.

The discontinuous reaction displays classical behaviour in that it begins at the austenite grain boundaries and proceeds as a result of

boundary migration in conjunction with precipitation to form extensive nodular regions of transformation product. Some nodules consist only of particulate precipitates in an austenitic matrix and these were found to develop when the misorientation between neighbouring grains was such that irrespective of its orientation, the boundary plane contained a low density of coincidence sites. More commonly, however, the nodules were found to contain both particulate and fibrous precipitates and when this occurred, two different precipitate distributions could be distinguished. These two distributions result from different nodule growth mechanisms which can be accounted for, at least in large part, if boundary migration proceeds in a manner leading to boundary energy minimization. In the first distribution, particulate precipitates occupy a region extending from the low coincidence portions of the advancing boundary to its original site, while the fibres lay behind, and normal to, comparatively long boundary segments containing a high density of coincidence sites. In the second, bands of particles alternate with bands of fibres which are associated with a series of short, inclined steps (ledges) on the nodule boundary, each of which lies in a high density coincidence orientation.

The sequence of events leading to the evolution of each of these distributions was determined deductively and has been described in detail. In short, the first of these distributions arises when the direction of nodule growth is everywhere normal to the plane of the advancing boundary, while in the case of the second distribution outward growth of the nodule occurs by the sideways movement of the ledges.

DECLARATION

To the author's knowledge and belief, the material in this thesis, except where due reference is made or common knowledge assumed, is original. No part of this work has been submitted for any other award or degree in any University.

M.H. AINSLEY

ACKNOWLEDGEMENTS

The author is indebted to Professor D.R. Miller and Dr. G.J. Cocks for their interest and guidance during the progress of this work.

The author would also like to thank his colleagues in the Materials Engineering Group of the Department of Chemical Engineering for many interesting and helpful discussions, and is particularly grateful to Mr L. Bray for his assistance with computer programming.

The research was supported by the Australian Research Grants Committee (F74/15142), whilst the author received a Commonwealth Post-graduate Award. Grateful acknowledgement is extended to all those authorities for provision of funds.

Grateful thanks are also given to the Broken Hill Proprietary Co. for supplying much of the material used in this work.

CHAPTER 1

INTRODUCTION

In recent years there has been much interest in the structures produced when austenite containing strong carbide forming elements transforms directly to ferrite (see, for example, the reviews by Honeycombe (1976, 1979)). It is well established that during transformation, alloy carbide precipitation takes place at the advancing austenite/ferrite (γ/α) boundaries and that in the main, this occurs in one of two ways. In the first, termed 'interphase precipitation', sheets of very fine discrete particles are formed, the precipitate being nucleated at successive positions of the transformation front (Davenport and Honeycombe (1971); Campbell and Honeycombe (1974); Howell et al. (1979a)). These particles may be present in either a series of planar sheets which lay parallel to the advancing boundary or in a series of curved sheets, in which case the individual precipitates can sometimes be distributed in a seemingly random array. In the second mode of precipitation, alloy carbides with a markedly fibrous morphology develop behind and in contact with the advancing boundary, the fibre growth direction being approximately parallel to the local direction of boundary migration (Berry and Honeycombe (1970); Edmonds (1972); Edmonds and Honeycombe (1973)).

It is now well established (Barbacki and Honeycombe (1976); Howell et al. (1979b)) that, other things (e.g. transformation kinetics and precipitate/matrix crystallography) being equal, the nature of the advancing boundary is the determining factor influencing which of these precipitate morphologies will develop. The association of the planar sheets of interphase precipitate with facetted boundary segments which appear to advance by a ledge mechanism has led to the view (Campbell and

Honeycombe (1974)) that these precipitates develop at the partially coherent boundary, i.e. $\{111\}_\gamma||\{110\}_\alpha$, between Kurdjumov-Sachs (K-S) orientation related phases. This idea is in accord with the general theory of precipitate/matrix interfacial structure proposed by Aaronson (1962) on the basis of morphological and kinetic studies of ferrite growth in austenite, and has recently received some support from the preliminary crystallographic studies of Howell et al. (1979b). On the other hand, fibrous precipitates and the less regular arrays of discrete particles are believed to form at boundaries which, according to Aaronson's theory, ought to be characterized by a structure considerably less ordered than that of their partially coherent counterpart and have thus been assumed (e.g. Howell et al (1979a)) to be incoherent. Boundaries of this type are those which are either K-S related but whose interfacial plane does not conform to the $\{111\}_\gamma$ habit, or those which are not characterized by a rational and well-defined orientation relationship.

Since the time of Aaronson's work, various theoretical and experimental developments have enabled significant advances to be made in our understanding of interphase boundary structure (see, for example, the reviews by van der Merwe (1974); Kinsman and Aaronson (1974) and Laird and Sankaran (1979)). As Purdy (1978) has recently emphasized, according to the present concept of interfacial structure based on the lattice matching approach - which can be best formally expressed in terms of the O-lattice model (Bollmann (1970)) whose applicability to the particular case of the γ/α boundary has been recently demonstrated (Howell et al. (1979c)) - neither close proximity to the K-S orientation relationship nor of the interfacial plane to $\{111\}_{fcc}$ are necessary conditions for fcc/bcc boundaries to exhibit some degree of lattice matching; moreover, because of the intrinsic complexity of the fcc/bcc system, there should exist a whole range of orientation relationships and boundary plane orientations

at which the extent of lattice matching is not insignificant. It is clear, then, that in order to delineate the precise conditions under which both fibrous and particulate carbides precipitate during the $\gamma \rightarrow \alpha$ transformation, a full description of the crystallography of the boundaries at which the different morphologies develop is required. It should be noted that a similar comment also applies to the conditions leading to the diverse and quite complex distributions in which these different morphologies are found; here again the nature of the advancing boundary is thought to play a major role, in this case through the influence it exerts on the ferrite growth mechanism (Berry and Honeycombe (1970); Edmonds and Honeycombe (1973); Campbell and Honeycombe (1974)). Further progress towards establishing these conditions is hampered, however, by the difficulty in carrying out detailed crystallographic studies of the γ/α boundaries associated with the different morphologies due to the parent austenite transforming to martensite on being cooled to room temperature.

Dippenaar (1970), in a study of the austenite to pearlite reaction, overcame this same difficulty by using a steel containing sufficient manganese and carbon (Fe - 13% Mn - 0.8%C)* to render the parent austenite stable to room temperature. On addition of a small amount of vanadium to this basic alloy he noted that under certain heat treatment conditions (namely, a solution treatment at 1250^{o}C, followed by water-quenching and then ageing in the range 450-700^{o}C) vanadium carbide precipitates with a markedly fibrous morphology are produced. Miller (private communication) later reported that under these same conditions discrete vanadium carbide particles can also form. The reaction giving

---

* All compositions given in this thesis are quoted in weight %.

rise to these precipitates does not, however, accompany the austenite to ferrite transformation but rather, as pointed out by Dippenaar, can be classified as a 'discontinuous precipitation' reaction (Smith (1953)) and can be expressed as follows:

$$\gamma_1 \rightarrow \gamma_2 + VC$$

where γ_1 refers to the austenite, supersaturated with respect to vanadium carbide (VC), into which the boundary migrates and γ_2 in the solute depleted austenite containing the precipitates. In this mode of precipitation, which occurs and has been extensively studied in a wide variety of alloy systems (Hornbogen (1972)), the reaction begins at the grain boundaries and proceeds by the growth of nodular regions of transformation product resulting from precipitation in conjunction with grain boundary migration.

Clearly, the discontinuous reaction in the Fe-Mn-V-C alloy system offers a very convenient opportunity to relate the nature of the precipitate and the mechanism of nodule growth to the crystallography (and through this the structure) of the boundary at which precipitation occurs. The interrelation between these various aspects of the reaction has been investigated in the present work which aims to examine the conditions leading to the observed precipitate morphologies and distributions.

From recent grain boundary modelling studies using computer simulation techniques (e.g. Smith et al. (1977); Pond and Vitek (1977); Pond, Smith and Vitek (1979); Nichols (1979)) and the experiments of Hermann et al. (1976) and Sautter et al. (1977) which demonstrate the importance of an electronic contribution to the boundary energy, it is apparent that a complete understanding of grain boundary structure must await the day when reliable computations can be made to determine atomic relaxations at grain

boundaries directly from a knowledge of the interatomic forces. For the most part, our current level of understanding of grain boundary structure is the result of a geometric approach, in which consideration is effectively given to the interaction between atomic nuclei at the boundary, electronic effects being disregarded. It is, perhaps, fair to say that the prominence with which this approach has figured in our current thinking is in no small measure due to the fact that the necessary experimental data required for the application of geometric boundary models can be acquired simply from microscopical investigation. Of the various geometric models which have been developed (see, for example, the reviews by Ralph (1975) and Gleiter and Pumphrey (1976)) the O-lattice model is, in principle, the most widely applicable and yields the most detailed description of the boundary structure, which is expressed in terms of the boundary defect configuration arising from atomic relaxations that serve to maximize the degree of registry between the two adjoining crystals. Much evidence from transmission electron microscopy of specially fabricated bicrystals with predetermined crystallographies (e.g. Schober and Balluffi (1970); Kegg et al. (1973)) supports this model; however, some difficulty arises in the practical case of applying the model to boundaries in real, polycrystalline materials due to the need to determine the crystallographic parameters with greater precision than is usually attainable (Ralph (1975)).

Because of the lower level of precision with which these parameters need be obtained, such boundaries can be more readily treated in terms of the Coincidence Site Lattice (CSL) model (Kronberg and Wilson (1949); Brandon et al. (1964); Brandon (1966)), though at the expense of detailed information on the boundary defect configuration. Despite this limitation, the CSL model has proved very useful in advancing our understanding of the structure of experimentally observed boundaries and in particular, in providing a framework for rationalizing the crystallographic

dependence of a wide range of boundary properties (e.g. energy (Dimou and Aust (1974)) and mobility (Demianczuk and Aust (1975)), processes (e.g. grain boundary diffusion (Ishida et al. (1976)), segregation (Aust and Rutter (1959); Gleiter (1970a)) and precipitation (Lorimer (1975))) and reactions (e.g. boundary dissociation (Ranganathan (1969); Goodhew (1979)) and boundary/lattice defect interactions (Dingley and Pond (1979); Clark and Smith (1979))). In view of this success, it was decided to also use the CSL model to interpret the crystallography of those boundaries of interest in the present work. For the benefit of the reader the following section (1.1) is given over to a detailed description of the model and a discussion of it's validity in the light of available experimental evidence.

Insofar as the role of boundary crystallography in influencing the precipitate morphology is concerned, the present study has shown that the essential distinction between the boundaries associated with the two kinds of precipitate - fibres and particles - lies in their markedly different propensity to nucleate precipitates. Accordingly, in seeking to explain this role, the literature concerning the effect of boundary crystallography on precipitate nucleation has been reviewed (section 1.2). It ought to be pointed out that this topic has received some coverage in a number of other reviews (Aaronson (1956); Aaron and Aaronson (1971); Aaronson et al. (1971); Lorimer (1975)) and these should be considered as supplementary reading. It should also be mentioned that as the present investigation is concerned with precipitation in well-annealed material, the recent studies (e.g. Jones et al. (1976a,b); Varin (1979)) into the effect on nucleation of 'non-equilibrium' components of grain boundary structure have been excluded from the review.

1.1 The Coincidence Site Lattice model

1.1.1 The construction, characterization and physical significance of the CSL

In this model it is noted that when two identical and interpenetrating crystal lattices are related by certain angular rotations about rational directions, a fraction of the atomic sites in each lattice are coincident. Provided a misorientation of this kind is not a rotational symmetry operation, these sites lie on a single lattice of larger cell dimensions. This larger lattice is the CSL and the special misorientations at which CSLs are generated are commonly referred to as coincidence site relationships; as an example, fig. 1 illustrates schematically the formation of the CSL generated between two primitive cubic lattices related by $[001]/36.9^{o}$. A CSL is commonly identified in the literature by an integer Σ which can be defined as either the reciprocal density of common lattice sites or the ratio of the volumes of the unit cells of the CSL and the crystal lattice; the CSL in fig. 1, for example, is characterized by $\Sigma = 5$. There exists an infinite number of coincidence site relationships and systematic relations for generating these together with the associated Σ values, which vary from unity to infinity, have been given by Ranganathan (1966); however, only those CSLs for which Σ is comparatively low, i.e. the volume density of coincident sites is high, are considered to have significance in the model.

A boundary between two grains in a coincidence site relationship becomes the appropriate planar section through the CSL. Because the latter has three dimensional regularity (due to the periodicity of the crystal lattices) the boundary therefore contains a two dimensional periodic array of coincidence sites, i.e. atoms shared by both grains.

FIGURE 1

Schematic illustration of the CSL formed by a 36.9° rotation of two simple cubic lattices about an [001] axis normal to the plane of the figure. ABCD defines the CSL unit cell.

o Grain A

+ Grain B

FIGURE 2

Two dimensional model of a bcc bicrystal in the coincidence site relationship [110]/50.5°, $\Sigma = 11$. The boundary follows the path ABCD to maximize the path with a high density of coincidence sites (After Brandon et al. (1964)).

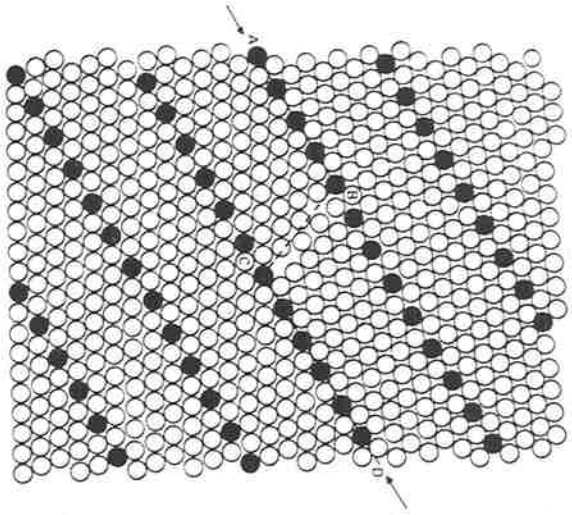
A
B
C
D

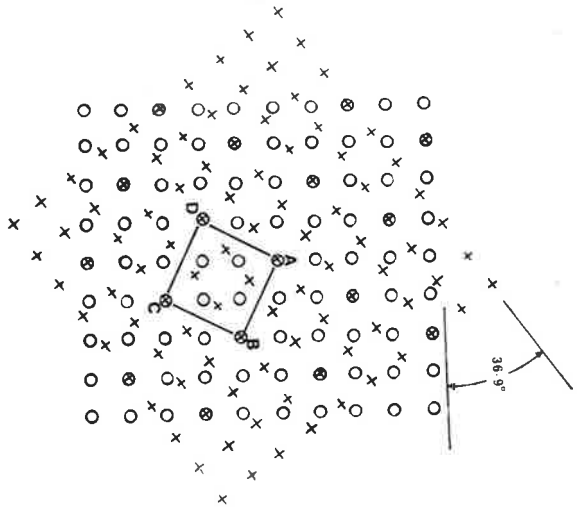
A
B
C
D
36.9°

The periodicity of this array will vary depending upon the plane of intersection with the CSL and as CSLs tend to be lattices of low symmetry (Pond (1974)) the coincidence sites in some CSL planes can be very much more closely spaced than in others (e.g. fig.2).

Brandon et al. (1964) postulated that a boundary lying in a densely packed CSL plane should have low energy (cf. a boundary with a comparatively disordered structure) because of its 'good fit' nature and that a grain boundary can be consequently expected to exhibit a preference to lie in such a plane; furthermore, when the precise crystallographic requirements for a boundary to conform to this plane are nearly - but not exactly - fulfilled, then rather than possessing a high energy 'poor fit' structure over its entire area the boundary will instead consist of regions of 'good fit' separated by specific defects which accommodate the deviation from exact coincidence. Two kinds of deviation from an ideal CSL boundary can occur; one is a deviation in the orientation of the boundary plane and the other a deviation in the misorientation of the neighbouring grains from the exact coincidence site relationship. Both of these can be reasonably expected to be exhibited by the majority of boundaries in real, polycrystalline materials since such boundaries may be subject to a number of influences that prevent perfect coincidence from being achieved - such influences include, for example, the establishment of a texture during fabrication and/or annealing which necessarily places a restriction on the relative orientations of neighbouring grains, and the requirement at grain boundary junctions for a boundary configuration that leads to a balance of the surface-tension forces.

According to Brandon et al. a deviation in the orientation of the boundary plane will be accommodated by the boundary taking up a stepped configuration (e.g. ABCD in fig. 2) so as to maximize its area in the

densely packed CSL plane, the good fit boundary segments so formed being separated by short and completely disordered steps whose frequency increases with the deviation. The reduction in the energy of the boundary as a result of its lying partially in the densely packed CSL plane will to some extent be offset by the concomitant increase in boundary area and this as well as the relative energies of the two kinds of boundary segments will determine the maximum allowable deviation.

On the other hand, a small angular deviation from an exact coincidence site misorientation is expected to be accommodated by a network of mismatch dislocations embedded in the nearby CSL boundary, in much the same way that small departures from a perfect crystal orientation (i.e. $\Sigma = 1$) are accommodated by a dislocation network in the Read-Schockley (1950) model for the 'low-angle' grain boundary. As with the low-angle grain boundary, the limiting angular deviation at which this description of a coincidence preserving array of dislocations retains physical significance is taken to be the point at which the dislocation spacing becomes comparable to the periodicity of the boundary structure, i.e. the spacing of the coincidence sites. Brandon (1966) has estimated that this should occur when the angular deviation is of the order of $15\Sigma^{-\frac{1}{2}}{}^{o}$, and thus the misorientation range over which a coincidence structure can persist is expected to decrease rapidly as Σ increases. On the basis of this limiting deviation, Warrington and Boon (1975) have calculated that for a random, polycrystalline aggregate only a few percent of all boundaries will possess a coincidence related structure; in real materials, however, this structure is usually exhibited by a very large percentage of the boundaries present as a result of material texture (e.g. Howell, Fleet, Welch and Ralph (1978)).

1.1.2 The validity of the model

No experimental technique has yet been developed which enables the precise disposition of atoms at a grain boundary to be determined unambiguously, and hence a rigorous comparison of the atomic arrangements at real grain boundaries with those predicted by the model has not been possible. However, on several occasions direct evidence has been obtained from electron diffraction studies of grain boundary material for the existence of a structural periodicity at boundaries lying between grains whose misorientation satisfies, or at least approximates, a coincidence site relationship (Sass et al. (1975); Tan et al. (1975)).

By contrast, information on grain boundary energy is far more accessible and in many studies where such information as well as details of the boundary crystallography have been obtained, the expectation that boundaries conforming to a CSL plane of comparatively high packing density have lower energy than 'poor fit' boundaries has been confirmed. The most convincing evidence for this correlation comes principally from the following sources:

(i) Studies involving the direct measurement of grain boundary energy (Rutter and Aust (1967); Murr et al. (1970); Gleiter (1970b); Hasson and Goux (1971); Dimou and Aust (1974)). On the basis of these studies it appears that with the exception of the $\Sigma = 3$ coherent twin boundary in low stacking fault energy fcc metals, where the energy is of the order of .02 - .05 E_R (E_R = energy of a fully disordered boundary), boundaries conforming to densely packed CSL planes have energies of the order of $0.7E_R$.

(ii) Electron and field-ion microscope observations of grain boundaries containing networks of dislocations whose characteristics (i.e. spacing, Burgers vector and diffraction contrast) are consistent

with their accommodating, in the manner described by Brandon et al., a small departure in misorientation from one defining a CSL (e.g. the Σ = 17 CSL in an Fe-Mn alloy (Ishida et al. (1969)); Σ = 3, 9, 11 and 17 in Au (Schober and Balluffi (1970, 1971a,b)); Σ = 33 in Al-Mg (Ishida et al. (1977)), Σ = 57 in Cu-Si (Forwood and Clarebrough (1977)); Σ = 3, 5, 7, 9, 31, 35 and 93 in stainless steel, Σ = 17 in Al, Σ = 19 in W and Σ = 15, 11 and 19 in Mo (Clark and Smith (1978))).

(iii) The presence in well-annealed metals of grain boundaries which have minimized their structure - dependent energy by preferentially facetting onto densely packed CSL planes. The most frequently quoted example in the literature of such a boundary is the Σ = 3 annealing twin boundary in fcc metals; in order to completely enclose the twinned grain this boundary assumes a stepped configuration, with the majority of the boundary being composed of segments lying in the most densely packed CSL plane, i.e. the common {111} twinning plane, and the remainder often lying normal to these segments and in the second most densely packed plane, i.e. the common {112} (Matthews (1962); Dickson and Pashley (1962); Pashley and Stowell (1963), Phillips (1972)). Other boundaries which have been observed to exhibit facetting behaviour in accordance with the orientation dependence of boundary energy predicted by the CSL model include the Σ = 19 and 41 boundaries in W (Ishida and Smith (1974)), the Σ = 3 and 5 (Wagner et al. (1974)) as well as the Σ = 11 and 33 (Goodhew et al. (1978)) boundaries in Au, and the Σ = 11, 13, 17, 19 and 29 boundaries in Nb (Andrejeva et al. (1978)).

In contrast to these findings, grain boundaries in some coincidence systems have been found to exhibit no preference to lie in a densely packed plane. For example, Goodhew et al. (1978) noted that whilst

a Σ = 33 boundary in Au exhibits a strong preference to lie in a densely packed plane, Σ = 19, 27 and 59 boundaries do not, even though the most densely packed plane in these CSLs contain a higher density of coincident sites (5.53, 4.63 and 3.13 coincidence sites/nm^2 of boundary area respectively) than the most densely packed Σ = 33 plane (2.41). Moreover, there has been a significant number of cases reported of boundaries which actually exhibit a preference to lie in planes which have no particular significance in the CSL model (see, for example, Goodhew et al.). It is clear, then, that in some instances grain boundary energy is not determined solely by the density of coincidence sites in the boundary plane.

Additional evidence in support of this conclusion has been obtained by Hermann et al. (1976) and Sautter et al. (1977), the nature of which strongly suggests that the inability of the CSL model to account for the total structure-dependent energy of all possible boundaries arises, at least in large part, because the model is based on geometrical concepts and not on the theory of metallic cohesion. Utilizing the idea (Shewmon (1966)) that if a pair of grains has a misorientation near that of an energy cusp their free energy will be reduced by the rotation of one grain, relative to the other until the cusp is reached, these workers were able to identify low energy boundaries in Cu, Ag and a number of Ag based alloys from the textures developed upon sintering small single crystal spheres of the metals onto a planar single crystal substrate of the same material. In all cases it was found that the strongly preferred orientations corresponded to low Σ coincidence site relationships; however, the frequency of occurrence of a particular orientation, which was taken to be a measure of the energy cusp depth, was often found to be different for the various metals examined. As these metals possess a similar lattice structure, but differ significantly in their electronic structures, these

workers concluded that in addition to the density of coincidence sites at a boundary, electronic factors can also influence the boundary energy. The precise nature of these factors has not yet been established; however, it has been suggested (Balluffi et al. (1975)) that the matching of wave functions across the boundary plane and conduction electron effects may be important.

Despite the considerable overall success the CSL model has had in accounting for the crystallographic dependence of grain boundary energy and behaviour, there is some doubt as to the validity of the shared atom concept for all grain boundaries. This is because, as Loberg and Norden (1976) have demonstrated, with the exception of the $\Sigma = 3$ coherent twin boundary in face centred cubic metals the shared atom configuration necessarily leads to certain atom pairs across the boundary possessing an interatomic spacing less than the equilibrium nearest neighbour spacing in the crystal lattice. Chalmers and Gleiter (1971) have suggested that such atomic overcrowding ought to be alleviated and the boundary energy therefore lowered by a rigid body translation, without rotation, of one crystal relative to it's neighbour away from the coincidence position. The bubble-raft experiments of Ishida (1972) and computer calculations of minimum energy boundary structures (e.g. Weins et al. (1971); Hasson et al. (1972); Pond et al. (1976)) have given considerable support to this idea, and the predicted translation at several boundaries has been verified experimentally using transmission electron microscopy (Pond and Smith (1974)). Although a translation of this kind eliminates the shared atom configuration, a periodic boundary structure is preserved in which certain points lying in equivalent positions in the unit cells of each adjoining crystal lattice are coincident. It can be readily shown (Bollmann (1970)) that the periodicity of this relaxed structure is identical to that when the atoms

are being shared so that despite it's being only an approximate description of grain boundary structure, the CSL model remains a powerful tool for investigating the degree of atomic fit at the boundary.

1.2 Grain boundary precipitation: the effect of boundary crystallography

Before proceeding to review the literature, it is appropriate that the underlying factors responsible for the pre-eminence of grain boundaries as sites for precipitation be identified.

According to classical nucleation theory, the driving force for precipitation is proportional to the reduction in Gibbs free energy ΔG given by:

$$\Delta G = \Delta G_C + \Delta G_S + \Delta G_{ST}$$

where ΔG_C is the chemical free energy term, and ΔG_S and ΔG_{ST} are the surface and strain energy terms associated with the creation of new interface. When ΔG is plotted as a function of the nucleus size, it passes through a maximum which represents the free energy barrier to nucleation. Clemm and Fisher (1955) were apparently the first to point out that this free energy barrier can be reduced if nucleation occurs at a grain boundary because of the energy released by the elimination of a portion of the boundary area. Thus, it is to be expected that grain boundaries will play a relatively more important role when the precipitation reaction is dominated by the surface energy term, i.e. when the chemical driving force for precipitation is small due to a low level of supersaturation, or when the nucleus interface is incoherent. Since the free energy of a high density coincidence site boundary is less than that of a disordered boundary, it is to be further expected (Pumphrey (1976)) that the former will be a less favoured site for precipitate nucleation.

Grain boundaries are also preferred sites for precipitation because of their ability to serve as high diffusivity paths. Accelerated diffusion in the boundary plane both assists in the assembly of atoms to form a stable nucleus and is important in promoting precipitate growth following the nucleation event. As there is good evidence that the diffusivity is lower at high coincidence boundaries than at disordered boundaries (Gleiter (1971); Ishida et al. (1976)), the former should be less favoured sites for precipitation on this basis also.

Unwin and Nicholson (1969), in a study of the nucleation and growth of grain boundary precipitates in Al-Zn-Mg and Al-Mg alloys, appear to have been the first to investigate the effect of grain boundary structure on precipitation using the CSL model to interpret the boundary crystallography. At high supersaturations (i.e. when precipitation took place at temperatures well below the solvus) precipitate densities and hence nucleation rates were found to be the same on all boundaries. These workers attributed this result to the boundary structure being of secondary importance in controlling nucleation when the chemical driving force for precipitation is high, i.e. when precipitate nucleation is easy. On the other hand, at low or moderate supersaturations (when nucleation occurred during the quench from a high temperature solution treatment) a large disparity in precipitate density from one boundary to another was observed. Specifically, it was found that when the boundary misorientation was within 4^{o} of that defining a CSL for which $\Sigma \lesssim 19$, and thus a misorientation lying approximately within the range of allowable deviations (Brandon (1966)) for the CSL model to retain significance, the density of precipitation was much lower than for grain boundaries deviating further from CSLs. No satisfactory correlation was found, however, between the precipitate density and the orientation of the boundary plane. It should be

pointed out, though, that the criterion for such was based on the assumption that only boundaries conforming to a close packed CSL plane contain a comparatively high density of coincidence sites whereas, in fact, if Σ is low a similar distinction may also apply when the CSL plane is one of rather modest packing density (Pond (1974)).

Butler and Swann (1976) have also studied grain boundary precipitation in the Al-Zn-Mg system and, in common with Unwin and Nicholson, found that very little precipitation occurred at boundaries between CSL related grains; moreover, this was the case regardless of any changes in the orientation of the boundary plane. As Butler and Swann gave no details of the crystallographic parameters defining the boundaries they examined, it is not altogether clear whether this apparent insensitivity to the boundary orientation signifies the absence of a correlation between the precipitate density and the density of coincidence sites at the boundary plane. On the grounds that the strong solute segregation during quenching Al-Zn-Mg (Doig and Edington (1975)) should occur preferentially to non-CSL boundaries in order to reduce their strain energy, Butler and Swann argued that the energies of the CSL and non-CSL boundaries should not differ significantly. Thus, they concluded that the lower precipitate density at the former boundaries was most probably due to the lower solute diffusivity and segregation levels at these, both effects making it more difficult for stable nuclei to form.

That the structural details as expressed in the CSL model can have a significant influence on precipitation has also been recently demonstrated by Williams and Edington (1976) in a study of the occurrence of discontinuous precipitation in Al-Li. In all cases examined, boundaries at which this reaction failed to initiate were found to lie between low Σ ($\Sigma \lesssim 11$) CSL related grains, while a significant departure from this

condition characterized boundaries at which the reaction was well established. As this discontinuous reaction simply involved coarsening at the grain boundary of a pre-existing dispersion of fine, general matrix precipitates, rather than the nucleation and growth of a new phase as is usually observed, it was concluded that the inhibition of the reaction at the CSL boundaries must be the result of a low boundary diffusivity.

In contrast to the behaviour expected when grain boundary structure is the determining factor influencing precipitation, on some occasions high density coincidence site boundaries have actually been found (Le Coze et al. (1970a,b)) to contain a higher density of precipitates that non-CSL boundaries, while in other cases a marked variation in the nature (Vaughan (1970)) or density (Butler and Swann (1976)) of precipitates at non-CSL boundaries has been observed. Vaughan (1970), for example, found that the few high angle grain boundaries in Al-4%Cu at which the transition phase θ' formed in preference to the equilibrium θ phase were 'normal' in the sense that their structure could not be described in terms of a low Σ CSL. The boundaries were, however, found to be special in one sense; namely, that the misorientation and grain boundary plane were such as to enable low energy θ'/matrix interfaces to be established with both neighbouring grains, hence bringing about a sizeable reduction in the free energy barrier to θ' nucleation. This finding was consistent with the results of an earlier study (Vaughan (1968)) in which it was observed that only one variant of the θ'/matrix orientation relationship was selected at a given low-angle grain boundary and that when the inclination of the boundary plane varied so did the orientation of θ'. Together, these observations were taken to indicate that the detailed crystallographic fit between the precipitate nucleus and one, or both of the adjacent grains was an important parameter governing the nucleation of the boundary precipitate.

On the basis of these observations, Pumphrey (1973) concluded that if a low energy interface (i.e. a well-defined habit plane) between precipitate and matrix exists, then it is the interfacial plane of the grain boundary rather than its structure that is the important factor influencing nucleation, which he argued would be favoured when the habit plane lies parallel to the boundary plane. Clough et al. (1974), while disagreeing with some of the steps in Pumphrey's argument, agreed in principle with his conclusion; however, in the light of a detailed theoretical investigation (Lee and Aaronson (1975)) into the effect of the nucleus boundary configuration on nucleation energetics, Clough et al. proposed that this conclusion should be broadened to 'the smaller the angle between low energy precipitate/matrix interfaces and the boundary plane, the more will precipitate nucleation be favoured'. Experimental evidence in support of this proposition has recently been obtained by Forest and Biscondi (1978) in a study of the precipitation of semicoherent θ' platelets at low angle grain boundaries in Cu-Al. As the angle between the precipitate habit plane and the plane of the boundary decreased, a marked increase in nucleation kinetics was observed and on the basis of thermodynamic considerations, this was attributed to a decrease in the free energy barrier for nucleation.

The foregoing experimental observations have been made during studies of precipitation at stationary grain boundaries. Although precipitation at migrating boundaries (as in the discontinuous precipitation reaction) has been the subject of many studies, only a few of these (e.g. Tu and Turnbull (1967); Liu and Aaronson (1968)) have been concerned with the influence of boundary crystallography on the precipitation reaction and then only insofar as was necessary to test the implied relationship (Smith (1953)) between the misorientation across the boundary and its

mobility - i.e., when the misorientation is small enough so that the discrete dislocation structure of the 'low-angle' grain boundary replaces a randomly disordered one, the boundary mobility (usually) becomes negligibly small and the discontinuous reaction will no longer take place. Whilst it would seem reasonable to expect that precipitation at migrating boundaries is influenced by both boundary structure and crystallographic matching at the precipitate/boundary plane in the same way as occurs at their static counterparts, it should be pointed out that at least two additional and essentially opposing factors, both related to the boundary mobility, may be important in influencing discontinuous precipitation.

The first is the effect of grain boundary migration on solute diffusion in the boundary, which is the principle means by which changes in composition occur during discontinuous precipitation (Sundquist (1973)). Recent work (Hillert and Purdy (1978); Smidoda et al. (1979)) has shown that the rate of solute diffusion at boundaries with appreciable mobility can be several orders of magnitude higher than at stationary or at least comparatively slow moving boundaries. The reason for this distinction is not yet clear; according to Hillert and Purdy it implies significant structural changes when grain boundaries become appreciably mobile; on the other hand Smidoda et al. suggest that it may be due to different solute transport mechanisms in the two cases, with diffusion in the latter boundaries occurring by the movement of the diffusing atom from one site of low potential energy to a neighbouring site while in the former boundaries by long range jumps of the diffusing atom which, according to their theoretical analysis, would require a much lower activation energy. Besides catalyzing nucleation through more rapid transport of solute to the nucleation site, it has been suggested (Westengen and Ryum (1978)) that this enhanced solute diffusivity may further aid the nucleation

process by enabling the criteria (Roy and Baver (1975)) for solute clustering to be more readily satisfied.

The second factor is the effect of boundary migration on the time available for nucleation, the importance of which has been emphasized by Campbell and Honeycombe (1974) in their study of discrete carbide precipitation (i.e. 'interphase' precipitation) at advancing austenite/ferrite boundaries. In contrast to the sort of behaviour expected when the boundary structure determines precipitate nucleation kinetics, these workers obtained convincing metallographic evidence that precipitate nucleation occurs more readily at partially coherent, low energy boundary segments - which experiments indicated to be virtually immobile insofar as their migration occurs exclusively by sideways ledge movement - than at these ledges which possess a considerably less ordered, high energy structure. Campbell and Honeycombe attributed this site selectivity for nucleation to the different mobilities of the two types of boundary segments, arguing that because of the high mobility of the ledges insufficient time is available for nucleation at these sites, whereas the partially coherent boundaries - although energetically less favoured sites - are sufficiently slow moving to allow carbide nucleation. This view has recently received support from a theoretical analysis (Aaronson et al. (1978)) of precipitate nucleation at migrating interphase boundaries.

CHAPTER 2

PRELIMINARY SURVEY OF THE TRANSFORMATION CHARACTERISTICS OF Fe-Mn-V-C ALLOYS

2.1 Introduction

As a precursor to studies concentrating on the more fundamental aspects of the discontinuous reaction in this alloy system an investigation was undertaken to delineate the optimum composition and heat-treatment conditions for observing the reaction in the presence of stable austenite, i.e. austenite containing sufficient manganese and carbon that it can be retained on cooling to room temperature. The results of the investigation are reported in this chapter.

In his preliminary work on the Fe-Mn-V-C system, Dippenaar (1970) found that discontinuous precipitates can be produced by suitable heat-treatment (i.e. a solution treatment at 1250^{o}C followed by a water-quench to retain the high temperature structure and then ageing in the range 450-700^{o}C) in an alloy of composition Fe-13Mn-2V-.8C and that this composition yields stable austenite. It seemed appropriate, therefore, to commence the present investigation with a detailed study of this alloy and then to assess the effect of alloy composition on the incidence of discontinuous precipitation by systematically varying the vanadium, carbon and manganese contents.

Details of the procedures used in the preparation and heat-treatment of the alloys examined here and the metallographic techniques used to assess their transformation characteristics are given in Appendix 1.

2.2 Results

In addition to discontinuous precipitation, several other competing precipitation reactions were found to occur in the alloys selected for study. A brief account of these reactions will be given before proceeding to a description of the transformation behaviour of the various alloys examined.

2.2.1 Nature of the precipitation reactions

Three quite distinct reactions were encountered over the range of ageing temperatures (400-900^{o}C) and times (≤200 hrs) considered.

In the first of these (general matrix precipitation) an exceedingly fine dispersion of discrete VC particles formed homogeneously throughout the austenite and resulted in a very significant age-hardening effect.

The second reaction was the familiar austenite to pearlite transformation, extensively studied by Dippenaar in Fe-Mn-C alloys, in which nodules with a lamellar structure of ferrite and cementite ($Fe(Mn)_3C$) developed at the austenite grain boundaries. Fine VC precipitates were present within the ferrite lamellae (fig. 3) and these formed in contact with the advancing ferrite/austenite boundary. However, unlike the carbide precipitates which form in association with the austenite to ferrite transformation in low alloy steels (Honeycombe (1976)), the precipitates within the ferrite lamellae displayed neither a fibrous morphology (though they appeared somewhat elongated in the direction of boundary movement) nor an 'interphase' morphology.

In the third reaction, supersaturated austenite decomposed in a discontinuous manner to yield a dispersion of VC precipitates in solute depleted austenite. This mode of precipitation proceeded in a similar

FIGURE 3

Thin foil micrograph of pearlite (X20,000)

FIGURE 4

Optical micrograph of a nodule containing coarse discontinuous precipitates (X500)

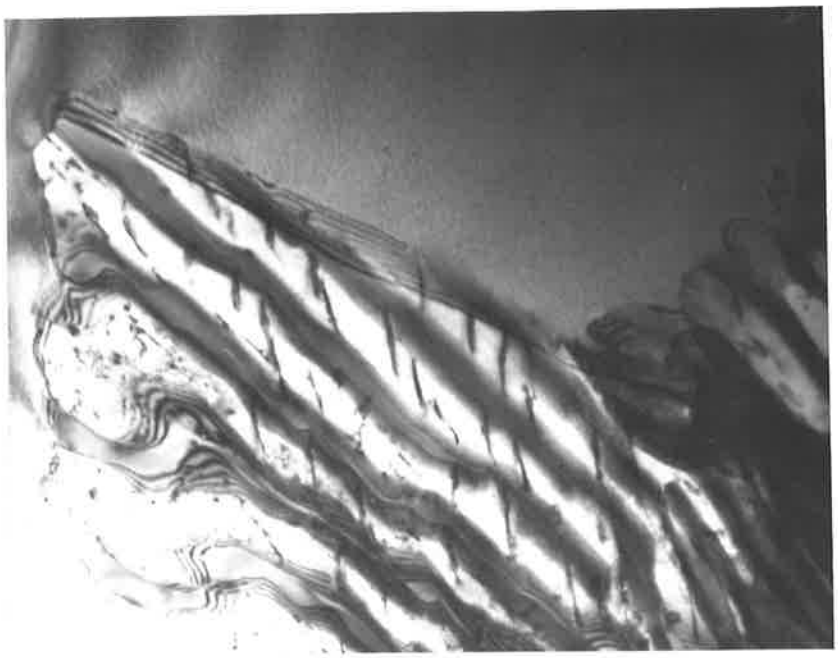

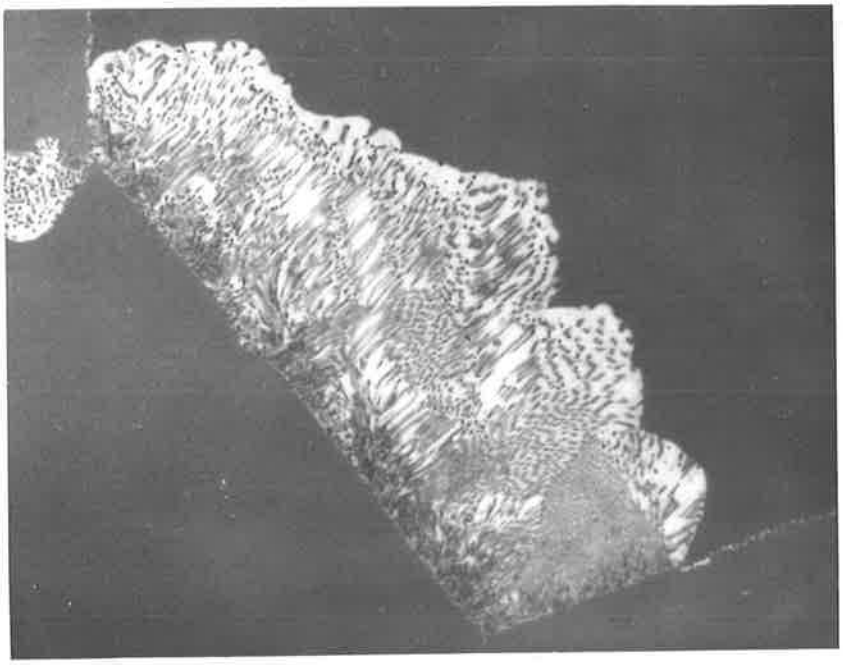

manner to the pearlite reaction in that nodular regions of transformation product developed at the austenite grain boundaries and advanced into the surrounding grains. Under some ageing conditions, coarse precipitates in the form of lamellae were produced and could easily be resolved in the optical microscope (fig. 4). Other ageing conditions, however, led to the development of nodules which simply appeared dark-etching in the optical microscope (fig. 5), this etching response being due to the presence of a dispersion of very fine precipitates. In the electron microscope these precipitates were seen to be present as either long, thin fibres or very small, discrete particles (fig. 6).

2.2.2 Composition and heat-treatment conditions leading to the development of fine discontinuous precipitates

The alloy Fe-13Mn-2V-.8C

The ageing response of this alloy, as revealed by optical metallography and hardness studies, is summarized in Table 1 and in the isothermal transformation diagram in fig. 7.

TABLE 1

Precipitation Reaction		Temperature Interval
Discontinuous Precipitation	fine	$550 \leqslant T \leqslant 710^{\circ}C$
	coarse	$640 \leqslant T \leqslant 900^{\circ}C$
Pearlite formation		$400 \leqslant T \leqslant 550^{\circ}C$
General Matrix precipitation		$400 \leqslant T \leqslant 900^{\circ}C$

Although the fine discontinuous reaction occurs over the temperature interval 550°-$710^{\circ}C$, a somewhat narrow interval than reported

FIGURE 5

Optical micrograph showing nodules of fine discontinuous precipitate (X425)

FIGURE 6

Extraction replica of a nodule containing fine, discontinuous precipitates (X23,000)

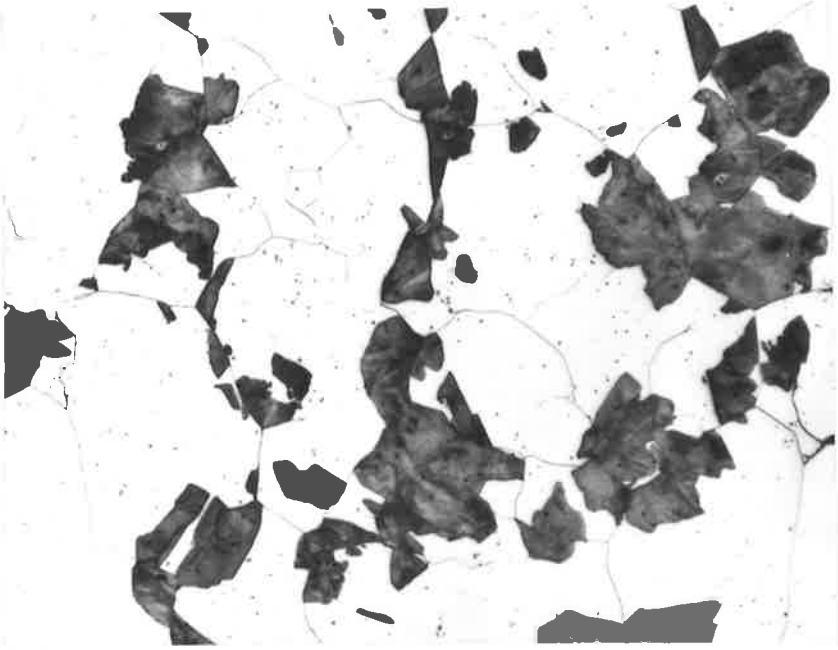

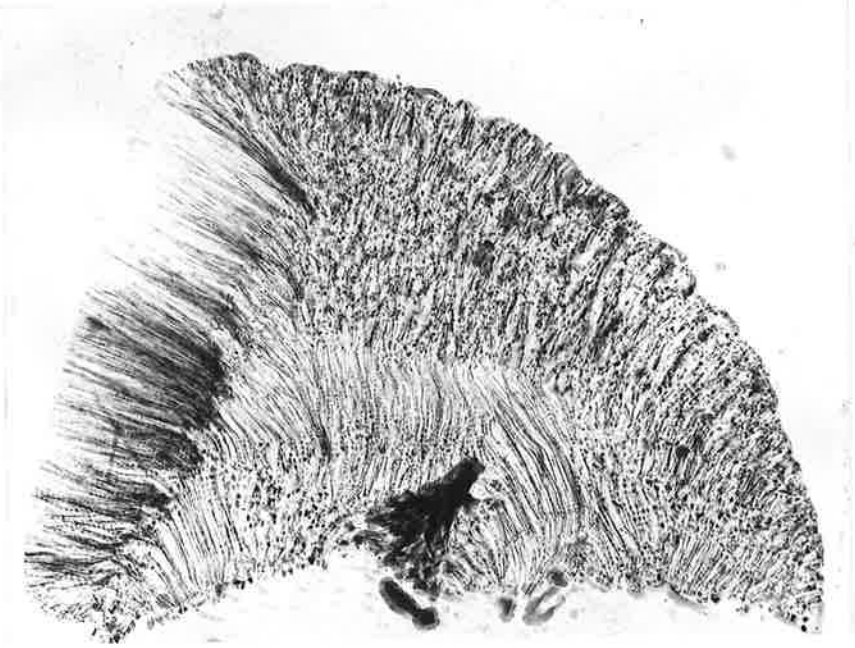

by Dippenaar (450-700°C), the reaction only proceeds to completion below 640°C (fig. 7). Above this temperature, extensive general matrix precipitation ahead of the fibrous nodules prevents complete transformation from taking place. Termination of the reaction coincides, in fact, with the attainment of peak hardness in the untransformed austenite, further ageing beyond this point resulting in the development of a uniform rim of coarse discontinuous precipitate around the nodules (fig. 8). Specimens aged at temperatures above 710°C contained no fibrous nodules of a size sufficient to be resolved in the optical microscope. At these temperatures, coarse discontinuous precipitates develop in the immediate vicinity of the grain boundaries (fig. 4). Below 550°C, fibrous precipitation is replaced by the pearlite reaction which requires a shorter incubation time (fig. 7).

In agreement with the observations of Dippenaar, x-ray diffraction studies revealed that despite the removal of carbon from solid solution due to VC precipitation, the austenite both ahead of and within the nodules remains completely stable to room temperature.

Other alloys

Systematic variations were made in the vanadium, carbon and manganese contents with Fe-13Mn-2V-.8C as the starting composition. In keeping with this systematic approach, the effect of variations in each constituent will be described separately. It should be pointed out that several similarities were apparent in the ageing response of the different alloys examined. Firstly, general matrix precipitation occurred over the entire range of ageing temperatures considered. Secondly, coarse discontinuous precipitates developed on ageing above 640°C and, as in the Fe-13Mn-2V-.8C alloy, formed only after the untransformed austenite containing the general matrix precipitate had attained peak hardness.

FIGURE 7

Isothermal transformation diagram
for the alloy Fe-13Mn-2V-.8C

FIGURE 8

Thin foil micrograph showing a rim
of coarse, discontinuous precipitates
ahead of fine, fibrous precipitates
(X60,000)

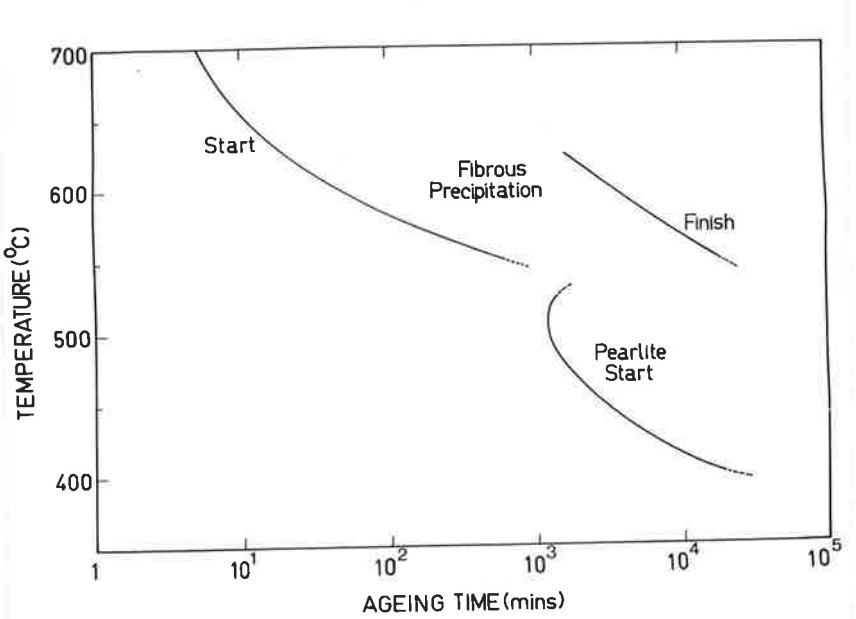
700
600
500
400
TEMPERATURE (°C)
Start
Fibrous
Precipitation
Finish
Pearlite
Start
1
10^1
10^2
10^3
10^4
10^5
AGEING TIME (mins)

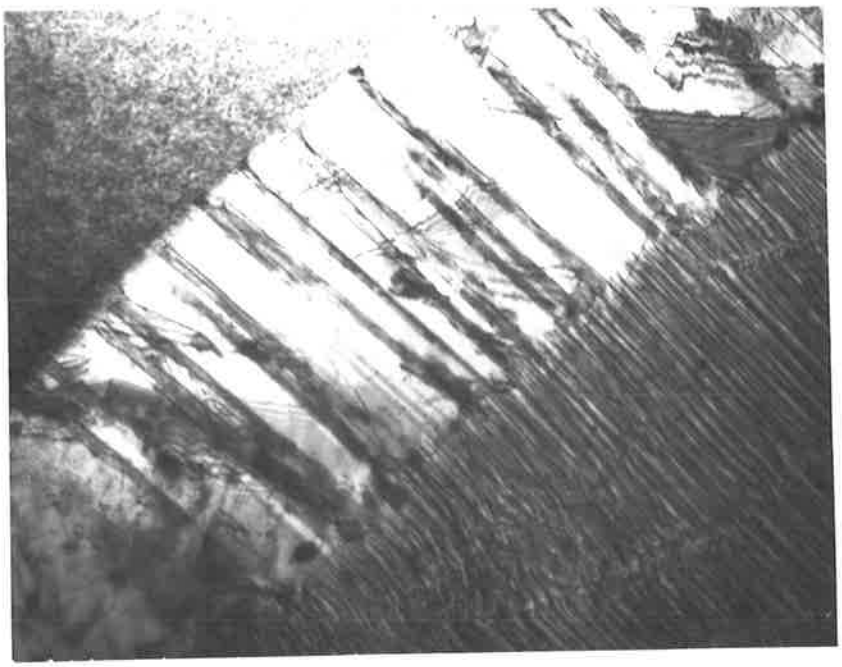

(a) The effect of vanadium content

The solid solubility of vanadium in the basic Fe-13Mn-.8C alloy is 2% at 1300°C and as this temperature is only some 20-30°C below the solidus temperature, vanadium additions in excess of 2% were not made.

In common with most other substitutional alloying elements, vanadium retards the rate of pearlite formation and hence, on reducing the vanadium content, pearlite formation is accelerated. Thus, when alloys containing 1.0% and 0.5% V were aged below the eutectoid temperature (~590°C in the presence of 13% Mn), the grain boundaries became rapidly occupied by pearlite. In neither of these alloys could the fine discontinuous reaction be detected.

(b) The effect of carbon content

The addition of carbon to the basic Fe-13Mn-2V-.8C alloy reduced the solidus temperature to the extent that only 0.2%C could be added without incipient melting at 1300°C. Increasing the carbon content by this much had no detectable influence on the temperature range over which the fine discontinuous reaction occurred but, because it resulted in a marked acceleration of the pearlite reaction, on ageing below the eutectoid temperature these two reactions proceeded simultaneously at the austenite grain boundaries. As pearlite occupied by far the greater proportion of the total boundary area, the extent to which the discontinuous reaction could proceed was very limited. Typically, this reaction accounted for only 5-10% of the transformation product in fully transformed specimens.

Reducing the carbon content below 0.8% (in the presence of 13%Mn and 2%V) reduced the stability of the austenite and as was expected from the behaviour of Fe-Mn-C alloys (White and Honeycombe (1962)), when the carbon content was less than 0.4%C the alloys were found to be partially martensitic at room temperature. Though reducing the carbon content from

0.8% to 0.5% did not render the 'as quenched' austenite unstable, the stability was lowered to the extent that the subsequent removal of carbon from solid solution, during either discontinuous or general matrix precipitation, resulted in a martensitic transformation on cooling from the ageing temperature.

(c) The effect of vanadium carbide content

It was thought that the absence of discontinuous precipitation in alloys containing 1.0% and 0.5% V might simply be due to a rapid exhaustion of suitable nucleation sites because of accelerated pearlite formation at the grain boundaries. In view of the marked effect of carbon content on the rate of pearlite formation, an attempt was made to suppress this reaction in low vanadium alloys (thereby leaving the way open for discontinuous precipitation) by examining alloys with an initially lower level of VC supersaturation. In the resulting alloys selected for study, namely Fe-13Mn-1V-0.63C and Fe-13Mn-.5V-.5C, pearlite formation was, as anticipated, greatly retarded. Despite this, the fine discontinuous reaction could not be detected even after ageing for as long as 200 hours in the temperature interval 450-700^{o}C. This strongly suggests that a minimum level of solute supersaturation is required for the discontinuous reaction to occur, as is found in many other alloy systems (Hornbogen (1972)).

(d) The effect of manganese content

Transformation studies on alloys containing in excess of 13%Mn were not undertaken since increasing the manganese content only marginally beyond this level (in the presence of 2%V and .8%C) lowered the solidus temperature below 1300^{o}C.

Reducing the manganese content had two effects: firstly, the

stability of the austenite was lowered to the extent that below 8%Mn, the 'as-quenched' alloys were partially martensitic; secondly, pearlite formation was enhanced with the result that in alloys containing 11% and 9%Mn aged below the eutectoid temperature, the pearlite reaction was once again found to occur at the expense of discontinuous precipitation.

2.3 Conclusions

The range of composition and heat-treatment conditions over which discontinuous precipitation of VC fibres and particles can occur, in the presence of stable austenite and without interference from competing precipitation modes, is very narrow. For a detailed study of the development of this discontinuous reaction, the alloy Fe-13Mn-2V-.8C, solution-treated at 1300^{o}C, water-quenched and then aged between 550-640^{o}C is close to optimum.

CHAPTER 3

DISCONTINUOUS PRECIPITATION: MICROSTRUCTURAL OBSERVATIONS

3.1 Introduction

The characteristics of the fine discontinuous precipitates, their distribution and the process of nodule development at the austenite grain boundaries are described in detail in this chapter. These various aspects of the reaction were studied using transmission electron microscopy of carbon extraction replicas and thin foils, and all observations reported here were made on the alloy Fe-13Mn-2V-0.8C, solution treated at 1300°C, water-quenched and unless otherwise indicated, aged at 600°C.

3.2 Results

3.2.1 Nature and crystallography of the precipitates

Two quite distinct precipitation processes were found to occur during the discontinuous reaction. In the first of these (particulate precipitation), VC is repeatedly nucleated at grain boundaries which are characteristically irregular as a result of local curvature. As these non-planar boundaries advance into the untransformed austenite, they leave behind a dispersion of fine, discrete particles (fig. 9). In the second process (fibrous precipitation), long thin VC fibres grew behind, and in contact with, comparatively planar boundaries (fig. 10). The fibres always appeared very straight and in all cases examined using trace analysis, the long fibre axis was found to lay normal to the plane of the boundary at which precipitation occurred. In fig. 10 for example, the long parallel fibres lay almost in the plane of the foil, which is ~(001) in the lower grain, while the boundary - viewed here 'edge-on' - is ~(541) in this grain.

FIGURE 9

Particulate precipitates behind a non-planar advancing boundary. Thin foil micrograph (X61,000)

FIGURE 10

Fibrous precipitates behind an advancing planar boundary (X35,000)

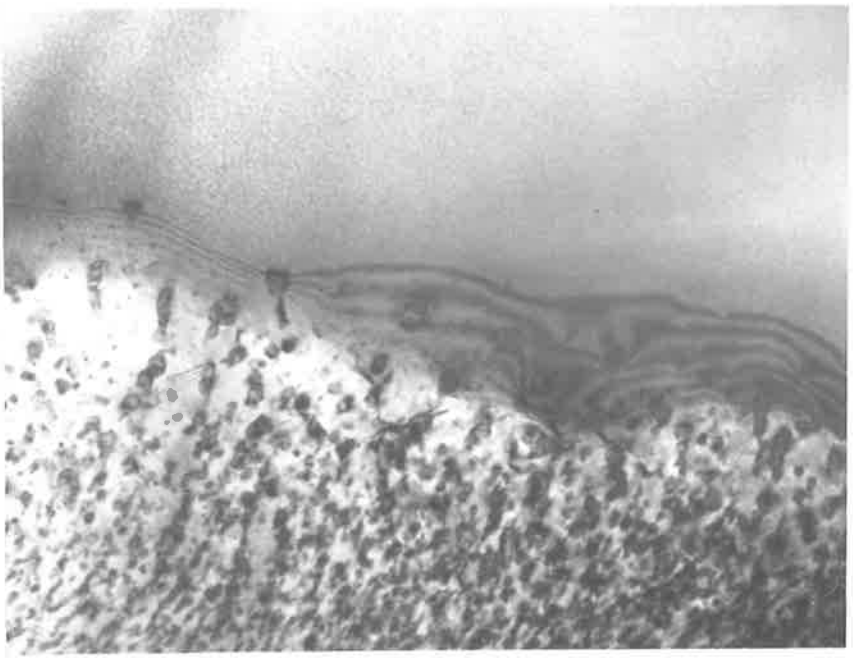

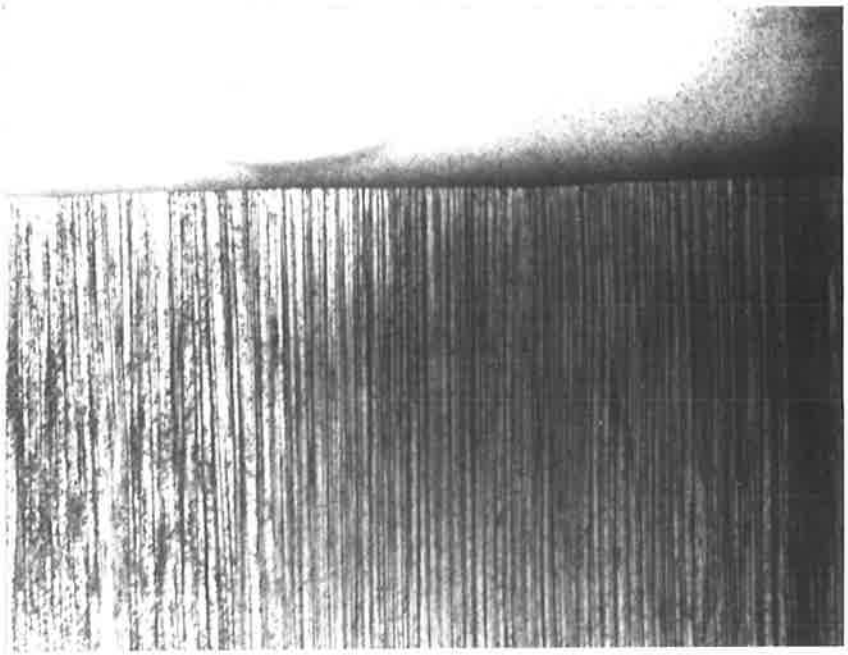

Whereas fibrous precipitation during the austenite to ferrite transformation represents a closer approach to equilibrium conditions than the development of discrete particles (Berry and Honeycombe (1970); Batte and Honeycombe (1973); Edmonds (1972)), as evidenced by the coarser nature of the fibres and the fact that these are present in greater amount when transformation proceeds more slowly, this does not appear to be the case in the discontinuous reaction. Both the average particle size and fibre width are comparable (~10-15nm), as are the interparticle and inter-fibre spacings (~50nm). Moreover, examination of large areas of extraction replicas taken from fully transformed specimens aged at 550°C and 640°C revealed no significant difference in the relative proportions of the two kinds of precipitate, even though the overall transformation kinetics of the discontinuous reaction differs considerably at these two temperatures (fig. 7).

In common with most other discontinuous precipitates, the VC exhibits an orientation relationship with the re-oriented matrix phase (fig. 11a,b), and not with the matrix which lies ahead of the advancing boundary. This relationship is the same for both fibrous and particulate precipitates and can be expressed as follows:

$$(001)_{VC} \;||\; (001)_{\gamma}$$

$$[010]_{VC} \;||\; [010]_{\gamma}$$

This, of course, is the familiar 'cube-cube' orientation relationship which is commonly encountered (e.g. Imai and Namekata (1970)) when VC or other isomorphous carbides precipitate in austenite.

3.2.2 The precipitate distribution

Some nodules were made up entirely of particulate precipitates

FIGURE 11(a)

Selected area electron diffraction pattern from a γ_2 region containing both fibrous and particulate precipitates. $\lambda L = 27mm$ Å

FIGURE 11(b)

Interpretation of above pattern.

- ● matrix reflection
- O VC reflection
- X Double diffraction

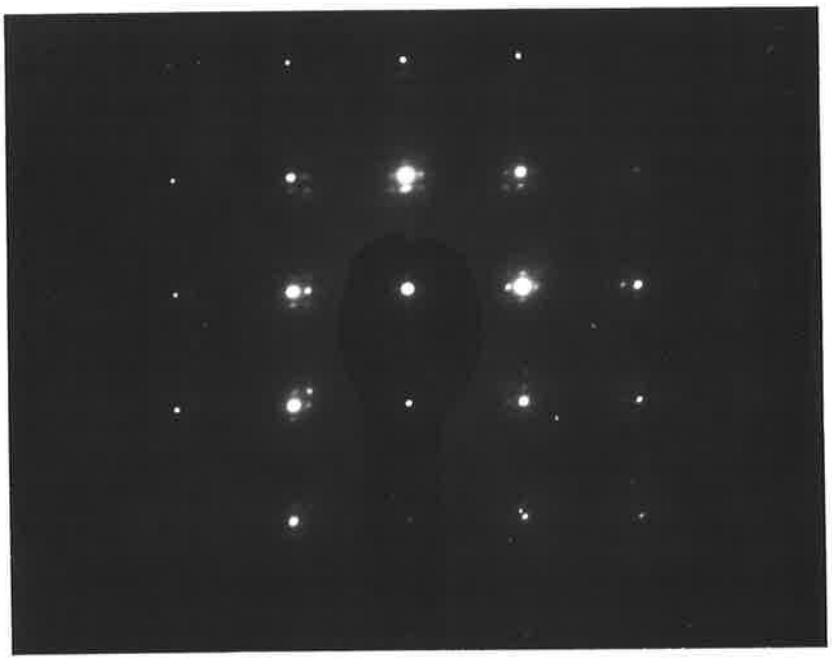

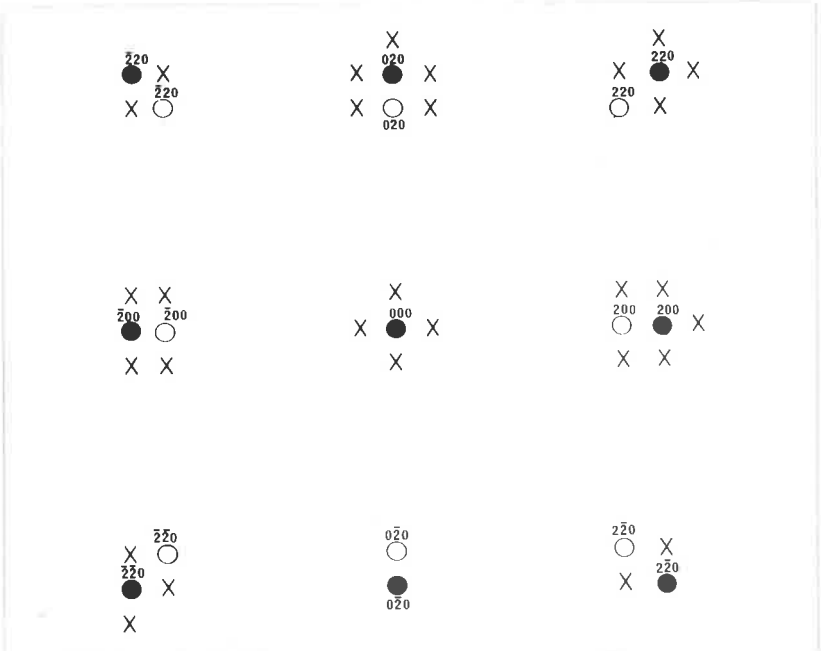
$\bar{2}\bar{2}0$
$\bar{2}20$
020
$0\bar{2}0$
220
200
$\bar{2}00$
000
$2\bar{2}0$
$0\bar{2}0$

randomly dispersed in the austenitic matrix; more commonly however, the nodules contained both fibrous and particulate precipitates and when this occurred, two different distributions of fibres and particles could be distinguished.

In the first (fig. 12), particulate precipitates are present over most of the nodule, occupying a region extending from the non-planar portions of the advancing boundary to the original site of this boundary, while the fibres lay behind, and normal to, comparatively long and straight boundary segments. It should be pointed out, however, that nodules containing this distribution were not all identical in structure. For example, in some nodules the fibrous region was reasonably uniform in width but in others (e.g. the larger of the two nodules in fig. 12) the fibrous region appeared distinctly wedge-shaped, converging to an apex at one end of the boundary segment at which the fibres developed. Also, in some nodules (fig. 12) the fibres lay (principally) behind only one straight boundary segment while in others extensive fibrous precipitation took place behind a number of boundary segments of different orientation (fig. 13) and where this occurred, the fibrous region consisted of arrays of parallel fibres, the fibre long axis in each array lying in a different crystallographic direction in the austenite (fig. 14).

In the second precipitate distribution (fig. 15), narrow bands of fibres separated considerably wider bands of roughly parallel fibres. In general, this banded structure was present over most of the nodule, with the individual bands lying more or less parallel to one another (fig. 16). Insofar as particulate precipitates are present in discrete bands, this structure bears some resemblance to the 'interphase' type distribution which occurs during the direct transformation of austenite to ferrite in low alloy steels. As with this latter distribution (see,

FIGURE 12

Extraction replica of two nodules, containing fibrous and particulate precipitates, which have nucleated between the same pair of austenite grains (X12,000)

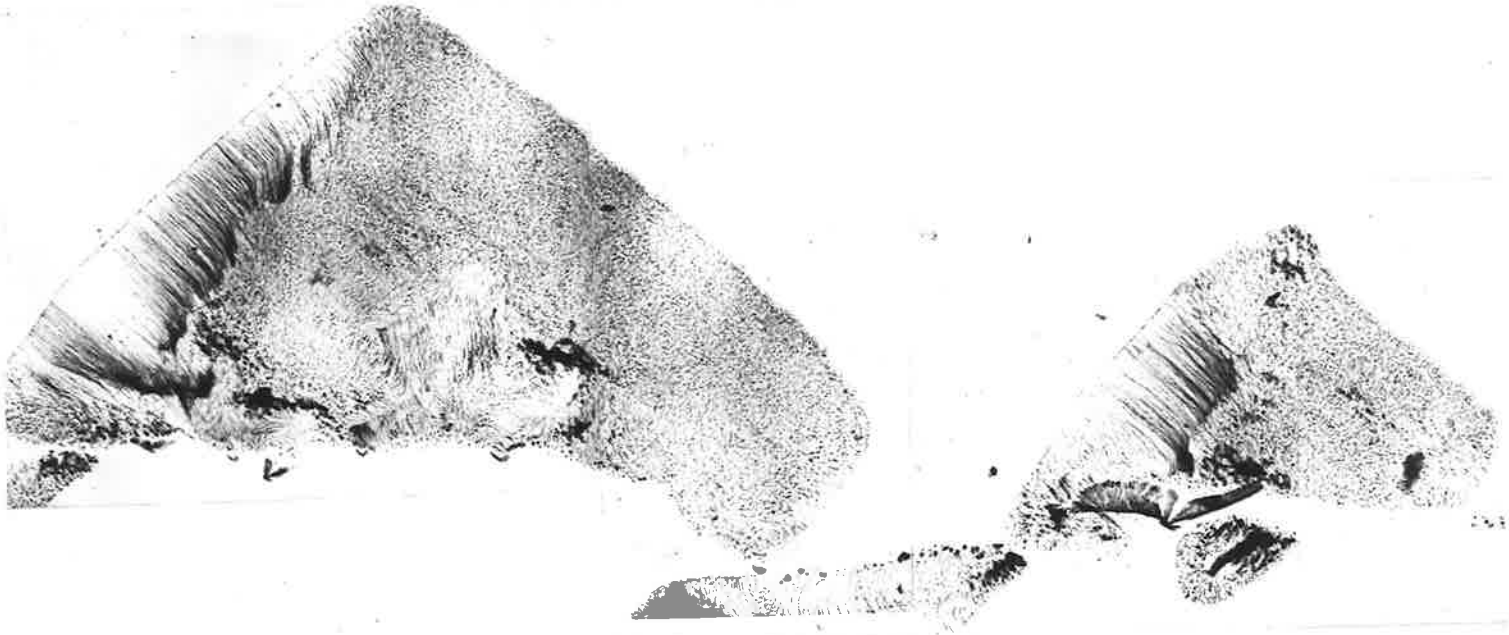

FIGURE 13

Extraction replica of a nodule whose boundary contains a number of straight segments of different orientation (X20,000)

FIGURE 14

Thin foil electron micrograph showing the fibrous region behind several planar boundary segments of different orientation (X30,000)

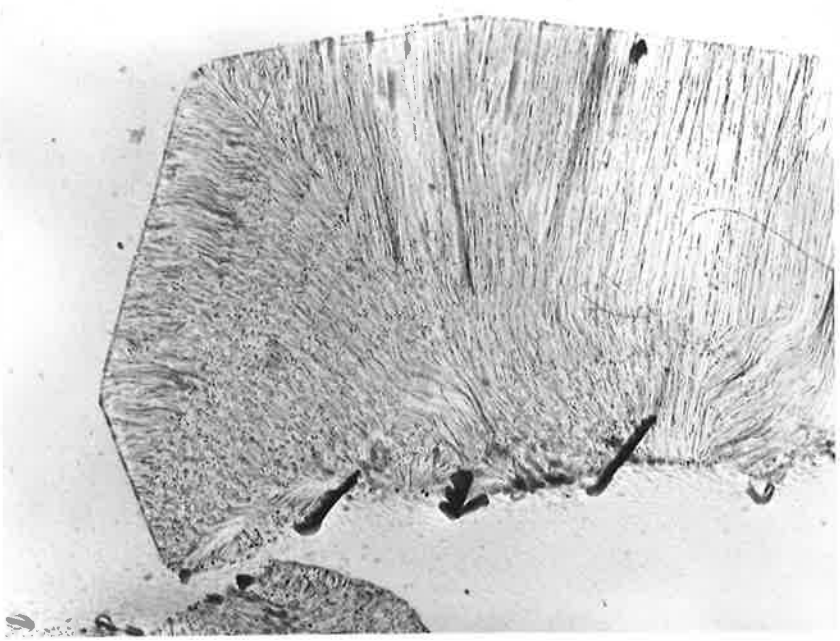

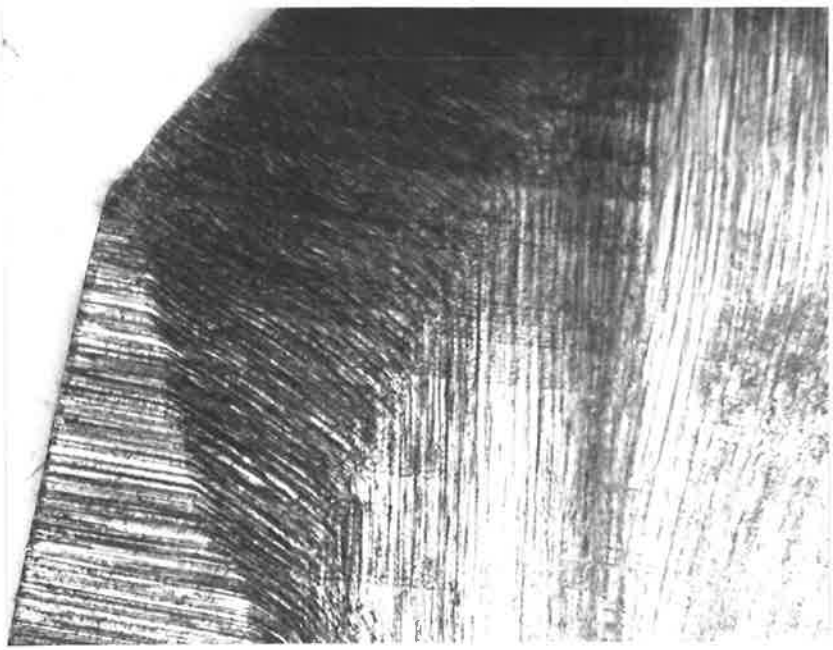

FIGURE 15

Banded distribution of fibres and particles.
Thin foil electron micrograph (X40,000)

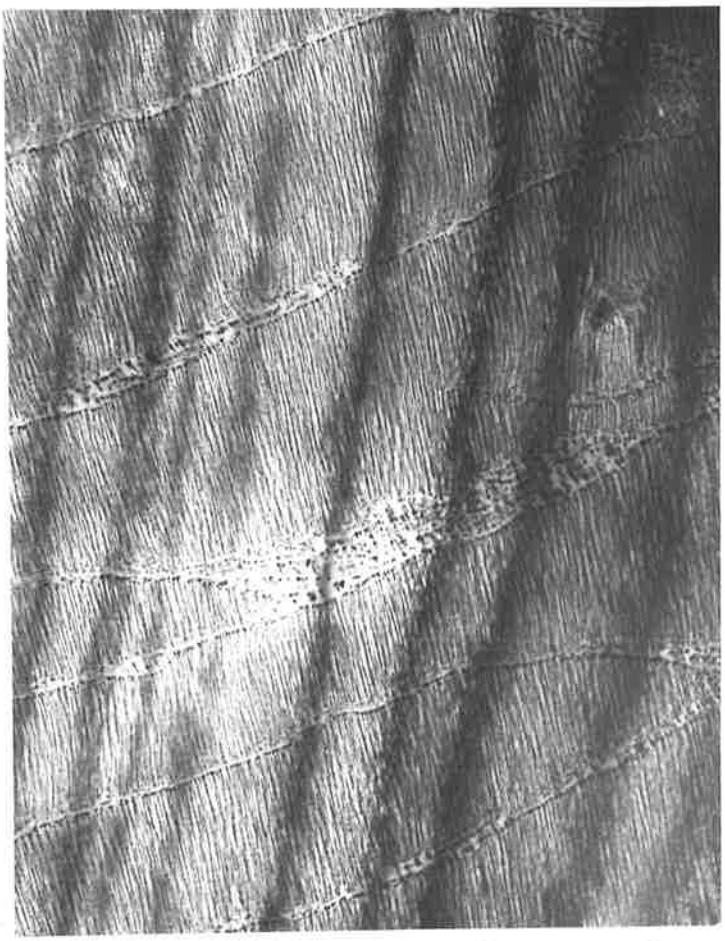

FIGURE 16

Extraction replica micrograph showing the association between the banded precipitate distribution and ledges on the nodule boundary (X13,000)

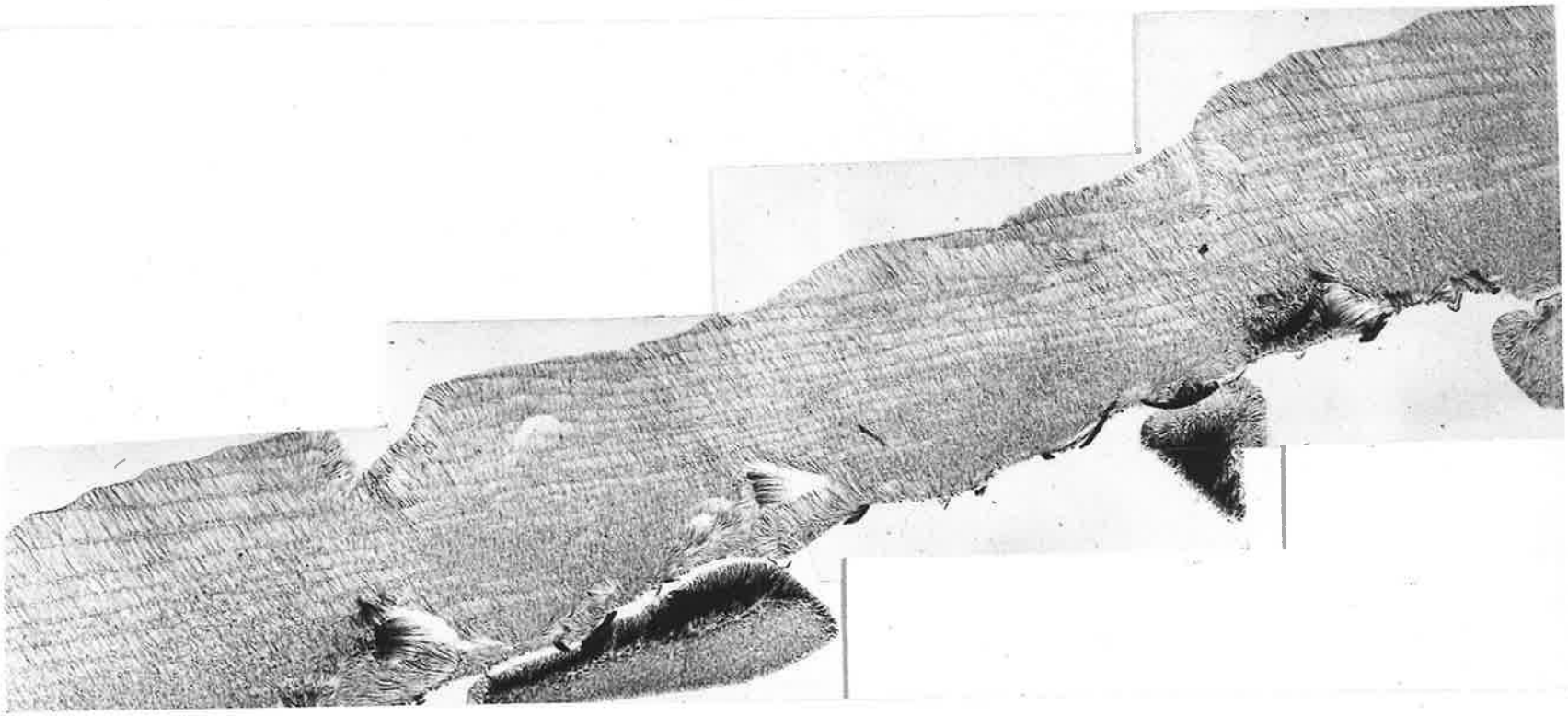

for example, Campbell and Honeycombe (1974)) the advancing boundaries frequently contained a series of short, inclined steps which were associated with the precipitate bands. This association is clearly evident in fig. 16. Thin foil electron microscopy revealed that these steps are, in fact, planar boundary segments behind which (and normal to which) fibrous precipitates develop (fig. 17a). On the other hand, the boundary segments between the steps appeared distinctly non-planar in the electron microscope and it is at these that particulate precipitation occurs, as can be seen in fig. 17b.

Close examination of this banded structure in thin foils tilted so as to minimize the extent of precipitate overlap in the image revealed that many of the particles in each band are attached to the ends of fibres in an adjacent band. Examples of this can be seen in the vicinity of arrowhead A in fig. 18. In virtually all of the cases where this attachment was encountered, the direction of fibre growth (indicated by arrowhead B in fig. 18) was consistent with the fibres having nucleated on these particles.

3.2.3 Nodule development

Confirming the results of optical metallographic studies (Chapter 2), electron microscopy revealed that the discontinuous reaction initiated at the pre-existing grain boundaries in the as-quenched alloy. It should be noted that the propensity to nucleate the reaction varied greatly from one boundary to another and often, from one segment to another of the same boundary. This particular aspect of the reaction will be examined in more detail in the next chapter.

The transformation commenced at the boundaries with the precipitation of particulate VC. As these particles formed, the boundaries began to migrate and as the reaction proceeded, migration

FIGURE 17(a)

Thin foil micrograph showing fibrous precipitation behind a planar ledge and particulate precipitates at adjacent non-planar boundary segments (X60,000)

FIGURE 17(b)

Same area as in (a) but at a different foil orientation

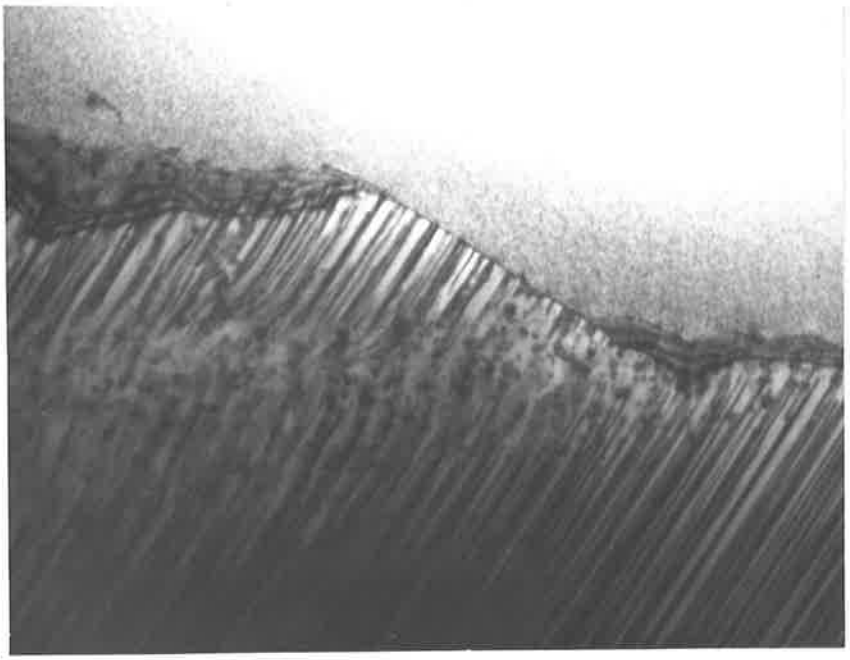

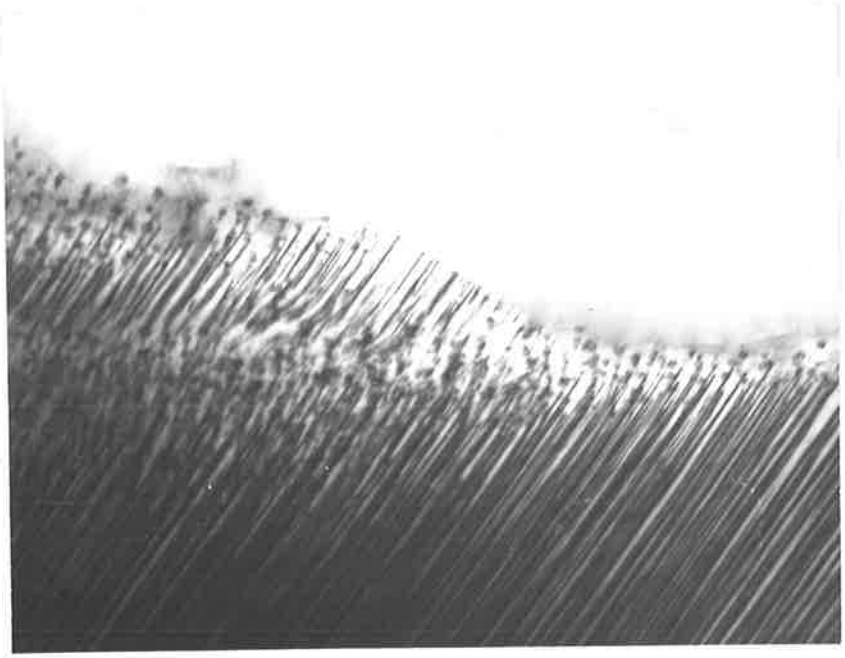

FIGURE 18

Thin foil electron micrograph showing fibres attached to particles (X85,000)

FIGURE 19

Early stages of nodule development.
Thin foil electron micrograph (X52,000)

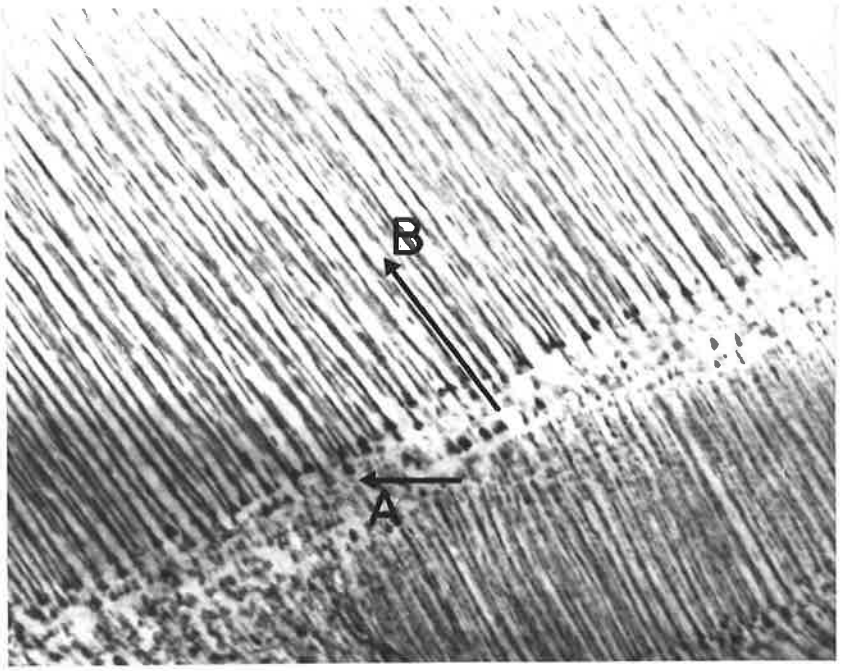
B
A

continued in association with further particulate precipitation. The nett effect of these simultaneous processes was to produce a highly convoluted grain boundary between adjacent grains (fig. 19), each convolution and the transformation product contained within constituting an individual nodule. In general, nodules in the very early stages of development were roughly hemispherical in shape (fig. 20) indicating that nodule growth occurs in an essentially radial manner. This shape was generally maintained until such time as either adjacent nodules impinged whereupon they coalesced to form quite complex shapes, or fibrous precipitation occurred in which case one or more growth directions became favoured.

The development of nodules in the manner described above - i.e., by the migration of pre-existing grain boundaries - establishes this process as being a classical discontinuous reaction (Smith (1953)). Further evidence for this manner of nodule development came from electron diffraction and dark-field studies which showed the orientation of the austenite to be continuous across the original site of the grain boundary.

Migration of the convoluted boundaries into one or other of the adjacent austenite grains continued until the entire volume of the specimen was occupied by nodules. It will be recalled from the previous section that some of these nodules consisted simply of a dispersion of particulate precipitates in an austenitic matrix; others, and these were by far the more common, contained both fibrous and particulate precipitates. In the former case, nodule growth involved continued particulate precipitation over the entire length of the advancing boundary which remained non-planar. In the latter case, however, it was apparent that at some stage of nodule growth a segment of the advancing boundary adopted a markedly planar configuration and this was accompanied by a transition

FIGURE 20

Nodule at an early stage of development containing only particulate precipitates. Thin foil electron micrograph (X115,000)

FIGURE 21

Thin foil electron micrograph of a nodule whose local direction of growth is everywhere normal to the boundary plane (X29,000)

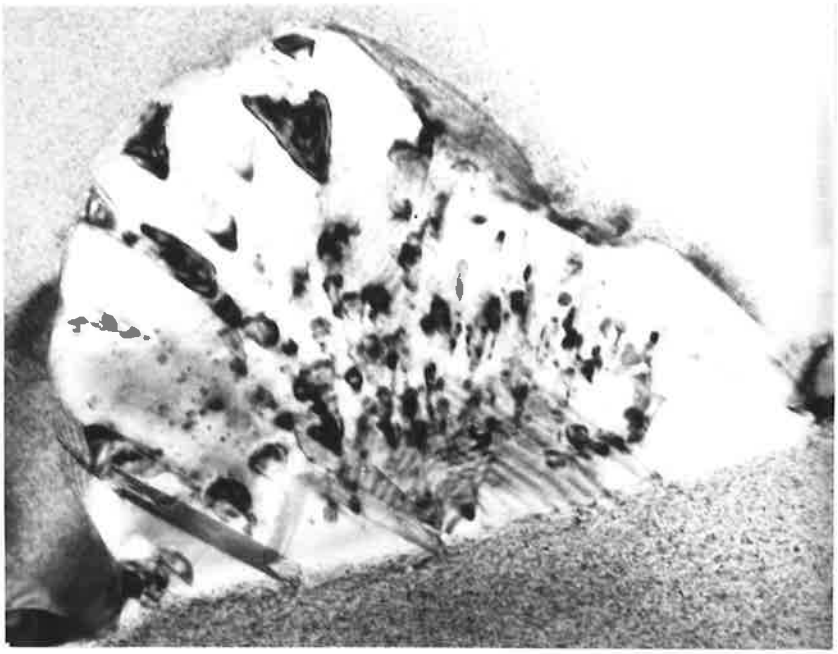

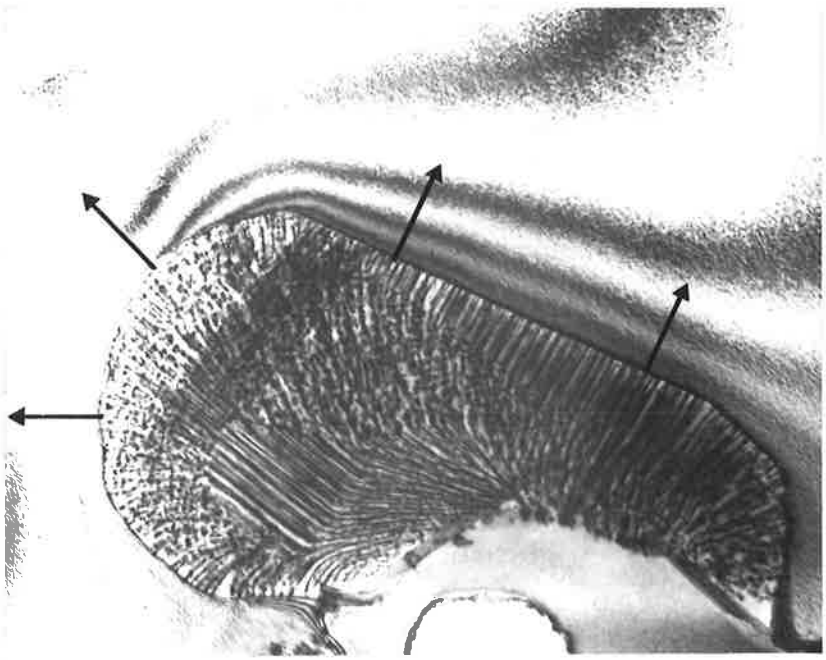

from particulate to fibrous precipitation. During the course of further nodule growth, particulate precipitates continued to form on those parts of the nodule boundary which remained non-planar so that at any one time, both types of precipitate formed concurrently behind different segments of the advancing boundary.

It was frequently the case that the boundary segments at which fibrous precipitation occurred, when present on either the one nodule or on adjacent nodules nucleated between the same two austenite grains, lay parallel or very nearly parallel to one another. Examples of this can be seen in figs. 12 and 16. Since electron diffraction analysis has shown that the orientation of the austenite containing the precipitate is continuous across the site of the transition, and that the transition occurs during nodule growth into super-saturated austenite of uniform orientation, it follows that fibres are generated behind those parts of the nodule boundary that lie in some preferred crystallographic orientation.

Nodule boundaries consisting of both planar and non-planar segments advanced in one or two ways, each giving rise to a different distribution of fibres and particles. As is now evident, these distributions are related to one another through the fact that it is behind favourably oriented boundary segments that fibrous precipitation takes place. In the case of the first distribution (fig. 12) and that which occurs when the favourably oriented segments are comparatively long, the local direction of nodule growth is normal to the plane of the boundary. This manner of growth can be readily visualised by referring to the thin foil micrograph in fig. 21. Growth of the nodule shown here involves the migration of both a planar boundary segment at which fibrous precipitation has occurred and a broadly curved segment at which particulate precipitates

FIGURE 22

Extraction replica micrograph showing a boundary protuberance (at A) at which ledges B and C have nucleated (X20,000)

have formed. Because the advancing boundary is viewed everywhere 'edge-on', the direction of boundary migration can be shown on the micrograph and is indicated at various points by arrows.

In the case of the banded precipitate distribution, the favourably oriented boundary segments are much shorter and constitute a series of inclined ledges on the nodule boundary. In this case, outward growth of the nodule involves the sideways movement of the ledges - a mechanism similar to that proposed by Aaronson (1962) and Davenport and Honeycombe (1971) for interphase precipitation in steels. For growth to continue in this way requires, of course, continued ledge development at the non-planar boundary segments. In this connection it is interesting to note that the initiation of fibrous precipitate bands and hence, ledge development, often occurs where there exists a comparatively large boundary protuberance, an example of which can be seen on the left-hand side of fig. 22. As will be seen in the later discussion, preferential ledge development at these sites closely parallels known behaviour in a number of other alloy systems.

3.3 Summary

A study has been made of the fine discontinuous reaction in the alloy Fe-13Mn-2V-.8C using electron microscopy of carbon extraction replicas and thin foils. The major points to emerge from this study are as follows:

(1) VC precipitates at the advancing grain boundaries as either long thin fibres (fibrous precipitation) or fine, discrete particles (particulate precipitation). Fibrous precipitates develop behind, and normal to, comparatively planar boundaries which lie in some favourable crystallographic orientation. In contrast, particulate precipitation occurs at boundaries which are non-planar and therefore

have no preference for a particular orientation. Both types of precipitate form in the familiar cube-cube orientation relationship with the nodule austenite.

(2) The discontinuous reaction is of the classical form in that it proceeds by the migration of pre-existing grain boundaries. In the initial stages of nodule growth the advancing boundary is entirely non-planar and hence the nodule contains only particulate precipitates. In the advanced stages however, one of two situations prevail: either the nodule boundary continues to remain non-planar over its entire length or, as is more likely, it consists of both planar and non-planar segments in which case both fibrous and particulate precipitates are present within the nodule.

(3) In the latter case, the precipitates are distributed in one of two ways. In the first, particulate precipitates are present in a random dispersion over most of the nodule and in a region extending from the non-planar portion of the nodule boundary to the original site of this boundary, while the fibres lay behind, and normal to, comparatively long and straight boundary segments. This distribution arises when the local direction of nodule growth is normal to the plane of the boundary. In the second distribution, narrow bands of particles separate considerably wider bands of fibres. In this case, the planar segments are much shorter and are present in the form of a series of inclined ledges on the nodule boundary. Outward growth of the nodule occurs by the sideways movement of the ledges.

CHAPTER 4

DISCONTINUOUS PRECIPITATION: THE EFFECT OF GRAIN BOUNDARY CRYSTALLOGRAPHY

4.1 Introduction

The fact that fibres, unlike particulate precipitates, are generated behind boundaries which lie in some favourable crystallographic orientation raises the possibility that the nature of the advancing boundary is a significant factor influencing precipitate morphology. This is further suggested by such behaviour as seen in figs. 12 and 17 where, as the orientation of the advancing boundary changes abruptly, so does the nature of the precipitate. In the present work this possibility has been investigated by carrying out detailed crystallographic analyses of a number of boundaries at which fibrous and particulate precipitation occur and interpreting the results of these analyses in terms of the Coincidence Site Lattice Model of grain boundary structure.

In addition to these studies, several pre-existing grain boundaries at which the discontinuous precipitation had not occurred after prolonged ageing have also been analyzed in order to study the effect of grain boundary crystallography on precipitate nucleation.

It will be recalled from chapter 1 that the CSL model envisages grain boundaries as consisting of a periodic array of coincidence sites which arise from geometrical matching between adjacent crystal lattices. As the essential distinction between the structure of one boundary and another is the difference in the (planar) density of coincidence sites (PDCS) at the boundary, i.e. the number of coincidence sites per unit boundary area, an appreciation of the factors which influence the PDCS is essential if the model is to be used to interpret crystallographic data.

These factors and their influence on the PDCS are briefly discussed in the following section.

The procedures used in the present work to obtain the crystallographic data required for the application of the model, and for the interpretation of this data, are described in section 4.3. The results of the crystallographic studies and their interpretation are presented in section 4.4, the details of which are summarized in section 4.5.

4.2 The density of coincidence sites at the grain boundary

In the CSL model a boundary becomes the appropriate planar section through the CSL which, it will be recalled, is the regular three-dimensional array formed by the fraction, $\frac{1}{\Sigma}$, of lattice sites common to the extended lattices of both neighbouring grains. The Σ value is determined by the misorientation between these grains and a procedure for its calculation has been given by Ranganathan (1966).

In a number of studies in which the model has been used to interpret crystallographic data for boundaries between cubic crystals (e.g. Ishida et al. (1976); Williams and Edington (1976)) an implicit relationship between Σ and the PDCS has been assumed; i.e. if Σ is comparatively low then the boundary will contain a relatively high PDCS and hence will have a well-ordered structure, and vice versa. However, as pointed out by Pond (1974) in a paper dealing with the geometrical properties of CSLs, no such simple relationship exists. In part, this is because CSLs possess low symmetry, i.e. the spatial distribution of coincidence sites is highly anisotropic, and partly because the characteristics of this distribution are sensitively dependent on the boundary misorientation. As a result of these factors, some CSLs contain planes with a similar or higher PDCS than that which can be achieved in CSLs with

significantly lower Σ values. For example, Pond has shown that because CSLs generated between f.c.c. crystals related by angular rotations about $\langle 100 \rangle$, $\langle 110 \rangle$ and $\langle 111 \rangle$ axes have, respectively, tetragonal, orthorhombic and trigonal type Bravais lattices, the maximum value of the PDCS in the $\Sigma = 41$ CSL ($\langle 100 \rangle$ / 12.1^{o}) is commensurate with that in the $\Sigma = 19$ CSL ($\langle 110 \rangle$ / 46.8^{o}) which in turn is less than half that in the $\Sigma = 27$ CSL ($\langle 110 \rangle$ / 31.6^{o}).

Thus, it is clear that in order to characterize grain boundary structure in terms of the PDCS, the spatial distribution of coincidence sites in the CSL defined by the boundary misorientation must first be determined, and then the appropriate planar section through this distribution, corresponding to the boundary plane orientation, be made.

It should be pointed out that although the PDCS is not simply related to Σ, it is nevertheless significantly influenced by this parameter (Smith, 1974). This influence arises because, in addition to being the reciprocal volume density of coincidence sites, Σ is also the ratio of the volume of the primitive unit cell of the CSL to that of the crystal lattices (Pond (1974)). It follows, then, that there must exist some upper limit to Σ beyond which the CSL unit cell volume is sufficiently large that irrespective of the boundary plane orientation, the PDCS will be so low as to render the boundary indistinguishable, for all practical purposes, from one with a completely disordered structure. Although as yet there exists no firm theoretical or experimental basis for deciding on the magnitude of Σ at which this occurs, there is some evidence (Goodhew et al, 1978) to suggest that CSLs with Σ values up to at least $\Sigma = 99$ may have physical significance in the model.

4.3 Experimental and interpretive procedures

4.3.1 Determination of the crystallographic parameters

The characterization of grain boundary structure in terms of the CSL model requires a knowledge of both the misorientation between the neighbouring grains and the orientation of the boundary plane. In the present work this information was obtained using transmission electron microscopy and selected area diffraction analysis of thin foil specimens.

(a) The boundary misorientation

There are several alternative ways of expressing the misorientation between a pair of grains. One of these is the axis/angle pair description, i.e. [hkl]/θ where [hkl] is a direction common to both grains and θ is the angle through which the lattice of one grain must be rotated about [hkl] in order to bring it into complete coincidence (Σ=1) with the lattice of the other grain. As a procedure has been given (Ranganathan (1966)) for generating CSL misorientations in this form, it was desirable for comparison purposes that the experimental misorientation also be expressed in this way. This description can be most simply obtained from electron diffraction patterns using a stereographic procedure (Johari and Thomas (1969)); however, a preliminary investigation by the author revealed that the inaccuracy introduced in plotting poles and in manipulating the stereogram can lead to errors in the misorientation determination of a magnitude commensurate with the difference between one coincidence site relationship and another. Accordingly, it was decided to determine the boundary misorientation using an inherently more accurate but less simple analytical procedure (Hancock and Lorimer (1970)) involving the use of matrix algebra. This procedure is briefly outlined below.

To obtain the information required for establishing the

misorientation, a Kikuchi diffraction pattern capable of being uniquely indexed (i.e. a pattern containing at least three non-parallel Kikuchi line pairs) was taken from each of the neighbouring grains. After being indexed, the patterns were used to obtain two sets of parallel directions in these grains, one set corresponding to the beam directions which were determined analytically using the procedure given by von Heimendahl et al. (1964) and the other set corresponding to some arbitrary direction in the plane of the patterns. These pairs of directions were then taken in combination to determine the misorientation matrix which relates crystallographic directions in one grain to directions in the other. The rotation axis [hkl], which is the direction common to both grains and hence is the eigen-vector of this matrix, and the rotation angle θ were then derived from the matrix elements using the relationships given by Hornstra (1960) and Lange (1967).

Because of this analytic procedure, only the errors associated with obtaining directions from the Kikuchi patterns limited the accuracy of the misorientation determination. The principal source of these errors was the diffuseness of the Kikuchi lines, an effect largely dependent on beam divergence and internal strain in the diffracting crystal. In obtaining a misorientation these errors interact in a rather complex way, the details of which have not been precisely established; however, a preliminary error analysis revealed that the overall inaccuracy in determining either the rotation axis or angle does not exceed the algebraic sum of the individual errors. On this basis it is estimated that these two parameters were determined to within 2^{o}.

(b) The boundary plane orientation

The determination of this required a knowledge of the direction of the boundary trace on the foil surface and the inclination of the

boundary in the foil. The former was obtained by correlating the boundary image with the relevant diffraction pattern and could be estimated to within $\pm 1^{\circ}$. The boundary inclination was determined from two-tilt boundary projected width measurements using the equation derived by von Heimendahl (1973) relating the change in the projected spacing of two image points, one on each foil surface, to the angle of specimen tilt. In order to gauge the accuracy of this determination a number {111} annealing twin boundaries were analysed since the angle of inclination of the twin boundary is known once the beam direction is specified. In all cases examined the inclination obtained from the two-tilt procedure was within 5° of the true value.

It should be pointed out that since the boundaries at which particulate precipitates form are irregular on a very fine scale, it was only possible to determine an 'average' boundary plane orientation for these. This determination was made from the mean direction of the boundary trace on the foil surface and the mean projected widths at the two-tilt settings.

4.3.2 Application of the CSL model

4.3.2.1 Selection of the appropriate CSL

To facilitate selection of a CSL for the interpretation of experimental results, reference is usually made to one of the several published lists (Brandon et al. (1964); Acton and Bevis (1971); Pumphrey and Bowkett (1971); Warrington and Buffalini (1971); Grimmer et al. (1974)) of axis-angle pairs defining CSLs up to some maximum Σ value. The choice of this Σ cut-off has necessarily been arbitrary since, as indicated earlier, it has not yet been established at what Σ value the model loses physical significance. Shortly after commencing the present work, however,

it became apparent that the model retains significance for boundaries lying between grains for which the Σ value exceeds those in the most extensive list so far published ($\Sigma \leqslant 49$, Grimmer et al.). To facilitate the CSL selection process a more extensive list was therefore compiled (see Table A2 (Appendix 2)), and the introductory part of this appendix for details of its construction).

From this extended list it was possible to readily identify the CSLs defined by axis/angle pairs in the vicinity of the experimental [hkl]/θ. Of these CSLs, the one used to interpret the experimental results was that defined by the axis/angle pair ([uvw]/θ') which lay sufficiently close to [hkl]/θ that the deviation of the latter from the exact coincidence condition was within the permissible deviation range of $15\Sigma^{-\frac{1}{2}o}$ given by Brandon (1966).

4.3.2.2 Construction of the CSL unit cell

Following selection of the appropriate CSL, its unit cell was constructed so that the coincidence plane in the vicinity of the boundary plane could be characterized in terms of the PDCS. Whilst the PDCS in any given CSL plane can be more readily determined by an analytical procedure (e.g. Andrejeva and Fionova (1979)), the approach used in the present work offers the distinct advantage of enabling all conceivable CSL planes in the vicinity of the boundary plane to be readily identified. This feature is important as quite significant variations in the PDCS can occur with small changes in the planar section through the CSL.

To simplify this construction use was made of the fact that in all cases examined, of the 24 different but equivalent descriptions of [uvw]/θ' which exist (Pumphrey and Bowkett (1971)) because of the symmetry relation between cubic crystals, at least one of these was a twinning operation, i.e. [UVW]/180^{o}. Because any given [UVW] crystal plane has, at

least, 2-fold symmetry it then follows that if one atom in such a plane is common to both neighbouring grains, then so are all the other atoms in that plane. Consequently, by utilizing the twin description the problem of constructing the CSL unit cell reduces to one of simply determining the positions of atoms in a small fraction ($\frac{1}{\Sigma}$) of the planes in the (UVW) stack containing sufficient planes to uniquely define the lattice of either of the adjacent grains.

A method for determining the twin description utilizing matrix algebra has been given by Pumphrey and Bowkett and this was used in the present work. Essentially, this approach involves first determining the misorientation matrix $\tilde{M}$ equivalent to [uvw]/θ' using the procedure given by Hornstra (1960), and then carrying out the following operation:

$$\tilde{M}_i = P_i\tilde{M} \qquad i = 1,.....24$$

where P_i is one of the cubic symmetry operations in matrix form as given by Jaswon (1956). This operation is continued until a misorientation matrix $\tilde{M}_i$ is obtained for which the rotation angle in the equivalent axis/angle pair description is 180^o.

To avoid tedious computations, a computer programme (see Appendix 3) was written to generate, using [UVW] as input data, plotted arrays showing the atom positions in the coincident (UVW) planes. From this computer output the CSL unit cell could be readily obtained by visual inspection.

4.4 Results and interpretation

4.4.1 Studies of the advancing boundary

The present investigation revealed that the precipitate morphology is significantly influenced by the nature of the advancing

boundary, with fibrous and particulate precipitation occurring, respectively, at boundaries containing comparatively high and low densities of coincidence sites. The following examples, which constitute a representative cross-section of the various boundaries examined, illustrate this influence. In addition, as these examples encompass boundaries advancing in the various different ways described in the previous chapter, they also provide the necessary information to enable the nodule growth process to be related to the boundary crystallography.

Details of the crystallography of the various nodule boundaries examined in this section are summarized below in Table 4.1.

TABLE 4.1

Example	γ_1/γ_2 misorientation	Boundary plane orientation in γ_2	
		Fibrous ppt.^{n}	Particulate ppt.^{n}
1	[.110,.640,.932]/34.62°	-	-
2	[.$\overline{768}$,.243,1.802]/80.78°	(.$\overline{129}$,.$\overline{577}$,.865)	(0.385.,726.,571)
3	[.346,.778,.378]/27.77°	(.$\overline{516}$,.$\overline{147}$,.844)	(.$\overline{322}$,.233,.918)
4	[.458,.629,.998]/140.60°	(.480,.872,.090)	-
5	[.$\overline{539}$,1.103,1.523]/102.06°	(.$\overline{174}$,.754,.$\overline{633}$) (.$\overline{499}$,.$\overline{809}$,.311)	-

Example 1

It will be recalled from Chapter 3 that the growth of some nodules is characterized by continued particulate precipitation over the entire advancing boundary which remains at all times non-planar. All (six) nodules which had nucleated between the pair of austenite grains in fig. 23 were found to exhibit this type of growth and one of these nodules is illustrated in this figure. (The rather large region of dark contrast

FIGURE 23

Nodule at an advanced stage of growth containing only particulate precipitates. Thin foil electron micrograph (X30,000). Beam direction $[\overline{17},44,88]$ in γ_1, $[\overline{20},59,78]$ in γ_2

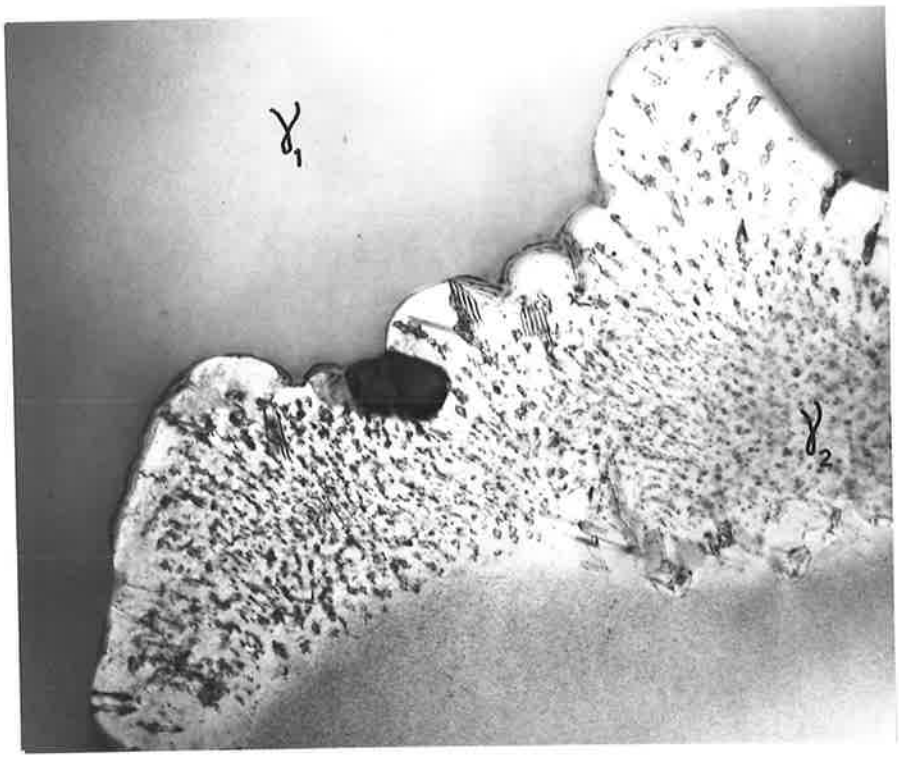
γ_1
γ_2

immediately behind the advancing boundary is a VC particle which is believed to have remained out of solution during the high temperature soak prior to the precipitation process).

The axis/angle pair describing the γ_1/γ_2 misorientation in fig. 23 is ~[169]/34.6°. From inspection of Table A2 it can be seen that no CLSs with $\Sigma \lesssim 99$ are generated by rotation angles in the vicinity of 34.6° about either [169] or other axes within a few degrees of this. The closest CSL relationships in Table A2 to the experimental misorientation are, in fact, rotations about [011], i.e. at 38.94°(Σ = 9), 34.89°(Σ = 89) and at 31.59°(Σ = 27), but in each of these cases the 12.5° deviation of the experimental rotation axis from [011] far exceeds the permissible deviation given by Brandon (1966), i.e. 5.0° for Σ = 9, 1.6° for Σ = 89 and 2.9° for Σ = 27.

In an attempt to characterize the γ_1/γ_2 misorientation in terms of a coincidence site relationship, a list was compiled of CSLs with $\Sigma > 99$ which are generated by rotations about [169] and at angles within several degrees of 34.6°. Although it was not possible to unambiguously determine from this list the appropriate coincidence site relationship since a number of CSLs (see Table 4.2) are generated at rotation angles which lie within the experimental error, it can be confidently stated that the CSL defined by the γ_1/γ_2 misorientation has a Σ value of at least 571. Because of their exceedingly high Σ values, it would be unrealistic to expect that the CSLs in Table 4.2 can be distinguished from one another in terms of a meaningful coincidence density at the boundary; hence, the inability to specify the coincidence site relationship defined by the γ_1/γ_2 misorientation is of no consequence insofar as the interpretation of the experimental results are concerned.

TABLE 4.2

Σ	θ
571	37.50
1207	36.44
637	35.44
1343	34.48
707	33.58
1487	32.72
781	31.91

Example 2

The portion of boundary seen in fig. 24 consists of two different segments lying roughly to one another; one of these (which is part of a ledge, in fact) is markedly planar and fibrous precipitation has occurred here, while the other is distinctly non-planar and has been the site of a limited amount of particulate precipitation.

In this case the γ_1/γ_2 misorientation is very close to the coincidence site relationship $[\bar{3}17] / 80.96^{\circ}$ where $\Sigma = 35$. Fig. 25 shows the unit cell of this CSL. The plane of the boundary segment at which fibrous precipitation has occurred lies almost parallel to the coincidence plane $(\bar{5}\bar{1}3)\gamma_1$ vs $(\bar{1}\bar{3}5)\gamma_2$ which is the twin plane and, as can be seen from inspection of fig. 25, is the most densely packed plane in the CSL (PDCS = 5.22 coinc. sites/nm^2). By contrast, the boundary segment at which particulate precipitation has occurred does not lie in the vicinity of a high density coincidence plane, but does lie very close to a number of CSL planes containing a comparatively low density of coincidence sites. Because

FIGURE 24

Thin foil electron micrograph showing part of a ledge and an adjacent non-planar boundary segment (X40,000). Beam direction $[\bar{2},12,99]$ in γ_1, $[\bar{29},48,83]$ in γ_2.

FIGURE 25

Unit cell of the $\Sigma = 35$ CSL.
Indices given with respect to γ_2

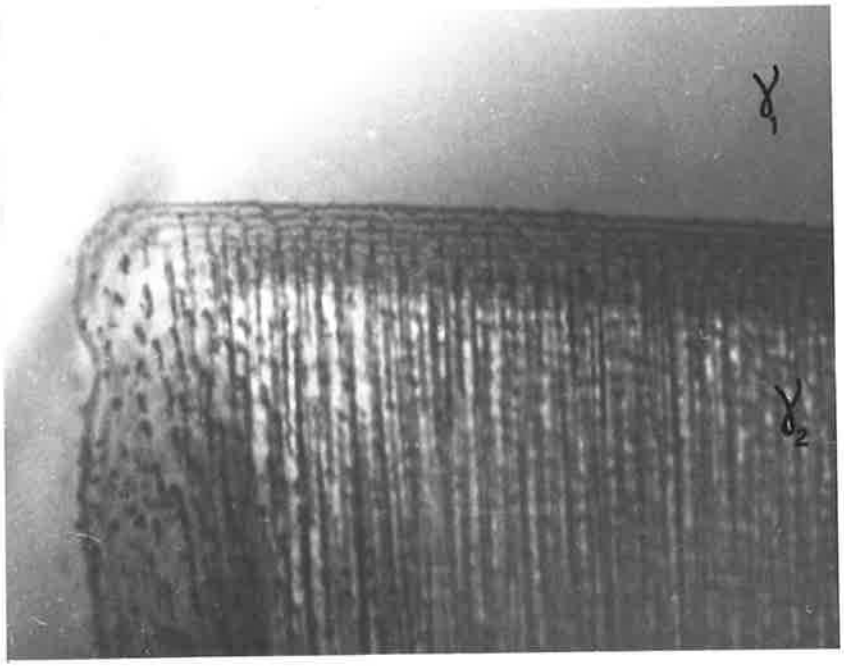
γ1
γ2

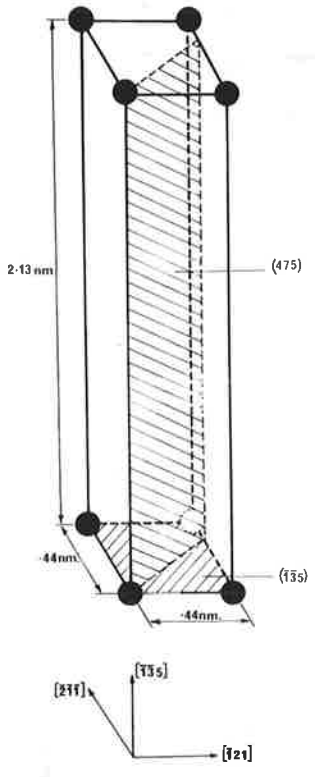
2·13 nm
(475)
·44nm.
(1̄35)
·44nm.
[1̄35]
[211]
[1̄21]

of the rather large error associated with the determination of the boundary plane orientation it is not possible to state which of these CSL planes most closely represents the boundary structure. However, since the most densely packed of these planes, i.e. $(5\bar{4}7)\gamma_1$ vs.$(475)\gamma_2$, contains a PDCS of 0.23 coinc. atoms/nm^2, it can be stated that the density of coincidence sites at the boundary does not exceed this value.

Example 3

A further example of a boundary consisting of planar and non-planar segments is shown in fig. 26 but unlike the previous example, this boundary is not advancing by the ledge mechanism. The arrowhead marks the junction of these different segments and is seen to be the site of a small change in the boundary orientation. To the left of the arrowhead fibrous precipitation has taken place behind the comparatively long planar segment while to the right, particulate precipitates have developed at the non-planar segment.

The γ_1/γ_2 misorientation in fig. 26 is very close to the coincidence site relationship $[121]/27.53^{o}$ which defines a CSL with $\Sigma = 53$ and a unit cell as shown in fig. 27. As in the previous example, the plane of the boundary segment at which fibrous precipitation has taken place conforms to the twin plane, i.e. $(\bar{6}14)\gamma_1$ vs.$(\bar{4}\bar{1}6)\gamma_2$, and again this plane contains the highest PDCS (2.24 coinc. sites/nm^2) in the CSL. Similarly, the boundary segment at which particulate precipitation has occurred does not conform to a densely packed CSL plane but does lie very close to a number of planes containing a very low density of coincidence sites. Of these $(\overline{123},100,135)\gamma_1$ vs.$(\overline{73},48,189)\gamma_2$ contains the highest PDCS (.08 coinc. sites/nm^2).

FIGURE 26

Thin foil electron micrograph showing fibrous precipitates behind a long, planar boundary segment differing slightly in orientation from a segment at which particulate precipitates have formed (X32,000). Beam direction [20,55,81] in γ_1, [43,46,77] in γ_2

FIGURE 27

Unit cell of the $\Sigma = 53$ CSL.
Indices given with respect to γ_2

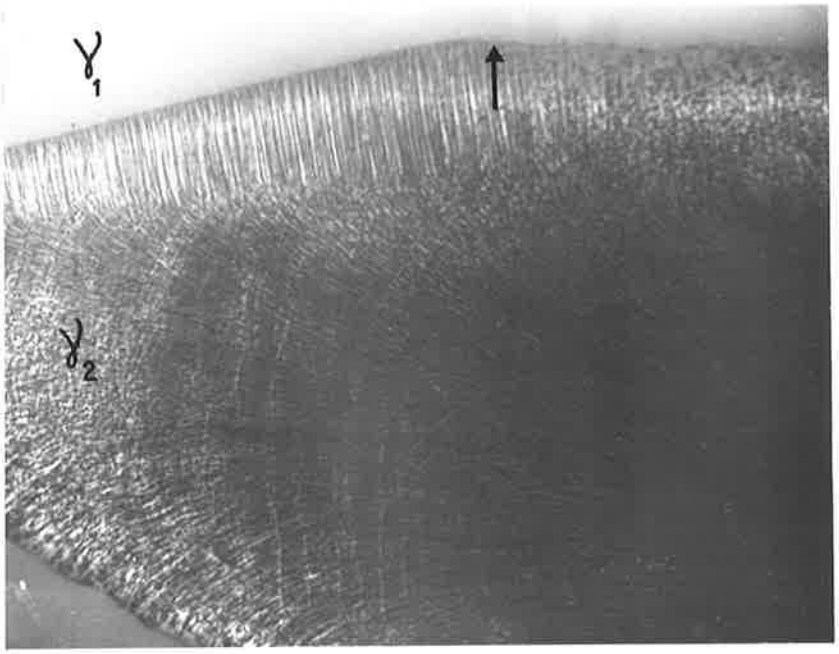
γ1
γ2

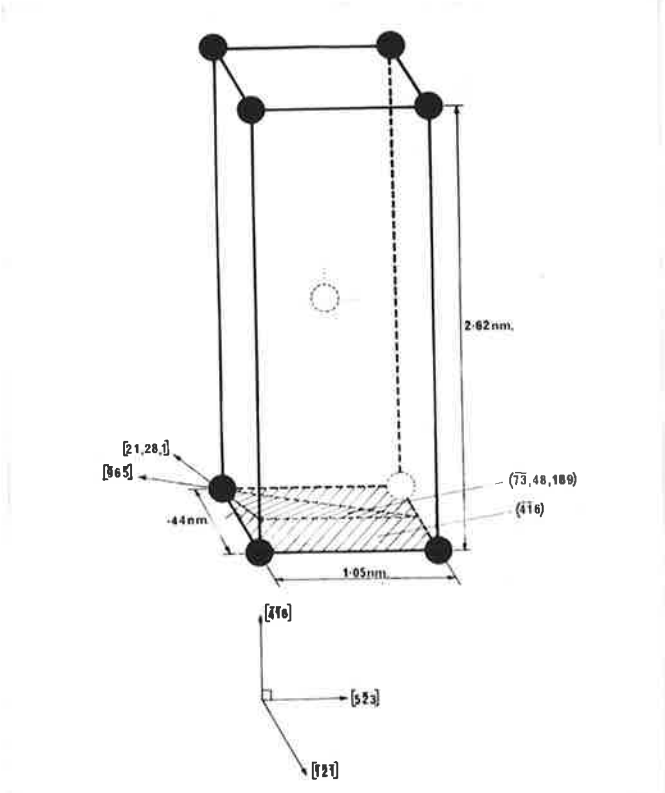
2·62nm.
[21,28,1]
[965]
(7̄3,48,189)
(4̄16)
·44nm
1·05nm
[4̄16]
[52̄3]
[72̄1]

Examples 4 and 5

In the previous examples the boundaries at which fibres are generated conform to the most densely packed plane in the CSL and this is also the twin plane. Not all such boundaries, however, were found to display these characteristics. In some cases the boundary conformed to the twin plane but, because of the particular CSL geometry, this was not the plane containing the highest PDCS, though it was always found to be one of the more densely packed planes in the CSL. The boundary whose crystallographic characteristics are listed in Table 4.1 under Example 4 falls into this category. This boundary conforms to the coincidence plane $(5\bar{2}9)\gamma_1$ vs. $(592)\gamma_2$ in the $\Sigma = 55$ CSL at $[5,7,11]/140.6^{o}$ and, as can be seen from inspection of the relevant CSL unit cell in fig. 28, this coincidence plane is the third most densely packed (PDCS = 1.47 coinc. sites/nm^2) in the CSL, the planes ADGF and BCHE containing the highest PDCS (1.86 coinc. sites/nm^2).

In other cases, the boundary at which fibrous precipitation occurred conformed to neither the twin plane nor the most densely packed CSL plane but instead, conformed to a coincidence plane of rather modest packing density relative to the latter. It should be pointed out, however, that where this occurred the PDCS value was always significantly higher than that typically associated with particulate precipitation. The crystallographic characteristics of two boundary segments on the one module which are of this type are listed in Table 4.1 (Example 5). The coincidence planes $(\overline{19},\overline{11},1)\gamma_1$ vs. $(\bar{5},17,\overline{13})\gamma_2$ and $(29,\bar{5},13)\gamma_1$ vs. $(\overline{17},\overline{25},11)\gamma_2$ in the $\Sigma = 23$ CSL at $[123]/120.56^{o}$ to which those boundary segments conform are identified in fig. 29 and contain, respectively, a PDCS of 1.40 and 0.96 coinc. sites/nm^2.

FIGURE 28

Unit cell of the $\Sigma = 55$ CSL.

Indices given with respect to γ_2

FIGURE 29

Unit cell of the $\Sigma = 23$ CSL.

Indices given with respect to γ_2

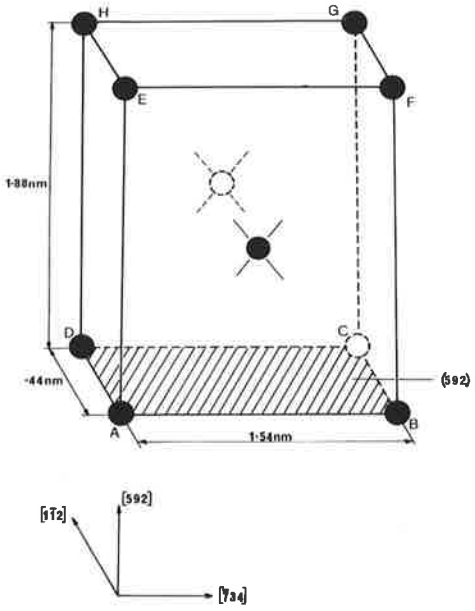
H
G
E
F
1·88nm
D
C
·44nm
(592)
A
B
1·54nm
[592]
[1$\bar{7}$2]
[$\bar{7}$34]

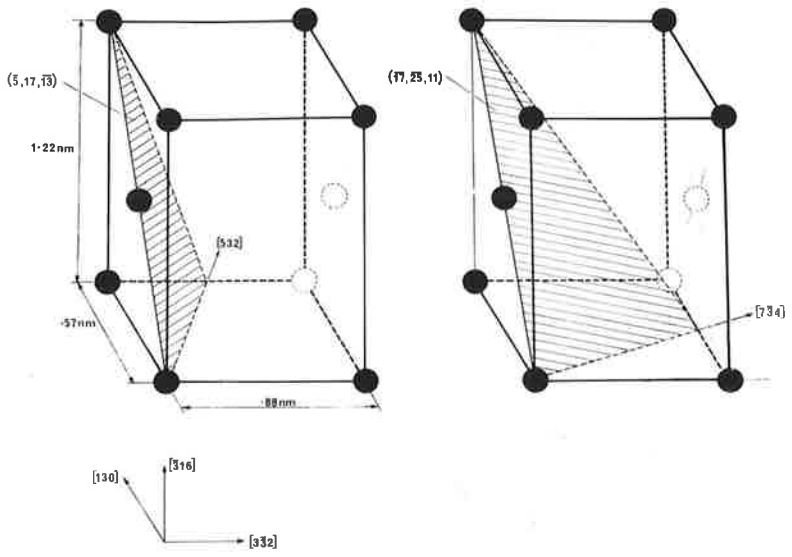
(5,17,$\bar{1}$3)
1·22nm
[532]
·57nm
·88nm
(17,25,11)
[734]
[130]
[$\bar{3}$16]
[33$\bar{2}$]

4.4.2 Studies of precipitate-free grain boundaries

Details of the crystallography of the several boundaries examined are summarized below in Table 4.3.

TABLE 4.3

Example	γ_1/γ_2 misorientation	Boundary plane orientation in γ_2
1	[.020,1.326,1.326]/69.66°	Segment A:- (.570,$\overline{.569}$,.592) Segment B:- ($\overline{.289}$,.565,.771)
2	[$\overline{.365}$,1.289,1.269]/112.06°	($\overline{.550}$,$\overline{.559}$,.622)

Example 1

As has been found (e.g. Petermann and Hornbogen (1968); Frebel and Schenk (1979)) in a number of other alloy systems, discontinuous precipitation was suppressed at annealing twin boundaries. An example of such a boundary, in a specimen in which the discontinuous reaction has proceeded almost to completion, is given in fig. 30. The boundary displays the usual stepped configuration and consists of two sets of planar, parallel segments which have been designated A and B. (The lines of dark contrast which are visible at the latter segments are believed to be dislocations as these segments appeared 'clean' on examination of extraction replicas).

The γ_1/γ_2 misorientation in fig. 30 is within several degrees of the coincidence site relationship [011]/70.53° defining the CSL with $\Sigma = 3$ and a unit cell as shown in fig. 31. The plane of the boundary segments designated A (Table 4.3) conforms to the twin plane, i.e. $(\bar{1}\bar{1}1)\gamma_1$ vs. $(1\bar{1}1)\gamma_2$,

FIGURE 30

Stepped annealing twin boundary after prolonged ageing. Thin foil electron micrograph (X30,000). Beam direction $[\bar{2},47,88]$ in γ_1 and $[28,59,76]$ in γ_2

FIGURE 31

Unit cell of the $\Sigma = 3$ CSL.
Indices given with respect to γ_2

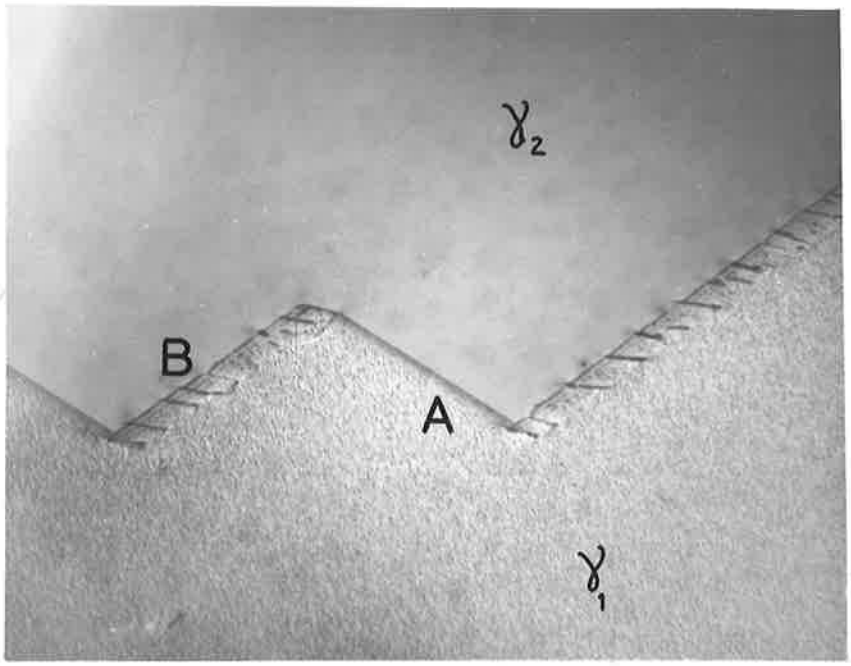
γ_2
B
A
γ_1

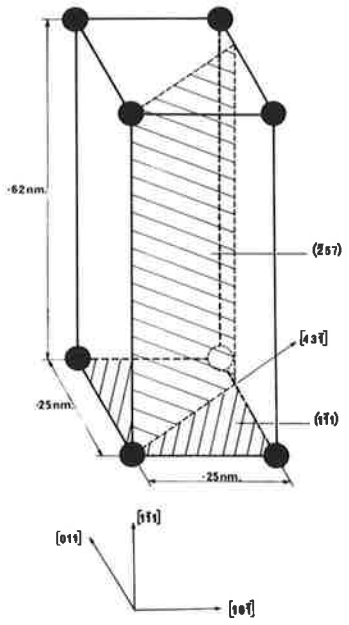
·62nm.
(25̄7)
[43̄]
(1̄1̄)
·25nm.
·25nm.
[1̄1]
[011]
[10̄]

FIGURE 32(a)

Thin foil electron micrograph of a boundary containing a precipitate-free segment (X46,000)

FIGURE 32(b)

Same area as in (a) but at a slightly different foil orientation

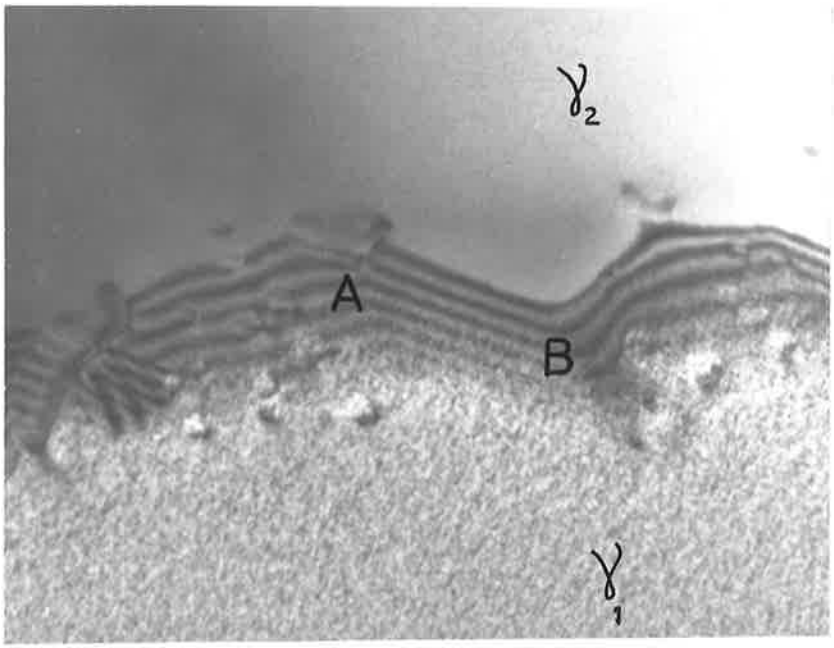
γ_2
A
B
γ_1

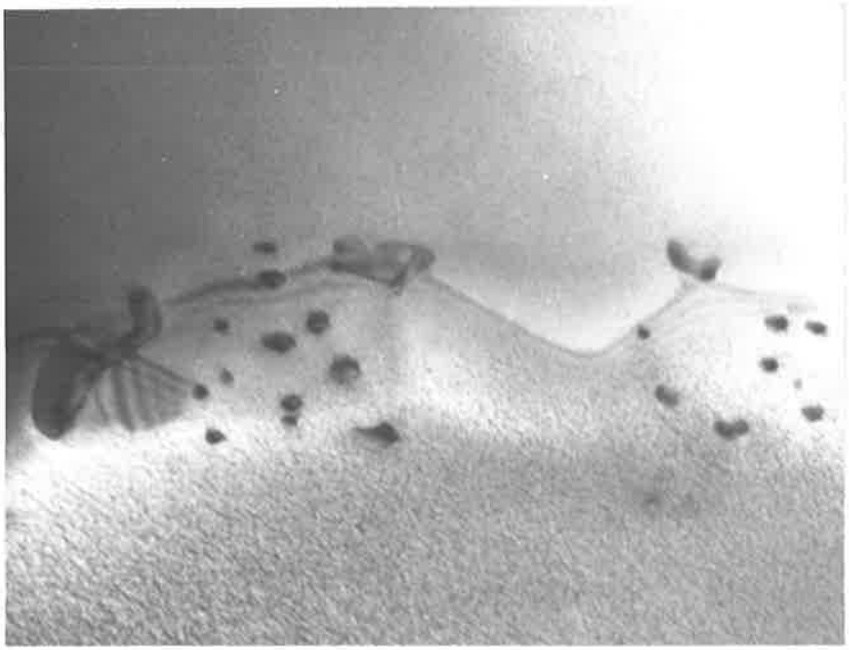

FIGURE 33

Same area as in fig. 32 but after a large foil tilt about an axis parallel to A-B (X46,000)

FIGURE 34

Unit cell of the $\Sigma = 7$ CSL.
Indices given with respect to γ_2

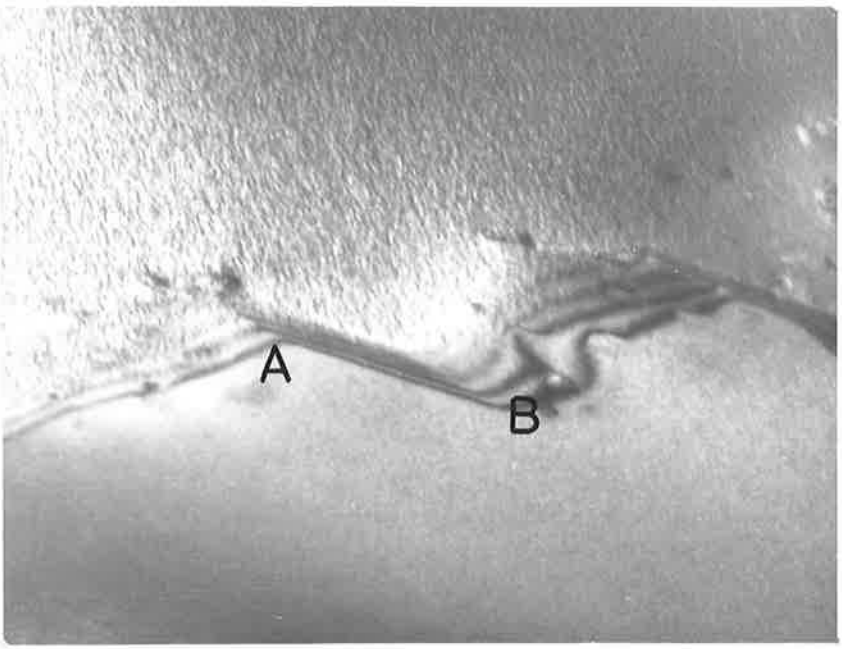
A
B

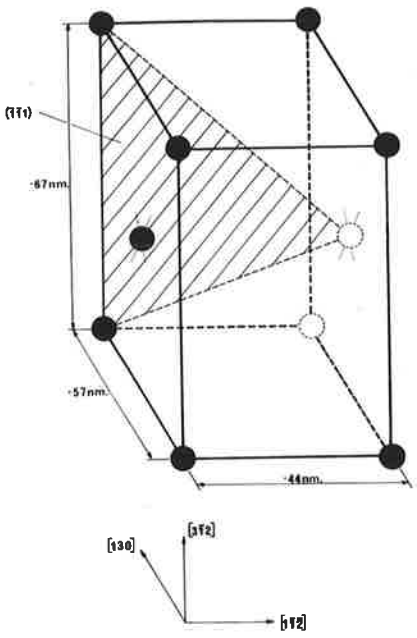
(11̄1)
·67nm.
·57nm.
·44nm.
[130]
[3̄12]
[1̄12]

which is the most densely packed plane in the CSL (PDCS = 17.82 coinc. sites/nm^2). Although the coincidence plane $(\bar{2}75)\gamma_1$ vs.$(\bar{2}57)\gamma_2$ to which boundary segments B conform is clearly not one of the more densely packed CSL planes (fig. 31), because of the small dimensions of the Σ = 3 CSL unit cell this plane still contains a reasonably high PDCS (1.75 coinc. sites/nm^2).

Example 2

Precipitate nucleation was found to be difficult not only at annealing twin interfaces but also at some segments of more 'general' grain boundaries. An example of the latter is seen in fig. 32, the micrograph in fig.(a) revealing the path of the boundary and that in fig.(b) the precipitate distribution. The boundary segment A-B, which in fact is a small planar step (as seen more clearly at the different foil orientation in fig. 33), has remained free of precipitate during ageing unlike the adjacent non-planar boundary segments which contain discrete VC particles. Close inspection of the remainder of this grain boundary revealed the presence of several other planar boundary steps which lay parallel to segment A-B and these too were observed to be free of precipitate.

The γ_1/γ_2 misorientation across this boundary is very close to the coincidence site relationship $[\bar{1}33]/110.92^{\circ}$ which defines a CSL with Σ = 7 and the unit cell depicted in fig. 34. Boundary segment A-B conforms to the coincidence plane $(\bar{1}1\bar{1})\gamma_1$ vs.$(\bar{1}\bar{1}1)\gamma_2$ which contains a comparatively high PDCS (2.55 coinc. sites/nm^2) in this CSL.

4.5 Summary

From the combined crystallographic and structural studies in section 4.4.1 it can be seen that the precipitate morphology is related to the nature of the advancing boundary as follows:-

(1) fibrous precipitates develop when the boundary (i) lies between grains for which the CSL has a comparatively high density of coincidence sites, i.e. a low Σ value, and (ii) has an orientation such that its plane conforms to a plane of modest or dense packing in the CSL; i.e. fibres develop at 'good fit' boundaries.

(2) particulate precipitates develop at 'poor fit' boundaries containing a very low density of coincidence sites. In this connection, two situations can be distinguished. Firstly, the misorientation between the adjacent grains may be such that Σ is very high, as is the case for the grains in fig. 23 where $\Sigma \gtrsim 571$. In this case, the boundary will be one of poor fit irrespective of the orientation of its plane and as a result, particulate precipitation occurs over the whole of the nodule boundary. Secondly, the misorientation between adjacent grains may be such that the density of coincidence sites in the CSL is comparatively high, as for the grains in fig. 24 where $\Sigma = 35$ and in fig. 26 where $\Sigma = 53$. In this case the boundary conforms to a plane containing a very low PDCS in the CSL.

Because of the limited nature of the present work, it is not possible to define either of the following:

(i) the limiting PDCS value(s) above which fibrous precipitation occurs and below which particulate precipitates develop. However, it can at least be stated that these two modes of precipitation occur when the PDCS is $\gtrsim 0.96$ and $\lesssim 0.23$ coinc. sites/nm^2 respectively.

(ii) the value of Σ above which only particulate precipitates form irrespective of the boundary orientation and below which either fibrous or particulate precipitates develop depending on the orientation of the boundary plane. It is most unlikely that the highest Σ value found to be associated with fibrous precipitation,

i.e. $\Sigma = 55$, even approximates this limiting value as calculations have shown that the most densely packed planes in a number of CSLs with $\Sigma > 55$ contain a higher PDCS (e.g. 4.01, 3.78 and 3.09 coinc. sites/nm^2 in the $\Sigma = 59([110]/46.0^{o})$, $\Sigma = 67([110]/62.4^{o})$ and $\Sigma = 99([110]/89.4^{o})$ CSLs respectively) than the minimum value (0.96 coinc. sites/nm^2) at which fibrous precipitation has been found to occur.

Several grain boundaries at which VC precipitation had not occurred after prolonged ageing have been examined in order to gain some insight into the effect of grain boundary crystallography on precipitate nucleation efficiency. It has been shown that, like the advancing boundaries behind which fibrous precipitation takes place, boundaries at which precipitate nucleation is difficult have the following characteristics: firstly, they are markedly planar which suggests at the outset that they lie in some favourable crystallographic orientation; secondly, they lie between low Σ CSL related grains and thirdly, their orientation is such that they contain a comparatively high PDCS (cf. boundaries at which repeated precipitate nucleation occurs).

CHAPTER 5

DISCUSSION

It has been shown that two types of VC precipitate - discrete particles and fibres - develop during the discontinuous reaction and that when present in the one nodule, these precipitates are distributed in one of two ways depending on the nodule growth process. This chapter discusses the conditions under which these precipitate morphologies and distributions develop.

5.1 The precipitate morphology

As fibres are reasonably straight and do not branch, it follows that each fibre, like a particulate precipitate, is the result of an individual nucleation event. However, whereas the particulate precipitates are repeatedly nucleated at a low coincidence boundary, the fibres - while developing behind a high coincidence boundary - appear to nucleate only on the particles which lie in the advancing boundary as it attains a high density coincidence orientation. This distinction suggests that the precipitate morphology is strongly influenced by the effect of grain boundary structure on the ease of precipitate nucleation and that, as Pumphrey (1976) has proposed, precipitate nucleation is comparatively easy at low coincidence boundaries but difficult at boundaries containing a high density of coincidence sites. As there is evidence (see later) that the nature of the precipitate is not significantly affected by the rate of boundary migration, the observation that precipitate nucleation is difficult at those (stationary) boundaries which already lie in a high coincidence orientation before the reaction commences would appear to be strong evidence in support of this correlation.

The comparative difficulty in nucleating precipitates at the high density coincidence boundary may be due to either the higher activation energy for nucleation at this site due to its lower interfacial energy (which is apparent from its highly facetted nature) or, as the principle means of solute transport during discontinuous precipitation is by grain boundary diffusion (Sundquist (1973)), the lower diffusivity at this boundary (Ishida et al. (1976); Williams and Edington (1976)). In view of the ability of the advancing high density coincidence boundary to support continued precipitate growth, the absence of precipitation at its stationary counterpart even after prolonged ageing might appear, at first sight, to rule out the latter of these possible explanations. However, a discrimination between these two possibilities cannot be undertaken on the basis of this observation alone as recent work (Hillert and Purdy (1978); Smidoda et al. (1979)) has shown that the diffusivity in migrating boundaries can be several orders of magnitude higher than in stationary boundaries.

It will be recalled (Chapter 1) that in addition to a boundary structure characterized by good fit, a high rate of boundary migration can also render precipitate nucleation more difficult. The evidence for this comes principally from studies of interphase precipitation during the ledge growth of ferrite in austenite. Here it is found that precipitate nucleation occurs preferentially at the immobile, partially coherent boundary segment which is displaced by ledge movement, rather than at the energetically more favourable disordered ledges. It is considered (e.g. Aaronson et al.(1978)) that this occurs because insufficient time is available for nucleation at the ledges on account of their high mobility. If, in the present reaction, the rate of boundary migration likewise significantly influences precipitate nucleation and similar considerations apply, it would of course follow that the high density coincidence boundary should

have a considerably higher mobility than its poor fit counterpart. Whilst this kinetic distinction clearly prevails when nodule growth proceeds by the ledge mechanism (fig. 16), in the case of nodules of the kind shown in figs.12 and 21 a significant difference in the rate of migration of the two kinds of boundaries does not appear to exist; - in fact, as will be seen later, in some cases the observed nodule structure can only be accounted for if the high density coincidence boundary advances more slowly than its poor fit counterpart. The absence of a significant influence of boundary mobility on the precipitate morphology suggested by this evidence is further highlighted by the observation (chapter 3) that an appreciable change in the overall transformation kinetics, brought about by varying the ageing temperature, produced no significant change in the relative proportions of fibrous and particulate precipitates in the transformation product.

By precipitating in a cube-cube orientation relationship with the solute depleted austenite (Chapter 3), the VC nucleates coherently (Imai and Namekata (1970)) and in such a way that the same crystallographic planes in the two phases lie parallel to one another. It follows, then, that the degree of crystallographic matching at the precipitate nucleus/boundary plane will be in direct proportion to the density of coincidence sites at the boundary, i.e. crystallographic matching will be poor at low coincidence boundaries but at boundaries containing a high density of coincidence sites relatively good matching will obtain. On this basis, it would be expected (Clough et al. (1974)) that the high coincidence boundaries should be the more favoured sites for precipitate nucleation. As this is not observed, it can be concluded that crystallographic matching of the precipitate with the plane of the boundary is of secondary importance to the structure of the boundary in controlling nucleation.

Summarizing then, it would appear that the boundary structure or more specifically, the degree of atomic fit at the boundary plane, is the determining factor influencing the precipitate morphology and that this influence arises predominantly through an effect on the ease of precipitate nucleation. With this established, the circumstances under which the two precipitate morphologies develop can now be proposed in more detail. Turning firstly to the case of particulate precipitation a dynamic process somewhat analogous to 'incoherent' interphase precipitation (Ricks et al. (1979)) at austenite/ferrite boundaries is envisaged, in which repeated nucleation and growth of new precipitates at the low coincidence boundary occurs at the expense of continued solute diffusion to the pre-existing boundary precipitates. The latter, when prevented from an adequate supply of solute to enable continued growth in contact with the advancing boundary, become detached from it and thereby incorporated in the solute depleted austenite as discrete particles. In the case of fibrous precipitation, nucleation occurs only on those particles lying in the boundary as it attains a high density coincidence orientation, the fibrous morphology developing as a result of continued precipitate growth at the high coincidence boundary as it advances into the grain ahead. Whereas in other discontinuous reactions involving continued precipitate growth a precipitate branching mechanism usually operates to compensate for the attendant increase in grain boundary area (e.g. Fournelle and Clark (1972)), thereby enabling roughly equidistant solute sinks to be maintained, no such compensation is required in the present reaction due to the planar nature of the high coincidence boundary. Consequently, precipitate growth at this boundary is essentially unidirectional, each fibre being the result of an individual nucleation event.

5.2 Nodule development and the precipitate distribution

It has been shown that depending on the manner of nodule growth, fibrous and particulate precipitates can be distributed in one of two ways. In the first (e.g. fig.12) fibrous precipitates lay behind, and normal to, comparatively long and straight boundary segments, while the particulate precipitates occupy a region extending from the non-planar portions of the advancing boundary to its original site. In the second (e.g. fig.16), bands of particles separate considerably wider bands of fibres which are associated with a series of short, planar ledges on the nodule boundary.

With the nature of the boundaries at which fibrous and particulate precipitates develop established, a description of the sequence of events leading to the evolution of these two different distributions can now be given. In both cases an essential requirement is that the misorientation across the nodule boundary defines a CSL with a Σ value sufficiently low that there exists at least one 'good fit' low-energy orientation which the boundary will prefer to lie in. As will be recalled from Chapter 3, the initial stages leading to the development of both distributions are similar in that the reaction commences with particulate precipitation at a (poor fit) grain boundary which then proceeds to migrate.

In the case of the first distribution, particulate precipitation continues in association with the boundary migration until a comparatively long segment of the advancing boundary adopts an orientation corresponding to one at which there is a high density of coincidence sites. At this stage a transition from particulate to fibrous precipitation takes place; thereafter, particulate precipitates continue to form at those parts of the advancing boundary which fail to attain a high coincidence orientation. As fibres develop normal to the plane of the boundary at which precipitation occurs and as they are reasonably straight, it follows that after this

transition fibrous precipitation takes place at a boundary which maintains a fixed orientation during further migration. Such behaviour simply reflects the fact that migration of a boundary out of a high density coincidence orientation is energetically unfavourable because neighbouring boundary plane orientations are associated with a low density of coincidence sites, a consequence of CSL geometry.

As the direction of fibre growth and the direction of migration of the boundary at which this occurs are the same, it further follows that those fibres which develop when the advancing boundary attains a high density coincidence orientation continue to lengthen during the further course of the reaction. In view of this, it now becomes apparent that the variation in fibre length behind the high coincidence boundary evident in some nodules (e.g. the larger of the two nodules in fig. 12) could only have arisen as a result of continued migration of the poor fit boundary into the high coincidence orientation following the initial transition from particulate to fibrous precipitation, i.e., as a result of continued lengthening of the high coincidence boundary segment at the expense of its poor fit counterpart (fig. 35). This sort of migrational behaviour, which is also believed (Aaronson (1962)) to occur during the growth of pro-eutectoid ferrite allotriomorphs in Fe-C alloys, strongly suggests - as Aaronson has pointed out - that minimization of the total boundary energy, i.e. $\gamma_i A_i$ where γ_i is the boundary free energy per unit area and A_i its area, is an important factor influencing the mechanism of boundary migration. Qualifying an earlier remark concerning the relative rates of migration of the low and high coincidence boundaries in the case of nodule growth leading to the kind of precipitate distribution being presently considered, it is pointed out that simple geometrical considerations dictate that in order for the high coincidence boundary to lengthen as it migrates, it must advance more slowly than its poor fit counterpart (note $d_1 < d_2$ in fig. 35).

FIGURE 35

Schematic diagram depicting successive stages of nodule growth involving lengthening of a high coincidence boundary. A-B-C defines initial boundary position and A'-B'-C' a later position. Hatched area delineates the fibrous precipitate region.

FIGURE 36

Schematic diagram illustrating the ledge mechanism of nodule growth

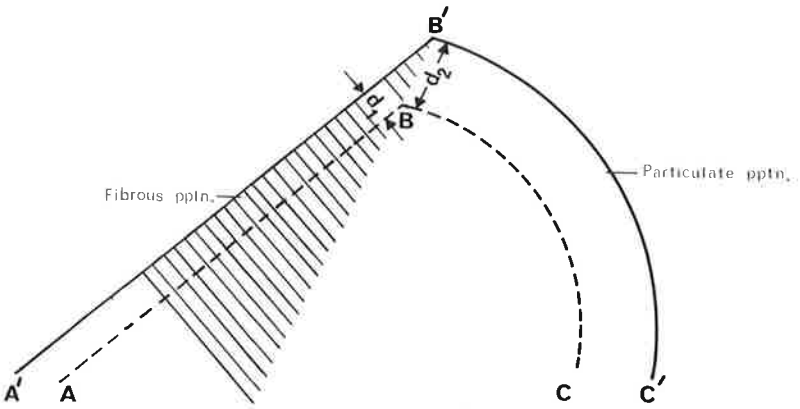
B′
d_1
d_2
B
Particulate pptn.
Fibrous pptn.
A′
A
C
C′

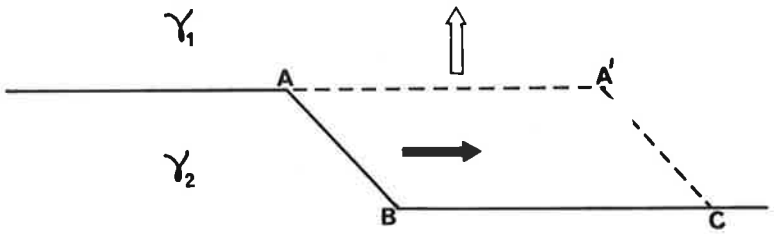
γ_1
A
A′
γ_2
B
C

For some pairs of austenite grains the boundary misorientation is such that the CSL contains a number of different planes at which the density of coincidence sites is high. For instance, the CSLs whose units are depicted in section 4.4.1 are of this type. It would therefore seem reasonable to expect that during the growth of nodules which have nucleated between such grains fibrous precipitation may occur at more than one orientation of the boundary plane with the result that the nodules contain a number of different arrays of parallel fibres. Nodules of this kind have, in fact, been observed on numerous occasions and an example of the fibrous region in one of these is seen in fig. 14.

In the second precipitate distribution, bands of particles alternate with bands of fibres which grow behind, and normal to, short planar boundary steps (ledges), each of which is the result of a segment of the advancing boundary facetting into a high density coincidence site orientation. The bands of particles are believed to delineate successive positions of a poor fit boundary which is displaced by the lateral movement of these ledges in the manner depicted schematically in fig. 36. Here, segment A-B represents a ledge and segment B-C part of the poor fit boundary. As segment A-B advances in the direction normal to itself, the ledge moves in the direction of the solid arrow across the poor fit boundary and in doing so, displaces this boundary in the direction of the hollow arrow so that with the ledge at C, the poor fit boundary has been displaced to A-A'. During the interval between the passage of one ledge and the next, particulate precipitates continue to form at the poor fit boundary and it appears (fig. 18) that some of these particles later serve as nuclei for the fibres generated behind this next ledge.

In view of the considerable orientation difference which can exist between ledges and the 'poor fit' boundaries they traverse (fig. 17), the

evidence (fig. 22) for repeated ledge development at sites where there exists a protuberance on the nodule boundary is not altogether unexpected, for at these sites the ledge orientation ought to be more readily achieved by the boundary than elsewhere. Such evidence closely parallels known behaviour in the Fe-C system (Kinsman et al. (1975)) where the evolution of sideplates from grain boundary ferrite allotriomorphs provides, by reason of the concave transition region, a continuous source of ledges.

The ledge growth mechanism for interphase boundary migration occurs not only during the austenite to ferrite transformation in iron base alloys, but is an important precipitate growth mechanism in many other alloy systems (e.g. Al-Cu (Weatherly and Sargent (1970); Garmong and Rhodes (1974)), Al-Ag (Laird and Aaronson (1967)) and Cu-Ga (Kittl and Massalski (1967))). In all of these alloy systems it has been found that, in accordance with a proposal by Aaronson (1962), the ledge mechanism overcomes a structural barrier to precipitate growth by displacing coherent or semi-coherent boundaries which are capable (Smith (1953)) of only very limited migration due to the accumulation of elastic strain energy. In the present discontinuous reaction, however, ledge movement displaces boundaries which, as would be expected from their comparatively disordered structure, are capable of extensive migration. It appears, then, that in this reaction the ledge growth process is a viable mechanism simply because those boundary segments in the high coincidence ledge orientation advance considerably more rapidly than their poor fit counterparts. The reason for this kinetic distinction is not immediately apparent, but it may well be due to one of the following factors:

(i) the high coincidence boundary possessing an inherently higher mobility, as Aust and Rutter (1959) and more recently Demianczuk and Aust (1975) have found in their studies of grain boundary migration in very dilute

solid solutions. The high mobility of this boundary was interpreted by these workers in terms of a selective boundary-solute interaction, the argument being that solute segregation to reduce boundary strain energy should be less at the good fit, highly coincident boundary which would therefore experience a lower solute drag effect. The applicability of this argument to the particular case of boundary migration in metals containing extensive amounts of solute is open to question, however, in view of the recent experimental evidence (Hillert and Purdy (1978); Cahn et al. (1979)) that in this instance, the presence of solute at the boundary (or more importantly, its rapid diffusion in the boundary plane) can in fact provide a driving force for boundary migration. So far, the experiments have been limited simply to demonstrating this effect in a range of alloy systems and have not attempted to examine the possible influence of boundary structure on the driving force.

(ii) an impediment to the migration of the low coincidence boundary due to the pinning force (Zener (1949)) exerted by the particulate precipitates opposing the process of boundary/precipitate detachment.

There is the further possibility of this distinction being due to the fact that migration of the high density coincidence boundary, unlike its poor fit counterpart; is able to proceed without the need for concomitant repeated precipitate nucleation. However, the fact that particulate precipitates are nucleated almost immediately on the newly displaced boundary following the passage of a ledge (fig. 17) would tend to suggest that a constraint imposed by nucleation kinetics on the rate of migration of the low coincidence boundary is most unlikely.

It should be emphasized that whilst this kinetic distinction permits the operation of the ledge mechanism, it does not dictate that nodule growth should occur in this way. Insofar as this mechanism enables nodule growth to proceed without an attendant increase in the area of the high energy poor fit boundary (fig. 36), its operation is certainly consistent with the earlier suggestion that minimization of the total grain boundary energy is a significant factor influencing the mode of nodule growth.

CHAPTER 6

CONCLUSIONS AND SUGGESTIONS FOR FURTHER WORK

Conclusions

The main findings of the present investigation may be summarized as follows:-

(1) The alloy Fe-13Mn-2V-0.8C, solution treated at 1300^{o}C, water quenched and aged in the range 550-710^{o}C undergoes a discontinuous reaction in which VC precipitates at the advancing grain boundary as either long, thin fibres or fine, discrete particles.

(2) The precipitate morphology is related to the CSL structure of the boundary at which precipitation occurs. Fibrous precipitates develop when the boundary (i) lies between grains for which the CSL has a comparatively high volume density of coincidence sites (Σ typically $\lesssim 55$) and (ii) has an orientation such that its plane conforms to one containing a high planar density of coincidence sites (PDCS typically $\gtrsim 1.0$ coincidence site/nm^2) in the CSL. Significant departures from these conditions (i.e. $\Sigma >> 55$ or a PDCS $\lesssim 0.1$ coincidence site/nm^2) leads to the development of particulate precipitates.

(3) The effect of grain boundary structure on the ease of precipitate nucleation is the important factor influencing the precipitate morphology. Nucleation is considerably more difficult at the high density coincidence boundary and this may be due either to its low energy or to reduced solute diffusivity in its plane.

(4) The discontinuous reaction is of the classical form in that it proceeds by the migration of pre-existing grain boundaries to form

nodular regions of transformation product. In the initial stages of nodule growth the advancing boundary is composed entirely of segments lying in a low coincidence orientation and hence the nodule contains only particulate precipitates. In some cases this state of affairs persists during the entire course of nodule growth but more commonly, at some stage of nodule growth, a segment of the advancing boundary attains a high density coincidence orientation and when this occurs, a transition from particulate to fibrous precipitation takes place.

(5) Fibrous and particulate precipitates within the one nodule are distributed in one of two ways depending upon the manner of nodule growth. In the first distribution, the fibres lay behind and in contact with comparatively long, high density coincidence segments of the nodule boundary while the particulate precipitates occupy a region extending from the poor fit portions of this boundary to its original site. In this case, the local direction of nodule growth is everywhere normal to the plane of the advancing boundary. In the second distribution, bands of particles alternate with bands of fibres which grow behind short planar ledges on the nodule boundary, each of which lies in a high density coincidence orientation. The bands of particles are believed to delineate successive positions of a low coincidence boundary which is displaced by the sideways movement of these ledges.

(6) Minimization of the total grain boundary energy appears to be an important factor determining the mechanism of nodule growth involving both fibrous and particulate precipitation.

Suggestions for further work

(i) The proposed nodule growth mechanisms were arrived at deductively from a consideration of the different precipitate distributions that form. The validity of these proposed mechanisms ought to be checked by utilizing one of the currently available experimental techniques enabling direct observation of phase transformations, e.g. photo emission or thermionic emission microscopy.

(ii) A particularly revealing experiment would be to examine how the limiting PDCS value for fibrous precipitation is affected by the presence of an interfacially active solute species such as boron or phosphorus, i.e. a solute which can significantly lower the austenite grain boundary energy. Clearly, a reduction in this limiting PDCS value brought about by the addition of such a solute would signify that it is primarily through an influence exerted upon the energetics of precipitate nucleation that the boundary structure affects precipitate morphology.

(iii) A similar transition from fine to coarse discontinuous precipitation as occurs in Fe-13Mn-2V-0.8C on ageing in the range 640-710^{o}C has not been previously reported in the literature; nor, in fact, has the possibility of such a transition been argued on the basis of theoretical considerations. Clearly, clarification of the reason for the observed transition would constitute a significant advance in our general understanding of precipitation behaviour at grain boundaries.

(iv) Because of their high toughness and work-hardening capacity, austenitic manganese steels find considerable commercial use in applications where resistance to impact and abrasion are required. Limits in this direction are set, however, by a relatively low yield

strength which renders these steels suitable for use only at low working loads when resistance to dimensional change is an important factor. It is well known that the presence of a fine precipitate distribution can lead to a significant increase in the yield strength, and it is therefore of some importance that mechanical tests be carried out to determine whether the fine discontinuous reaction can prove beneficial in this regard without, at the same time, having a detrimental effect on the toughness and work-hardening capacity.

APPENDIX 1

EXPERIMENTAL MATERIALS AND TECHNIQUES

A1.1 Materials and alloy preparation

Preliminary transformation studies (Chapter 2) were undertaken using alloys prepared by melting high purity constituents in an argon-arc furnace. The analysis of the principal component (iron) is given in Table A1.1, the total impurity level in the other constituent elements, carbon, manganese and vanadium being <0.01%, <0.02% and <0.2% by weight respectively.

These constituents were weighed out to produce 50-60 gram ingots of desired composition and a small excess of manganese (approximately 10% by weight of the nominal manganese content) was then added to compensate for losses resulting from evaporation during melting. The charge was then placed in a depression in the water cooled copper hearth of the furnace. After evacuation to 1Pa the furnace chamber was flushed with high purity argon, this sequence being repeated twice more. A titanium getter was then melted for 10 minutes in order to remove residual impurities in the argon. To obtain a reasonably homogenous melt, the ingot was bridged over the hearth depression and the arc then used to extend the molten pool from the ingot centre to each end until the depression was filled - this procedure was repeated at least six times.

The principal alloy used in this work, of nominal composition Fe-13Mn-2V-0.8C, was supplied by the Broken Hill Pty. Co. Ltd. The alloy was prepared by vacuum induction melting, and its analysis is given in Table A1.2.

A1.2 Alloy fabrication and heat-treatment

The as-cast ingots were initially hot rolled to 8mm diam. bar, and following mechanical abrasion to remove the oxide scale and decarburized layer, the ingots were then sealed in argon filled mullite tubes and homogenized for 50 hours at 1200°C. This heat-treatment resulted in the formation of a large quantity of undissolved VC and homogenization was considered complete on the basis of a uniform distribution of these particles along the length of the ingot.

After homogenization the alloys were hot rolled and swaged to 3mm diameter rod. Hot working was always performed above 1150°C, since there was a tendency for the alloys to crack at lower temperatures.

Specimens for transformation studies were solution treated at 1300°C ±10° for one hour in argon filled silica capsules. It was observed that a chemical reaction occurred when the high manganese steels were in direct contact with the silica. To overcome this problem, the specimens were wrapped in a single layer of mild steel shim before encapsulation. Solution treatment was followed by a water quench during which the tube was broken to improve the quench efficiency. Specimens for ageing were re-encapsulated in evacuated silica tubes. Temperature control during ageing was ±3°C, and the ageing treatment was always terminated by a water quench.

A1.3 Metallographic techniques

A1.3.1 Optical microscopy

Specimens were initially ground to a sufficient depth to remove unrepresentative surface layer, and then polished to a fine diamond finish. Mechanical polishing can produce many artefacts in austenitic manganese steels and it therefore was often necessary to employ a final electropolish

using the following electrolyte at 0-10°C:

10% Perchloric Acid

20% Glycerol

70% Ethanol

Electropolishing was carried out using a stainless steel cathode at a potential of 10-15V and a current density of 0.1-0.15A/cm^2. 2% nital (nitric acid in ethanol) was found to be a suitable etchant for all phases examined by optical microscopy.

Percentage transformation was determined by point counting, using a grid of approximately 1000 points.

A1.3.2 Electron microscopy

(a) Extraction Replicas

The surface for replication was mechanically polished in the normal manner, lightly etched with picral (1% picric acid and 5% HCl in ethanol) and then coated with a thin layer of carbon. After scoring the film into small squares, the replica was stripped from the specimen in an electrolyte of 10% HCl in ethanol, using a stainless steel cathode and a potential of 7 volts. The replica was then floated off in distilled water and collected on a support grid.

(b) Thin foils

Thin foils were prepared from discs which had been sliced from 3mm diameter bar using a water cooled carborundum slitting wheel. After mechanically grinding the discs to a thickness of 0.1 mm they were dished and perforated in a commercial twin jet Fischione+ electropolishing cell

---

+ Manufactured by E.A. Fischione Instrument Mfg. Co., Verona, Pa., USA.

using the same electrolyte and polishing conditions reported in A1.3.1. Following perforation, the foils were thoroughly washed in ethanol and rapidly dried in a hot air stream.

Because of the highly localized nature of the discontinuous precipitation reaction, initial perforations rarely occurred at desired locations. This problem was partly overcome by controlled enlargement of the perforation by ion-beam thinning in a commercial Ion Tech Microlap[++] unit using the following conditions:

Accelerating potential:	5 - 6 KV
Ion beam current density:	4 - 5 mA/cm^2
Ion source angle:	20 - 25^{o}
Specimen rotation rate:	20 - 30 r.p.m.

A1.4 Instrumental methods

The majority of replica and thin foil studies were undertaken on a Philips EM200 electron microscope operating at 100 KV. This machine was equipped with a double tilt stage, a tilt-rotation stage and beam tilt facilities. Several thin foils were also examined in a JSEM-200 microscope at 200 KV.

In order to achieve high resolution in the electron microscope it was necessary to make a correction for specimen magnetism.[+++] Freeman (1971) has described a beam tilting technique for this correction and his method was used in the present study.

++ Manufactured by Ion Tech Ltd., Teddington, Middlesex, England.

+++ Although austenitic manganese steels are non-magnetic, a detectable influence of the specimen on the electron beam was apparent. This resulted from a ferritic rim around the edge of the 3mm disc due to decarburization and a surface loss of manganese during heat treatment.

Several calibrations were necessary before accurate measurements could be obtained from electron micrographs. Image magnifications were determined using a cross grating replica, and the rotation between the diffraction pattern and image was calculated from a superimposed exposure of an MoO_3 crystal and its diffraction pattern. Camera constants were determined for a number of lens settings using a thin gold foil.

TABLE A1.1

Element	Wt.%	Element	Wt.%
C	0.012	Al	<.003
Si	<.015	Co	<.003
Mn	<.01	Cu	0.01
P	0.005	Nb	<.004
S	0.008	Ti	<.003
Cr	<.02	V	<.004
Mo	<.01	N_2	0.002
Ni	<.01	O_2	0.005

TABLE A1.2

Element	Wt.%	Element	Wt.%
C	0.85	Al	<.004
Si	0.02	Co	<.01
Mn	13.6	Cu	0.04
P	0.011	Nb	0.01
S	0.032	Ti	<0.01
Cr	0.11	V	2.0
Mo	0.01	N_2	0.0035
Ni	0.02	O_2	0.0034

APPENDIX 2

TABULATION OF CSLs

Table A2, which lists all coincidence site relationships defining CSLs for which $\Sigma \lesssim 99$, was generated in order to facilitate the process of selecting CSLs to interpret the crystallographic data. The table was generated using the following equations given by Ranganathan (1966):

$$\text{(i)} \qquad \theta' = 2 \arctan \left(\frac{x}{y}\right)\sqrt{N}$$

and

$$\text{(ii)} \qquad \Sigma = x^2 + Ny^2$$

where θ' is the rotation angle about the axis [uvw],

$N = u^2 + v^2 + w^2$, and x and y are co-prime integer variables.

Since for CSLs generated between cubic crystal lattices Σ can only take odd values (Grimmer et al, 1974), if (ii) gave an even number it was divided by two repeatedly until an odd number was obtained.

For the sake of brevity, the table lists only coincidence site relationships corresponding to angular rotations about axes in the stereographic triangle [001] - [011] - [111]. It should be noted, however, that a similar list of θ' and Σ values would obtain if rotations were performed about crystallographically equivalent axes in any other stereographic triangle.

TABLE A.2

[uvw]	x y Σ θ′	x y Σ θ′	x y Σ θ′	x y Σ θ′	x y Σ θ′	x y Σ θ′
0 0 1	1 13 85 171.26	1 11 61 169.61	1 9 41 167.32	1 8 65 165.75	1 7 25 163.74	1 6 37 161.08
	1 5 13 157.38	2 9 85 154.94	3 13 89 154.01	1 4 17 151.93	3 11 65 149.49	2 7 53 148.11
	1 3 5 143.13	3 8 73 138.99	5 13 97 137.92	2 5 29 136.40	3 7 29 133.60	4 9 97 132.08
	5 11 73 131.11	1 2 5 126.87	5 9 53 121.89	4 7 65 120.51	3 5 17 118.07	5 8 89 115.99
	7 11 85 115.06	2 3 13 112.62	5 7 37 108.92	3 4 25 106.26	7 9 65 104.25	4 5 41 102.68
	5 6 61 100.39	6 7 85 98.80	7 6 85 81.20	6 5 61 79.61	5 4 41 77.32	9 7 65 75.75
	4 3 25 73.74	7 5 37 71.08	3 2 13 67.38	11 7 85 64.94	8 5 89 64.01	5 3 17 61.93
	7 4 65 59.49	9 5 53 58.11	2 1 5 53.13	11 5 73 48.89	9 4 97 47.92	7 3 29 46.40
	5 2 29 43.60	13 5 97 42.08	8 3 73 41.11	3 1 5 36.87	7 2 53 31.89	11 3 65 30.51
	4 1 17 28.07	13 3 89 25.99	9 2 85 25.06	5 1 13 22.62	6 1 37 18.92	7 1 25 16.26
	8 1 65 14.25	9 1 41 12.68	11 1 61 10.39	13 1 85 8.80		
0 1 1	1 7 99 168.46	1 6 73 166.56	1 5 51 163.90	2 9 83 162.14	1 4 33 159.95	2 7 51 157.16
	1 3 19 153.47	2 5 27 148.41	4 9 89 145.11	1 2 9 141.06	4 7 57 136.00	3 5 59 134.02
	2 3 11 129.52	3 4 41 124.12	4 5 33 121.01	5 6 97 118.98	6 7 67 117.56	1 1 3 109.47
	8 7 81 102.12	6 5 43 99.37	5 4 57 97.05	4 3 17 93.37	7 5 99 90.58	10 7 99 89.42
	3 2 17 86.63	8 5 57 82.95	5 3 43 80.63	7 4 81 77.88	2 1 3 70.53	7 3 67 62.44
	12 5 97 61.02	5 2 33 58.99	8 3 41 55.88	3 1 11 50.48	10 3 59 45.98	7 2 57 44.00
	4 1 9 38.94	9 2 89 34.89	5 1 27 31.59	6 1 19 26.53	7 1 51 22.84	8 1 33 20.05
	9 1 83 17.86	10 1 51 16.10	12 1 73 13.44	14 1 99 11.54		
0 1 2	0 1 5 180.00	1 5 63 169.78	1 4 81 167.24	1 3 23 163.04	1 2 21 154.79	3 5 67 149.96
	2 3 49 146.80	3 4 89 142.92	1 1 3 131.81	4 3 61 118.39	7 5 87 115.90	3 2 29 112.29
	5 3 35 106.60	2 1 9 96.38	7 3 47 87.56	5 2 45 83.62	3 1 7 73.40	7 2 69 65.15
	11 3 83 62.75	4 1 21 58.41	5 1 15 48.19	6 1 41 40.88	7 1 27 35.43	8 1 69 31.23
	9 1 43 27.91	11 1 63 22.98	13 1 87 19.52			
0 1 3	0 1 5 180.00	1 3 91 167.97	1 2 41 162.03	2 3 47 156.19	1 1 11 144.90	4 3 53 134.28
	3 2 49 129.25	2 1 7 115.38	5 2 65 103.34	8 3 77 99.72	3 1 19 93.02	10 3 95 86.98
	7 2 89 84.20	4 1 13 76.66	5 1 35 64.62	6 1 23 55.58	7 1 59 48.62	8 1 37 43.14
	9 1 91 38.72	10 1 55 35.10	12 1 77 29.53			
0 1 4	0 1 17 180.00	1 3 77 170.76	1 2 69 166.17	1 1 9 152.73	3 2 77 140.02	5 3 89 135.98
	2 1 21 128.25	5 2 93 117.54	3 1 13 107.92	4 1 33 91.74	5 1 21 79.02	6 1 53 68.99
	7 1 33 61.00	8 1 81 54.53	9 1 49 49.23	11 1 69 41.09	13 1 93 35.19	
0 1 5	0 1 13 180.00	1 1 27 157.81	2 1 15 137.17	3 1 35 119.06	4 1 21 103.77	5 1 51 91.12
	6 1 31 80.72	7 1 75 72.14	8 1 45 65.03	10 1 63 54.03	12 1 85 46.04	
0 1 6	0 1 37 180.00	1 1 19 161.33	2 1 41 143.60	3 1 23 127.50	4 1 53 113.34	5 1 31 101.16
	6 1 73 90.78	7 1 43 81.98	9 1 59 68.11	11 1 79 57.88		
0 1 7	0 1 25 180.00	1 1 51 163.90	2 1 27 148.41	3 1 59 134.02	4 1 33 121.01	5 1 75 109.47
	6 1 43 99.37	7 1 99 90.58	8 1 57 82.95	10 1 75 70.53	12 1 97 61.02	
0 1 8	0 1 65 180.00	1 1 33 165.86	2 1 69 152.14	3 1 37 139.18	4 1 81 127.22	5 1 45 116.39
	7 1 57 98.07	9 1 73 83.71	11 1 93 72.48			
0 1 9	0 1 41 180.00	1 1 83 167.40	2 1 43 155.09	3 1 91 143.34	4 1 49 132.34	6 1 59 112.94
	8 1 73 97.08	10 1 91 84.32				
0 1 10	1 1 51 168.64	3 1 55 146.76	5 1 63 127.10	7 1 75 110.28	9 1 91 96.31	
0 1 11	0 1 61 180.00	2 1 63 159.47	4 1 69 140.19	6 1 79 122.98	8 1 93 108.17	
0 1 12	1 1 73 170.51	3 1 77 152.02	5 1 85 134.90	7 1 97 119.66		
0 1 13	0 1 85 180.00	2 1 87 162.56	4 1 93 145.89			
0 1 14	1 1 99 171.85					
0 2 3	0 1 13 180.00	1 3 59 169.44	1 2 53 164.21	1 1 7 149.00	3 2 61 134.82	5 3 71 130.38
	2 1 17 121.97	7 3 83 116.18	5 2 77 110.53	3 1 11 100.48	4 1 29 84.06	5 1 19 71.59
	6 1 49 62.01	7 1 31 54.50	8 1 77 48.52	9 1 47 43.66	11 1 67 36.30	13 1 91 31.00
0 2 5	0 1 29 180.00	1 1 15 158.96	2 1 33 139.25	3 1 19 121.76	4 1 45 106.79	5 1 27 94.25
	6 1 65 83.82	7 1 39 75.14	8 1 93 67.89	9 1 55 61.79	11 1 75 52.17	13 1 99 45.00
0 2 7	0 1 53 180.00	1 1 27 164.36	2 1 57 149.28	3 1 31 135.21	4 1 69 122.43	5 1 39 111.04
	6 1 89 101.01	7 1 51 92.25	9 1 67 77.94	11 1 87 67.00		
0 2 9	0 1 85 180.00	1 1 43 167.62	2 1 89 155.52	3 1 47 143.95	5 1 55 123.06	7 1 67 105.58
	9 1 83 91.38					
0 2 11	1 1 63 169.78	3 1 67 149.96	5 1 75 131.81	7 1 87 115.90		
0 2 13	1 1 87 171.30	3 1 91 154.30	5 1 99 138.37			
0 3 4	0 1 25 180.00	1 1 13 157.38	2 1 29 136.40	3 1 17 118.07	4 1 41 102.68	5 1 25 90.00
	6 1 61 79.61	7 1 37 71.08	8 1 89 64.01	9 1 53 58.11	11 1 73 48.89	13 1 97 42.08
0 3 5	0 1 17 180.00	1 1 35 160.54	2 1 19 142.14	3 1 43 125.55	4 1 25 111.10	5 1 59 98.77
	6 1 35 88.36	7 1 83 79.59	8 1 49 72.17	10 1 67 60.49	12 1 89 51.83	

[uvw]	x y Σ θ′	x y Σ θ′	x y Σ θ′	x y Σ θ′	x y Σ θ′	x y Σ θ′
0 3 7	0 1 29 180.00 6 1 47 103.54	1 1 59 165.04 8 1 61 87.18	2 1 31 150.57 10 1 79 74.58	3 1 67 137.00	4 1 37 124.58	5 1 83 113.43
0 3 8	0 1 73 180.00 7 1 61 101.35	1 1 37 166.65 9 1 77 87.02	2 1 77 153.65 11 1 97 75.67	3 1 41 141.31	4 1 89 129.83	5 1 49 119.33
0 3 10	1 1 55 169.06	3 1 59 147.94	5 1 67 128.82	7 1 79 112.32	9 1 95 98.47	
0 3 11	0 1 65 180.00	2 1 67 160.10	4 1 73 141.34	6 1 83 124.49	8 1 97 109.89	
0 3 13	0 1 89 180.00	2 1 91 162.95	4 1 97 146.62			
0 4 5	0 1 41 180.00 6 1 77 93.72	1 1 21 162.25 7 1 45 84.90	2 1 45 145.31 9 1 61 70.86	3 1 25 129.79 11 1 81 60.41	4 1 57 116.01	5 1 33 104.03
0 4 7	0 1 65 180.00 7 1 57 98.07	1 1 33 165.86 9 1 73 83.71	2 1 69 152.14 11 1 93 72.48	3 1 37 139.18	4 1 81 127.22	5 1 45 116.39
0 4 9	0 1 97 180.00	1 1 49 168.40	3 1 53 146.12	5 1 61 126.17	7 1 73 109.19	9 1 89 95.16
0 4 11	1 1 69 170.23	3 1 73 151.25	5 1 81 133.74	7 1 93 118.24		
0 4 13	1 1 93 171.59	3 1 97 155.12				
0 5 6	0 1 61 180.00 6 1 97 104.94	1 1 31 165.41 7 1 55 96.26	2 1 65 151.27 9 1 71 81.90	3 1 35 137.98 11 1 91 70.75	4 1 77 125.76	5 1 43 114.75
0 5 7	0 1 37 180.00 6 1 55 110.21	1 1 75 166.74 8 1 69 94.16	2 1 39 153.82 10 1 87 81.41	3 1 83 141.55	4 1 45 130.12	5 1 99 119.67
0 5 8	0 1 89 180.00 9 1 85 92.70	1 1 45 167.90	2 1 93 156.06	3 1 49 144.72	5 1 57 124.15	7 1 69 106.85
0 5 9	0 1 53 180.00	2 1 55 158.01	4 1 61 137.54	6 1 71 119.54	8 1 85 104.30	
0 5 11	0 1 73 180.00	2 1 75 161.20	4 1 81 143.37	6 1 91 127.19		
0 5 12	1 1 85 171.20	3 1 89 154.01	5 1 97 137.92			
0 5 13	0 1 97 180.00	2 1 99 163.66				
0 6 7	0 1 85 180.00 9 1 83 91.38	1 1 43 167.62	2 1 89 155.52	3 1 47 143.95	5 1 55 123.06	7 1 67 105.58
0 6 11	1 1 79 170.87	3 1 83 153.07	5 1 91 136.49			
0 7 8	1 1 57 169.25	3 1 61 148.48	5 1 69 129.62	7 1 81 113.27	9 1 97 99.49	
0 7 9	0 1 65 180.00	2 1 67 160.10	4 1 73 141.34	6 1 83 124.49	8 1 97 109.89	
0 7 10	1 1 75 170.63	3 1 79 152.38	5 1 87 135.45	7 1 99 120.33		
0 7 11	0 1 85 180.00	2 1 87 162.56	4 1 93 145.89			
0 7 12	1 1 97 171.77					
0 8 9	1 1 73 170.51	3 1 77 152.02	5 1 85 134.90	7 1 97 119.66		
0 8 11	1 1 93 171.59	3 1 97 155.12				
0 9 10	1 1 91 171.50	3 1 95 154.86				
1 1 1	0 1 3 180.00 3 11 93 162.10 5 9 67 144.43 4 5 91 130.42 3 2 21 98.21 2 1 7 81.79 8 3 91 66.01 13 3 49 43.57 7 1 13 27.80 17 1 73 11.64	1 11 91 173.99 1 3 7 158.21 3 5 21 141.79 11 9 91 109.58 11 7 67 95.57 15 7 93 77.90 3 1 3 60.00 9 2 93 42.10 8 1 67 24.43 19 1 91 10.42	1 9 61 172.66 2 5 79 153.99 2 3 31 137.90 5 4 73 108.36 5 3 13 92.20 11 5 49 76.43 17 5 91 53.99 5 1 7 38.21 9 1 21 21.79	1 7 37 170.57 3 7 39 152.20 5 7 43 135.18 9 7 57 106.83 7 4 97 89.41 7 3 19 73.17 7 2 61 52.66 17 3 79 33.99 11 1 31 17.90	1 5 19 166.83 5 11 97 150.59 3 4 57 133.17 4 3 43 104.82 9 5 39 87.80 5 2 37 69.43 11 3 37 50.57 6 1 39 32.20 13 1 43 15.18	1 4 49 163.57 1 2 13 147.80 7 9 73 131.64 7 5 31 102.10 13 7 79 86.01 13 5 61 67.34 4 1 19 46.83 19 3 97 30.59 15 1 57 13.17
1 1 2	0 1 3 180.00 4 5 83 143.83 2 1 5 101.54 4 1 11 62.96 10 1 53 27.53	1 4 97 168.34 1 1 7 135.58 5 2 49 88.83 5 1 31 52.20 12 1 75 23.07	1 3 55 164.50 6 5 93 127.80 8 3 59 65.14 6 1 21 44.42	2 5 77 161.45 4 3 35 122.88 3 1 15 78.46 7 1 55 38.57	1 2 25 156.93 3 2 33 117.04 10 3 77 72.62 8 1 35 34.05	2 3 29 149.55 5 3 79 111.54 7 2 73 69.97 9 1 97 30.45

[uvw]	x y Σ θ′	x y Σ θ′	x y Σ θ′	x y Σ θ′	x y Σ θ′	x y Σ θ′
1 1 3	0 1 11 180.00	1 5 69 173.10	1 3 25 168.52	1 2 45 162.85	3 5 71 159.49	1 1 3 146.44
	7 5 81 134.23	3 2 53 131.33	5 3 31 126.64	9 5 89 123.02	2 1 15 117.82	11 5 99 112.89
	7 3 37 109.75	5 2 69 105.98	3 1 5 95.74	7 2 93 86.92	11 3 55 84.26	4 1 27 79.33
	13 3 67 74.86	5 1 9 67.11	17 3 97 60.68	6 1 47 57.97	7 1 15 50.70	8 1 75 45.04
	9 1 23 40.46	11 1 33 33.56	13 1 45 28.62	15 1 59 24.94	17 1 75 22.08	19 1 93 19.60
1 1 4	0 1 9 180.00	1 2 73 166.56	2 3 83 162.14	1 1 19 153.47	4 3 89 145.11	3 2 31 141.06
	2 1 11 129.52	5 2 97 118.98	3 1 27 109.47	4 1 17 93.37	5 1 43 80.63	6 1 27 70.53
	7 1 67 62.44	8 1 41 55.88	9 1 99 50.48	10 1 59 45.98	12 1 81 38.94	
1 1 5	0 1 27 180.00	1 3 61 172.66	1 1 7 158.21	5 3 67 144.43	2 1 31 137.90	7 3 73 131.64
	3 1 9 120.00	11 3 91 109.58	4 1 43 104.82	5 1 13 92.20	6 1 63 81.79	7 1 19 73.17
	8 1 91 66.01	9 1 27 60.00	11 1 37 50.57	13 1 49 43.57	15 1 63 38.21	17 1 79 33.99
	19 1 97 30.59					
1 1 6	0 1 19 180.00	1 1 39 161.57	2 1 21 144.05	3 1 47 128.10	4 1 27 114.04	5 1 63 101.91
	6 1 37 91.55	7 1 87 82.74	8 1 51 75.23	10 1 69 63.30	12 1 91 54.38	
1 1 7	0 1 51 180.00	1 1 13 164.06	2 1 55 148.71	3 1 15 134.43	4 1 67 121.49	5 1 19 110.01
	6 1 87 99.93	7 1 25 91.15	9 1 33 76.86	11 1 43 65.98	13 1 55 57.56	15 1 69 50.92
	17 1 85 45.57					
1 1 8	0 1 33 180.00	1 1 67 165.97	2 1 35 152.34	3 1 75 139.46	4 1 41 127.57	5 1 91 116.78
	6 1 51 107.10	8 1 65 90.88	10 1 83 78.18			
1 1 9	0 1 83 180.00	1 1 21 167.47	2 1 87 155.24	3 1 23 143.55	4 1 99 132.59	5 1 27 122.48
	7 1 33 104.93	9 1 41 90.70	11 1 51 79.26	13 1 63 70.05	15 1 77 62.55	17 1 93 56.37
1 1 10	0 1 51 180.00	2 1 53 157.60	4 1 59 136.79	6 1 69 118.57	8 1 83 103.23	
1 1 11	1 1 31 169.70	3 1 33 149.73	5 1 37 131.46	7 1 43 115.48	9 1 51 101.88	11 1 61 90.47
	13 1 73 80.94	15 1 87 72.96				
1 1 12	0 1 73 180.00	2 1 75 161.20	4 1 81 143.37	6 1 91 127.19		
1 1 13	1 1 43 171.25	3 1 45 154.16	5 1 49 138.15	7 1 55 123.68	9 1 63 110.92	11 1 73 99.86
	13 1 85 90.34	15 1 99 82.16				
1 1 14	0 1 99 180.00					
1 1 15	1 1 57 172.41	3 1 59 157.48	5 1 63 143.28	7 1 69 130.16	9 1 77 118.30	11 1 87 107.73
	13 1 99 98.42					
1 1 17	1 1 73 173.29	3 1 75 160.05	5 1 79 147.33	7 1 85 135.38	9 1 93 124.37	
1 1 19	1 1 91 173.99	3 1 93 162.10	5 1 97 150.59			
1 2 2	0 1 9 180.00	1 3 41 167.32	1 2 37 161.08	2 3 85 154.94	1 1 5 143.13	4 3 97 132.08
	3 2 45 126.87	5 3 53 121.89	2 1 13 112.62	7 3 65 104.25	5 2 61 100.39	3 1 9 90.00
	7 2 85 81.20	4 1 25 73.74	5 1 17 61.93	6 1 45 53.13	7 1 29 46.40	8 1 73 41.11
	9 1 45 36.87	11 1 65 30.51	13 1 89 25.99			
1 2 3	0 1 7 180.00	1 2 57 164.78	2 3 65 159.79	1 1 15 150.07	4 3 71 140.77	3 2 65 136.31
	2 1 9 123.75	5 2 81 112.50	8 3 95 109.05	3 1 23 102.56	4 1 15 86.18	5 1 39 73.62
	6 1 25 63.90	7 1 63 56.25	8 1 39 50.13	9 1 95 45.15	10 1 57 41.03	12 1 79 34.64
1 2 4	0 1 21 180.00	1 3 95 171.68	1 2 85 167.55	1 1 11 155.38	3 2 93 143.75	2 1 25 132.84
	3 1 15 113.58	4 1 37 97.77	5 1 23 85.01	6 1 57 74.74	7 1 35 66.42	8 1 85 59.61
	9 1 51 53.97	11 1 71 45.23	13 1 95 38.84			
1 2 5	0 1 15 180.00	1 1 31 159.31	2 1 17 139.88	3 1 39 122.58	4 1 23 107.72	5 1 55 95.22
	6 1 33 84.78	7 1 79 76.08	8 1 47 68.80	10 1 65 57.42	12 1 87 49.07	
1 2 6	0 1 41 180.00	1 1 21 162.25	2 1 45 145.31	3 1 25 129.79	4 1 57 116.01	5 1 33 104.03
	6 1 77 93.72	7 1 45 84.90	9 1 61 70.86	11 1 81 60.41		
1 2 7	0 1 27 180.00	1 1 55 164.50	2 1 29 149.55	3 1 63 135.58	4 1 35 122.88	5 1 79 111.54
	6 1 45 101.54	8 1 59 85.14	10 1 77 72.62	12 1 99 62.96		
1 2 8	0 1 69 180.00	1 1 35 166.27	2 1 73 152.92	3 1 39 140.28	4 1 85 128.57	5 1 47 117.91
	7 1 59 99.76	9 1 75 85.41	11 1 95 74.12			
1 2 9	0 1 43 180.00	1 1 87 167.69	2 1 45 155.66	3 1 95 144.15	4 1 51 133.34	6 1 61 114.19
	8 1 75 98.43	10 1 93 85.68				
1 2 10	1 1 53 166.85	3 1 57 147.36	5 1 65 127.98	7 1 77 111.32	9 1 93 97.41	
1 2 11	0 1 63 180.00	2 1 65 159.79	4 1 71 140.77	6 1 81 123.75	8 1 95 109.05	
1 2 12	1 1 75 170.63	3 1 79 152.38	5 1 87 135.45	7 1 99 120.33		

[uvw]	x y Σ θ'	x y Σ θ'	x y Σ θ'	x y Σ θ'	x y Σ θ'	x y Σ θ'
1 2 13	0 1 87 180.00	2 1 89 162.76	4 1 95 146.26			
1 3 3	0 1 19 180.00	1 3 43 171.25	1 2 77 166.91	1 1 5 154.16	3 2 85 142.02	5 3 49 138.15
	2 1 23 130.71	7 3 55 123.68	3 1 7 110.92	11 3 73 99.86	4 1 35 94.92	13 3 85 90.34
	5 1 11 82.16	6 1 55 72.00	7 1 17 63.82	8 1 83 57.17	9 1 25 51.68	11 1 35 43.23
	13 1 47 37.07	15 1 61 32.41	17 1 77 28.76	19 1 95 25.84		
1 3 4	0 1 13 180.00	1 1 27 157.81	2 1 15 137.17	3 1 35 119.06	4 1 21 103.77	5 1 51 91.12
	6 1 31 80.72	7 1 75 72.14	8 1 45 65.03	10 1 63 54.03	12 1 85 46.04	
1 3 5	0 1 35 180.00	1 3 79 173.55	1 1 9 160.81	5 3 85 148.53	2 1 39 142.64	7 3 91 136.95
	3 1 11 126.22	4 1 51 111.87	5 1 15 99.59	6 1 71 89.19	7 1 21 80.41	8 1 99 72.97
	9 1 29 66.64	11 1 39 56.54	13 1 51 48.94	15 1 65 43.05	17 1 81 38.38	19 1 99 34.59
1 3 6	0 1 23 180.00	1 1 47 163.23	2 1 25 147.14	3 1 55 132.28	4 1 31 118.94	5 1 71 107.20
	6 1 41 97.00	7 1 95 88.19	8 1 55 80.58	10 1 73 68.29	12 1 95 58.95	
1 3 7	0 1 59 180.00	1 1 15 165.16	2 1 63 150.81	3 1 17 137.33	4 1 75 124.98	5 1 21 113.88
	6 1 95 104.01	7 1 27 95.31	9 1 35 80.96	11 1 45 69.85	13 1 57 61.15	15 1 71 54.23
	17 1 87 48.63					
1 3 8	0 1 37 180.00	1 1 75 166.74	2 1 39 153.82	3 1 83 141.55	4 1 45 130.12	5 1 99 119.67
	6 1 55 110.21	8 1 69 94.16	10 1 87 81.41			
1 3 9	0 1 91 180.00	1 1 23 168.03	2 1 95 156.32	3 1 25 145.08	5 1 29 124.68	7 1 35 107.46
	9 1 43 93.33	11 1 53 81.86	13 1 65 72.54	15 1 79 64.91	17 1 95 58.60	
1 3 10	0 1 55 180.00	2 1 57 158.41	4 1 63 138.25	6 1 73 120.45	8 1 87 105.33	
1 3 11	1 1 33 170.01	3 1 35 150.63	5 1 39 132.80	7 1 45 117.10	9 1 53 103.64	11 1 63 92.27
	13 1 75 82.72	15 1 89 74.69				
1 3 12	0 1 77 180.00	2 1 79 161.69	4 1 85 144.27	6 1 95 128.39		
1 3 13	1 1 45 171.45	3 1 47 154.72	5 1 51 139.02	7 1 57 124.76	9 1 65 112.14	11 1 75 101.15
	13 1 87 91.65					
1 3 15	1 1 59 172.54	3 1 61 157.85	5 1 65 143.87	7 1 71 130.91	9 1 79 119.17	11 1 89 108.68
1 3 17	1 1 75 173.38	3 1 77 160.31	5 1 81 147.74	7 1 87 135.92	9 1 95 125.01	
1 3 19	1 1 93 174.06	3 1 95 162.29	5 1 99 150.90			
1 4 4	0 1 33 180.00	1 1 17 160.25	2 1 37 141.61	3 1 21 124.85	4 1 49 110.30	5 1 29 97.93
	6 1 69 87.51	7 1 41 78.75	8 1 97 71.36	9 1 57 65.10	11 1 77 55.15	
1 4 5	0 1 21 180.00	1 1 43 162.46	2 1 23 145.70	3 1 51 130.32	4 1 29 116.63	5 1 67 104.70
	6 1 39 94.41	7 1 91 85.59	8 1 53 78.02	10 1 71 65.89	12 1 93 56.74	
1 4 6	0 1 53 180.00	1 1 27 164.36	2 1 57 149.28	3 1 31 135.21	4 1 69 122.43	5 1 39 111.04
	6 1 89 101.01	7 1 51 92.25	9 1 67 77.94	11 1 87 67.00		
1 4 7	0 1 33 180.00	1 1 67 165.97	2 1 35 152.34	3 1 75 139.46	4 1 41 127.57	5 1 91 116.78
	6 1 51 107.10	8 1 65 90.88	10 1 83 78.18			
1 4 8	0 1 81 180.00	1 1 41 167.32	2 1 85 154.94	3 1 45 143.13	4 1 97 132.08	5 1 53 121.89
	7 1 65 104.25	9 1 81 90.00				
1 4 9	0 1 49 180.00	1 1 99 168.46	2 1 51 157.16	4 1 57 136.00	6 1 67 117.56	8 1 81 102.12
	10 1 99 89.42					
1 4 10	1 1 59 169.44	3 1 63 149.00	5 1 71 130.38	7 1 83 114.18	9 1 99 100.48	
1 4 11	0 1 69 180.00	2 1 71 160.68	4 1 77 142.39	6 1 87 125.89		
1 4 12	1 1 81 170.99	3 1 85 153.40	5 1 93 136.99			
1 4 13	0 1 93 180.00	2 1 95 163.31				
1 5 5	0 1 51 180.00	1 1 13 164.06	2 1 55 148.71	3 1 15 134.43	4 1 67 121.49	5 1 19 110.01
	6 1 87 99.93	7 1 25 91.15	9 1 33 76.86	11 1 43 65.98	13 1 55 57.56	15 1 69 50.92
	17 1 85 45.57					
1 5 6	0 1 31 180.00	1 1 63 165.52	2 1 33 151.50	3 1 71 138.29	4 1 39 126.14	5 1 87 115.17
	6 1 49 105.39	8 1 63 89.09	10 1 81 76.43			
1 5 7	0 1 75 180.00	1 1 19 166.83	2 1 79 153.99	3 1 21 141.79	4 1 91 130.42	5 1 25 120.00
	7 1 31 102.10	9 1 39 87.80	11 1 49 76.43	13 1 61 67.34	15 1 75 60.00	17 1 91 53.99

[uvw]	x y Σ θ′	x y Σ θ′	x y Σ θ′	x y Σ θ′	x y Σ θ′	x y Σ θ′
1 5 8	0 1 45 180.00 8 1 77 99.72	1 1 91 167.97 10 1 95 86.98	2 1 47 156.19	3 1 99 144.90	4 1 53 134.28	6 1 63 115.38
1 5 9	1 1 27 168.96 13 1 69 77.02	3 1 29 147.65 15 1 83 69.18	5 1 33 128.40 17 1 99 62.64	7 1 39 111.83	9 1 47 97.95	11 1 57 86.48
1 5 10	0 1 63 180.00	2 1 65 159.79	4 1 71 140.77	6 1 81 123.75	8 1 95 109.05	
1 5 11	1 1 37 170.57 13 1 79 86.01	3 1 39 152.20 15 1 93 77.90	5 1 43 135.18	7 1 49 120.00	9 1 57 106.83	11 1 67 95.57
1 5 12	0 1 85 180.00	2 1 87 162.56	4 1 93 145.89			
1 5 13	1 1 49 171.81 13 1 91 94.10	3 1 51 155.75	5 1 55 140.60	7 1 61 126.75	9 1 69 114.40	11 1 79 103.54
1 5 15	1 1 63 172.78	3 1 65 158.56	5 1 69 144.97	7 1 75 132.32	9 1 83 120.80	11 1 93 110.45
1 5 17	1 1 79 173.55	3 1 81 160.81	5 1 85 148.53	7 1 91 136.95	9 1 99 126.22	
1 5 19	1 1 97 174.18	3 1 99 162.66				
1 6 6	0 1 73 180.00 7 1 61 101.35	1 1 37 166.65 9 1 77 87.02	2 1 77 153.65 11 1 97 75.67	3 1 41 141.31	4 1 89 129.83	5 1 49 119.33
1 6 7	0 1 43 180.00 8 1 75 98.43	1 1 87 167.69 10 1 93 85.68	2 1 45 155.66	3 1 95 144.15	4 1 51 133.34	6 1 61 114.19
1 6 8	1 1 51 168.64	3 1 55 146.76	5 1 63 127.10	7 1 75 110.28	9 1 91 96.31	
1 6 9	0 1 59 180.00	2 1 61 159.14	4 1 67 139.57	6 1 77 122.17	8 1 91 107.26	
1 6 10	1 1 69 170.23	3 1 73 151.25	5 1 81 133.74	7 1 93 118.24		
1 6 11	0 1 79 180.00	2 1 81 161.92	4 1 87 144.70	6 1 97 128.97		
1 6 12	1 1 91 171.50	3 1 95 154.86				
1 7 7	0 1 99 180.00 11 1 55 84.26	1 1 25 168.52 13 1 67 74.86	3 1 27 146.44 15 1 81 67.11	5 1 31 126.64 17 1 97 60.68	7 1 37 109.75	9 1 45 95.74
1 7 8	0 1 57 180.00	2 1 59 158.78	4 1 65 138.92	6 1 75 121.33	8 1 89 106.31	
1 7 9	1 1 33 170.01 13 1 75 82.72	3 1 35 150.63 15 1 89 74.69	5 1 39 132.80	7 1 45 117.10	9 1 53 103.64	11 1 63 92.27
1 7 10	0 1 75 180.00	2 1 77 161.45	4 1 83 143.83	6 1 93 127.80		
1 7 11	1 1 43 171.25 13 1 85 90.34	3 1 45 154.16 15 1 99 82.16	5 1 49 138.15	7 1 55 123.68	9 1 63 110.92	11 1 73 99.86
1 7 12	0 1 97 180.00	2 1 99 163.66				
1 7 13	1 1 55 172.27 13 1 97 97.40	3 1 57 157.08	5 1 61 142.66	7 1 67 129.37	9 1 75 117.39	11 1 85 106.75
1 7 15	1 1 69 173.10	3 1 71 159.49	5 1 75 146.44	7 1 81 134.23	9 1 89 123.02	11 1 99 112.89
1 7 17	1 1 85 173.78	3 1 87 161.49	5 1 91 149.61	7 1 97 138.37		
1 8 8	1 1 65 169.94	3 1 69 150.41	5 1 77 132.48	7 1 89 116.71		
1 8 9	0 1 73 180.00	2 1 75 161.20	4 1 81 143.37	6 1 91 127.19		
1 8 10	1 1 83 171.10	3 1 87 153.71	5 1 95 137.46			
1 8 11	0 1 93 180.00	2 1 95 163.31				
1 9 9	1 1 41 171.04 13 1 83 88.96	3 1 43 153.55 15 1 97 80.81	5 1 47 137.23	7 1 53 122.53	9 1 61 109.64	11 1 71 98.50
1 9 10	0 1 91 180.00	2 1 93 163.13	4 1 99 146.97			
1 9 11	1 1 51 171.97 13 1 93 95.24	3 1 53 156.22	5 1 57 141.32	7 1 63 127.67	9 1 71 115.44	11 1 81 104.66

[uvw]	x y Σ θ′	x y Σ θ′	x y Σ θ′	x y Σ θ′	x y Σ θ′	x y Σ θ′
1 9 13	1 1 63 172.78	3 1 65 158.56	5 1 69 144.97	7 1 75 132.32	9 1 83 120.80	11 1 93 110.45
1 9 15	1 1 77 173.47	3 1 79 160.57	5 1 83 148.15	7 1 89 136.45	9 1 97 125.62	
1 9 17	1 1 93 174.06	3 1 95 162.29	5 1 99 150.90			
1 11 11	1 1 61 172.66	3 1 63 158.21	5 1 67 144.43	7 1 73 131.64	9 1 81 120.00	11 1 91 109.58
1 11 13	1 1 73 173.29	3 1 75 160.05	5 1 79 147.33	7 1 85 135.38	9 1 93 124.37	
1 11 15	1 1 87 173.85	3 1 89 161.70	5 1 93 149.95	7 1 99 138.81		
1 13 13	1 1 85 173.78	3 1 87 161.49	5 1 91 149.61	7 1 97 138.37		
1 13 15	1 1 99 174.24					
2 2 3	0 1 17 180.00 2 1 21 128.25 7 1 33 61.00	1 3 77 170.76 5 2 93 117.54 8 1 81 54.53	1 2 69 166.17 3 1 13 107.92 9 1 49 49.23	1 1 9 152.73 4 1 33 91.74 11 1 69 41.09	3 2 77 140.02 5 1 21 79.02 13 1 93 35.19	5 3 89 135.98 6 1 53 68.99
2 2 5	0 1 33 180.00 6 1 69 87.51	1 1 17 160.25 7 1 41 78.75	2 1 37 141.61 8 1 97 71.36	3 1 21 124.85 9 1 57 65.10	4 1 49 110.30 11 1 77 55.15	5 1 29 97.93
2 2 7	0 1 57 180.00 6 1 93 103.05	1 1 29 164.91 7 1 53 94.33	2 1 61 150.33 9 1 69 79.98	3 1 33 136.66 11 1 89 68.93	4 1 73 124.17	5 1 41 112.97
2 2 9	0 1 89 180.00 9 1 85 92.70	1 1 45 167.90	2 1 93 156.06	3 1 49 144.72	5 1 57 124.15	7 1 69 106.85
2 2 11	1 1 65 169.94	3 1 69 150.41	5 1 77 132.48	7 1 89 116.71		
2 2 13	1 1 89 171.40	3 1 93 154.59				
2 3 3	0 1 11 180.00 4 1 19 99.08 12 1 83 42.70	1 2 89 167.83 5 1 47 86.34	1 1 23 155.93 6 1 29 76.03	3 2 97 144.53 7 1 71 67.65	2 1 13 133.81 8 1 43 60.77	3 1 31 114.79 10 1 61 50.26
2 3 4	0 1 29 180.00 6 1 65 83.82	1 1 15 158.96 7 1 39 75.14	2 1 33 139.25 8 1 93 67.89	3 1 19 121.76 9 1 55 61.79	4 1 45 106.79 11 1 75 52.17	5 1 27 94.25 13 1 99 45.00
2 3 5	0 1 19 180.00 6 1 37 91.55	1 1 39 161.57 7 1 87 82.74	2 1 21 144.05 8 1 51 75.23	3 1 47 128.10 10 1 69 63.30	4 1 27 114.04 12 1 91 54.38	5 1 63 101.91
2 3 6	0 1 49 180.00 6 1 85 98.80	1 1 25 163.74 7 1 49 90.00	2 1 53 148.11 9 1 65 75.75	3 1 29 133.60 11 1 85 64.94	4 1 65 120.51	5 1 37 108.92
2 3 7	0 1 31 180.00 6 1 49 105.39	1 1 63 165.52 8 1 63 89.09	2 1 33 151.50 10 1 81 76.43	3 1 71 138.29	4 1 39 126.14	5 1 47 115.17
2 3 8	0 1 77 180.00 7 1 63 102.84	1 1 39 167.00 9 1 79 88.55	2 1 81 154.32 11 1 99 77.16	3 1 43 142.25	4 1 93 130.99	5 1 51 120.65
2 3 9	0 1 47 180.00 10 1 97 88.23	1 1 95 168.22	2 1 49 156.69	4 1 55 135.16	6 1 65 116.50	8 1 79 100.95
2 3 10	1 1 57 169.25	3 1 61 148.48	5 1 69 129.62	7 1 81 113.27	9 1 97 99.49	
2 3 11	0 1 67 180.00	2 1 69 160.40	4 1 75 141.88	6 1 85 125.20	8 1 99 110.70	
2 3 12	1 1 79 170.87	3 1 83 153.07	5 1 91 136.49			
2 3 13	0 1 91 180.00	2 1 93 163.13	4 1 99 146.97			
2 4 5	0 1 45 180.00 6 1 81 96.38	1 1 23 163.04 7 1 47 87.96	2 1 49 146.80 9 1 63 73.40	3 1 27 131.81 11 1 83 62.75	4 1 61 118.39	5 1 35 106.60
2 4 7	0 1 69 180.00 7 1 59 99.76	1 1 35 166.27 9 1 75 85.41	2 1 73 152.92 11 1 95 74.12	3 1 39 140.28	4 1 85 128.57	5 1 47 117.91
2 4 9	1 1 51 168.64	3 1 55 146.76	5 1 63 127.10	7 1 75 110.28	9 1 91 96.31	
2 4 11	1 1 71 170.37	3 1 75 151.64	5 1 83 134.33	7 1 95 118.96		
2 4 13	1 1 95 171.60	3 1 99 155.38				
2 5 5	0 1 27 180.00 6 1 45 101.54	1 1 55 164.50 8 1 59 85.14	2 1 29 149.55 10 1 77 72.62	3 1 63 135.58 12 1 99 62.96	4 1 35 122.88	5 1 79 111.54

[uvw]	x y Σ θ′	x y Σ θ′	x y Σ θ′	x y Σ θ′	x y Σ θ′	x y Σ θ′
2 5 6	0 1 65 180.00 7 1 57 98.07	1 1 33 165.86 9 1 73 83.71	2 1 69 152.14 11 1 93 72.48	3 1 37 139.18	4 1 81 127.22	5 1 45 116.39
2 5 7	0 1 39 180.00 6 1 71 95.66	1 1 79 167.08 10 1 89 82.90	2 1 41 154.48	3 1 87 142.48	4 1 47 131.27	6 1 57 111.62
2 5 8	0 1 93 180.00 9 1 87 93.95	1 1 47 168.16	2 1 97 156.57	3 1 51 145.44	5 1 59 125.19	7 1 71 108.05
2 5 9	0 1 55 180.00	2 1 57 158.41	4 1 63 138.25	6 1 73 120.45	8 1 87 105.33	
2 5 10	1 1 65 169.94	3 1 69 150.41	5 1 77 132.48	7 1 89 116.71		
2 5 11	0 1 75 180.00	2 1 77 161.45	4 1 83 143.83	6 1 93 127.80		
2 5 12	1 1 87 171.30	3 1 91 154.30	5 1 99 138.37			
2 5 13	0 1 99 180.00					
2 6 7	0 1 89 180.00 9 1 85 92.70	1 1 45 167.90	2 1 93 156.06	3 1 49 144.72	5 1 57 124.15	7 1 69 106.85
2 6 9	1 1 61 169.61	3 1 65 149.49	5 1 73 131.11	7 1 85 115.06		
2 6 11	1 1 81 170.99	3 1 85 153.40	5 1 93 136.99			
2 7 7	0 1 51 180.00	2 1 53 157.60	4 1 59 136.79	6 1 69 118.57	8 1 83 103.23	
2 7 8	1 1 59 169.44	3 1 63 149.00	5 1 71 130.38	7 1 83 114.18	9 1 99 100.48	
2 7 9	0 1 67 180.00	2 1 69 160.40	4 1 75 141.88	6 1 85 125.20	8 1 99 110.70	
2 7 10	1 1 77 170.76	3 1 81 152.73	5 1 89 135.98			
2 7 11	0 1 87 180.00	2 1 89 162.76	4 1 95 146.26			
2 7 12	1 1 99 171.85					
2 8 9	1 1 75 170.63	3 1 79 152.38	5 1 87 135.45	7 1 99 120.33		
2 8 11	1 1 95 171.68	3 1 99 155.38				
2 9 9	0 1 83 180.00	2 1 85 162.35	4 1 91 145.51			
2 9 10	1 1 93 171.59	3 1 97 155.12				
3 3 4	0 1 17 180.00 6 1 35 88.36	1 1 35 160.54 7 1 83 79.59	2 1 19 142.14 8 1 49 72.17	3 1 43 125.55 10 1 67 60.49	4 1 25 111.10 12 1 89 51.83	5 1 59 98.77
3 3 5	0 1 43 180.00 5 1 17 105.35 15 1 67 47.23	1 3 97 174.18 6 1 79 95.08 17 1 83 42.19	1 1 11 162.66 7 1 23 86.26	2 1 47 146.08 9 1 31 72.15	3 1 13 130.83 11 1 41 61.60	4 1 59 117.23 13 1 53 53.53
3 3 7	0 1 67 180.00 7 1 29 98.93	1 1 17 166.07 9 1 37 84.57	2 1 71 152.54 11 1 47 73.31	3 1 19 139.74 13 1 59 64.39	4 1 83 127.91 15 1 73 57.24	5 1 23 117.16 17 1 89 51.42
3 3 8	0 1 41 180.00 8 1 73 97.08	1 1 83 167.40 10 1 91 84.32	2 1 43 155.09	3 1 91 143.34	4 1 49 132.34	6 1 59 112.94
3 3 10	0 1 59 180.00	2 1 61 159.14	4 1 67 139.57	6 1 77 122.17	8 1 91 107.26	
3 3 11	1 1 35 170.30 13 1 77 84.41	3 1 37 151.45 15 1 91 76.33	5 1 41 134.04	7 1 47 118.60	9 1 55 105.29	11 1 65 93.97
3 3 13	1 1 47 171.64 13 1 89 92.90	3 1 49 155.25	5 1 53 139.83	7 1 59 125.79	9 1 67 113.30	11 1 77 102.37
3 3 17	1 1 77 173.47	3 1 79 160.57	5 1 83 148.15	7 1 89 136.45	9 1 97 125.62	
3 3 19	1 1 95 174.12	3 1 97 162.48				
3 4 4	0 1 41 180.00 6 1 77 93.72	1 1 21 162.25 7 1 45 84.90	2 1 45 145.31 9 1 61 70.86	3 1 25 129.79 11 1 81 60.41	4 1 57 116.01	5 1 33 104.03
3 4 5	0 1 25 180.00 6 1 43 99.37	1 1 51 163.90 7 1 99 90.58	2 1 27 148.41 8 1 57 82.95	3 1 59 134.02 10 1 75 70.53	4 1 33 121.01 12 1 97 61.02	5 1 75 109.47

[uvw]	x y Σ θ′	x y Σ θ′	x y Σ θ′	x y Σ θ′	x y Σ θ′	x y Σ θ′
3 4 6	0 1 61 180.00 6 1 97 104.94	1 1 31 165.41 7 1 55 96.26	2 1 65 151.27 9 1 71 81.90	3 1 35 137.98 11 1 91 70.75	4 1 77 125.76	5 1 43 114.75
3 4 7	0 1 37 180.00 6 1 55 110.21	1 1 75 166.74 8 1 69 94.16	2 1 39 153.82 10 1 87 81.41	3 1 83 141.55	4 1 45 130.12	5 1 99 119.67
3 4 8	0 1 89 180.00 9 1 85 92.70	1 1 45 167.90	2 1 93 156.06	3 1 49 144.72	5 1 57 124.15	7 1 69 106.85
3 4 9	0 1 53 180.00	2 1 55 158.01	4 1 61 137.54	6 1 71 119.54	8 1 85 104.30	
3 4 10	1 1 63 169.76	3 1 67 149.96	5 1 75 131.81	7 1 87 115.90		
3 4 11	0 1 73 180.00	2 1 75 161.20	4 1 81 143.37	6 1 91 127.19		
3 4 12	1 1 85 171.20	3 1 89 154.01	5 1 97 137.92			
3 4 13	0 1 97 180.00	2 1 99 163.66				
3 5 5	0 1 59 180.00 6 1 95 104.01 17 1 87 48.63	1 1 15 169.16 7 1 27 95.31	2 1 63 150.81 9 1 35 80.96	3 1 17 137.33 11 1 45 69.85	4 1 75 124.98 13 1 57 61.15	5 1 21 113.88 15 1 71 54.23
3 5 6	0 1 35 180.00 6 1 53 108.71	1 1 71 166.37 8 1 67 92.57	2 1 37 153.11 10 1 85 79.84	3 1 79 140.55	4 1 43 128.90	5 1 95 118.27
3 5 7	0 1 83 180.00 7 1 33 104.93	1 1 21 167.47 9 1 41 90.70	2 1 87 155.24 11 1 51 79.26	3 1 23 143.55 13 1 63 70.05	4 1 99 132.59 15 1 77 62.55	5 1 27 122.48 17 1 93 56.37
3 5 8	0 1 49 180.00 10 1 99 89.42	1 1 99 168.46	2 1 51 157.16	4 1 57 136.00	6 1 67 117.56	8 1 81 102.12
3 5 9	1 1 29 169.35 13 1 71 79.04	3 1 31 148.74 15 1 85 71.12	5 1 35 130.01	7 1 41 113.73	9 1 49 99.99	11 1 59 88.54
3 5 10	0 1 67 180.00	2 1 69 160.40	4 1 75 141.88	6 1 85 125.20	8 1 99 110.70	
3 5 11	1 1 39 170.82 13 1 81 87.52	3 1 41 152.90 15 1 95 79.38	5 1 45 136.24	7 1 51 121.31	9 1 59 108.27	11 1 69 97.08
3 5 12	0 1 89 180.00	2 1 91 162.95	4 1 97 146.62			
3 5 13	1 1 51 171.97 13 1 93 95.24	3 1 53 156.22	5 1 57 141.32	7 1 63 127.67	9 1 71 115.44	11 1 81 104.66
3 5 15	1 1 65 172.89	3 1 67 158.88	5 1 71 145.48	7 1 77 132.99	9 1 85 121.57	11 1 95 111.29
3 5 17	1 1 81 173.63	3 1 83 161.05	5 1 87 148.91	7 1 93 137.44		
3 5 19	1 1 99 174.24					
3 6 7	0 1 47 180.00 10 1 97 88.23	1 1 95 168.22	2 1 49 156.69	4 1 55 135.16	6 1 65 116.50	8 1 79 100.95
3 6 8	1 1 55 169.06	3 1 59 147.94	5 1 67 128.82	7 1 79 112.32	9 1 95 98.47	
3 6 10	1 1 73 170.51	3 1 77 152.02	5 1 85 134.90	7 1 97 119.66		
3 6 11	0 1 83 180.00	2 1 85 162.35	4 1 91 145.51			
3 7 7	1 1 27 168.96 13 1 69 77.02	3 1 29 147.65 15 1 83 69.18	5 1 33 128.40 17 1 99 62.64	7 1 39 111.83	9 1 47 97.95	11 1 57 86.48
3 7 8	0 1 61 180.00	2 1 63 159.47	4 1 69 140.19	6 1 79 122.98	8 1 93 108.17	
3 7 9	1 1 35 170.30 13 1 77 84.41	3 1 37 151.45 15 1 91 76.33	5 1 41 134.04	7 1 47 118.60	9 1 55 105.29	11 1 65 93.97
3 7 10	0 1 79 180.00	2 1 81 161.92	4 1 87 144.70	6 1 97 128.97		
3 7 11	1 1 45 171.45 13 1 87 91.65	3 1 47 154.72	5 1 51 139.02	7 1 57 124.76	9 1 65 112.14	11 1 75 101.15
3 7 13	1 1 57 172.41 13 1 99 98.42	3 1 59 157.48	5 1 63 143.28	7 1 69 130.16	9 1 77 118.30	11 1 87 107.73

[uvw]	x y Σ ε′	x y Σ ε′	x y Σ ε′	x y Σ ε′	x y Σ ε′	x y Σ ε′
3 7 15	1 1 71 173.20	3 1 73 159.78	5 1 77 146.89	7 1 83 134.81	9 1 91 123.71	
3 7 17	1 1 87 173.85	3 1 89 161.70	5 1 93 149.95	7 1 99 138.81		
3 8 8	1 1 69 170.23	3 1 73 151.25	5 1 81 133.74	7 1 93 118.24		
3 8 9	0 1 77 180.00	2 1 79 161.69	4 1 85 144.27	6 1 95 128.39		
3 8 10	1 1 87 171.30	3 1 91 154.30	5 1 99 138.37			
3 8 11	0 1 97 180.00	2 1 99 163.66				
3 9 10	0 1 95 180.00	2 1 97 163.49				
3 9 11	1 1 53 172.12 13 1 95 96.35	3 1 55 156.66	5 1 59 142.01	7 1 65 128.54	9 1 73 116.44	11 1 93 105.73
3 9 13	1 1 65 172.89	3 1 67 158.88	5 1 71 145.48	7 1 77 132.99	9 1 85 121.57	11 1 95 111.29
3 9 17	1 1 95 174.12	3 1 97 162.48				
3 11 11	1 1 63 172.78	3 1 65 158.56	5 1 69 144.97	7 1 75 132.32	9 1 83 120.80	11 1 93 110.45
3 11 13	1 1 75 173.38	3 1 77 160.31	5 1 81 147.74	7 1 87 135.92	9 1 95 125.01	
3 11 15	1 1 89 173.92	3 1 91 161.91	5 1 95 150.28			
3 13 13	1 1 87 173.85	3 1 89 161.70	5 1 93 149.95	7 1 99 138.81		
4 4 5	0 1 57 180.00 6 1 93 103.05	1 1 29 164.91 7 1 53 94.33	2 1 61 150.33 9 1 69 79.98	3 1 33 136.66 11 1 89 68.93	4 1 73 124.17	5 1 41 112.97
4 4 7	0 1 81 180.00 7 1 65 104.25	1 1 41 167.32 9 1 81 90.00	2 1 85 154.94	3 1 45 143.13	4 1 97 132.08	5 1 53 121.89
4 4 9	1 1 57 169.25	3 1 61 148.48	5 1 69 129.62	7 1 81 113.27	9 1 97 99.49	
4 4 11	1 1 77 170.76	3 1 81 152.73	5 1 89 135.98			
4 5 5	0 1 33 180.00 6 1 51 107.10	1 1 67 165.97 8 1 65 90.88	2 1 35 152.34 10 1 83 78.18	3 1 75 139.46	4 1 41 127.57	5 1 91 116.78
4 5 6	0 1 77 180.00 7 1 63 102.84	1 1 39 167.00 9 1 79 88.55	2 1 81 154.32 11 1 99 77.16	3 1 43 142.25	4 1 93 130.99	5 1 51 120.65
4 5 7	0 1 45 180.00 8 1 77 99.72	1 1 91 167.97 10 1 95 86.98	2 1 47 156.19	3 1 99 144.90	4 1 53 134.28	6 1 63 115.38
4 5 8	1 1 53 168.85	3 1 57 147.36	5 1 65 127.98	7 1 77 111.32	9 1 93 97.41	
4 5 9	0 1 61 180.00	2 1 63 159.47	4 1 69 140.19	6 1 79 122.98	8 1 93 108.17	
4 5 10	1 1 71 170.37	3 1 75 151.64	5 1 83 134.33	7 1 95 118.96		
4 5 11	0 1 81 180.00	2 1 83 162.14	4 1 89 145.11	6 1 99 129.52		
4 5 12	1 1 93 171.59	3 1 97 155.12				
4 6 7	1 1 51 168.64	3 1 55 146.76	5 1 63 127.10	7 1 75 110.28	9 1 91 96.31	
4 6 9	1 1 67 170.09	3 1 71 150.84	5 1 79 133.12	7 1 91 117.49		
4 6 11	1 1 87 171.30	3 1 91 154.30	5 1 99 138.37			
4 7 7	0 1 57 180.00	2 1 59 158.78	4 1 65 138.92	6 1 75 121.33	8 1 89 106.31	
4 7 8	1 1 65 169.94	3 1 69 150.41	5 1 77 132.48	7 1 89 116.71		
4 7 9	0 1 73 180.00	2 1 75 161.20	4 1 81 143.37	6 1 91 127.19		
4 7 10	1 1 83 171.10	3 1 87 153.71	5 1 95 137.46			
4 7 11	0 1 93 180.00	2 1 95 163.31				

[uvw]	x y Σ θ′	x y Σ θ′	x y Σ θ′	x y Σ θ′	x y Σ θ′	x y Σ θ′
4 8 9	1 1 81 170.99	3 1 85 153.40	5 1 93 136.99	0 1 89 180.00	2 1 91 162.95	4 1 97 146.62
4 9 10	1 1 99 171.85					
5 5 6	0 1 43 180.00 8 1 75 98.43	1 1 87 167.69 10 1 93 85.68	2 1 45 155.66	3 1 95 144.15	4 1 51 133.34	6 1 61 114.19
5 5 7	0 1 99 180.00 11 1 55 84.26	1 1 25 168.52 13 1 67 74.86	3 1 27 146.44 15 1 81 67.11	5 1 31 126.64 17 1 97 60.68	7 1 37 109.75	9 1 45 95.74
5 5 8	0 1 57 180.00	2 1 59 158.78	4 1 65 138.92	6 1 75 121.33	8 1 89 106.31	
5 5 9	1 1 33 170.01 13 1 75 82.72	3 1 35 150.63 15 1 89 74.69	5 1 39 132.80	7 1 45 117.10	9 1 53 103.64	11 1 63 92.27
5 5 11	1 1 43 171.25 13 1 85 90.34	3 1 45 154.16 15 1 99 82.16	5 1 49 138.15	7 1 55 123.68	9 1 63 110.92	11 1 73 99.86
5 5 12	0 1 97 180.00	2 1 99 163.66				
5 5 13	1 1 55 172.27 13 1 97 97.40	3 1 57 157.08	5 1 61 142.66	7 1 67 129.37	9 1 75 117.39	11 1 85 106.75
5 5 17	1 1 85 173.78	3 1 87 161.49	5 1 91 149.61	7 1 97 138.37		
5 6 6	0 1 97 180.00	1 1 49 168.40	3 1 53 146.12	5 1 61 126.17	7 1 73 109.19	9 1 89 95.16
5 6 7	0 1 55 180.00	2 1 57 158.41	4 1 63 138.25	6 1 73 120.45	8 1 87 105.33	
5 6 8	1 1 63 169.78	3 1 67 149.96	5 1 75 131.81	7 1 87 115.90		
5 6 9	0 1 71 180.00	2 1 73 160.94	4 1 79 142.89	6 1 89 126.55		
5 6 10	1 1 81 170.99	3 1 85 153.40	5 1 93 136.99			
5 6 11	0 1 91 180.00	2 1 93 163.13	4 1 99 146.97			
5 7 7	1 1 31 169.70 13 1 73 80.94	3 1 33 149.73 15 1 87 72.96	5 1 37 131.46	7 1 43 115.48	9 1 51 101.88	11 1 61 90.47
5 7 8	0 1 69 180.00	2 1 71 160.68	4 1 77 142.39	6 1 87 125.89		
5 7 9	1 1 39 170.82 13 1 81 87.52	3 1 41 152.90 15 1 95 79.38	5 1 45 136.24	7 1 51 121.31	9 1 59 108.27	11 1 69 97.08
5 7 10	0 1 87 180.00	2 1 89 162.76	4 1 95 146.26			
5 7 11	1 1 49 171.81 13 1 91 94.10	3 1 51 155.75	5 1 55 140.60	7 1 61 126.75	9 1 69 114.40	11 1 79 103.54
5 7 13	1 1 61 172.66	3 1 63 158.21	5 1 67 144.43	7 1 73 131.64	9 1 81 120.00	11 1 91 109.58
5 7 15	1 1 75 173.38	3 1 77 160.31	5 1 81 147.74	7 1 87 135.92	9 1 95 125.01	
5 7 17	1 1 91 173.99	3 1 93 162.10	5 1 97 150.59			
5 8 8	1 1 77 170.76	3 1 81 152.73	5 1 89 135.98			
5 8 9	0 1 85 180.00	2 1 87 162.56	4 1 93 145.89			
5 8 10	1 1 95 171.68	3 1 99 155.38				
5 9 9	1 1 47 171.64 13 1 89 92.90	3 1 49 155.25	5 1 53 139.83	7 1 59 125.79	9 1 67 113.30	11 1 77 102.37
5 9 11	1 1 57 172.41 13 1 99 98.42	3 1 59 157.48	5 1 63 143.28	7 1 69 130.16	9 1 77 118.33	11 1 87 107.73
5 9 13	1 1 69 173.10	3 1 71 159.49	5 1 75 146.44	7 1 81 134.23	9 1 89 123.02	11 1 99 112.89
5 9 15	1 1 83 173.71	3 1 85 161.27	5 1 89 149.27	7 1 95 137.91		
5 9 17	1 1 99 174.24					

[uvw]	x y Σ θ′	x y Σ θ′	x y Σ θ′	x y Σ θ′	x y Σ θ′	x y Σ θ′
5 11 11	1 1 67 173.00	3 1 69 159.19	5 1 73 145.97	7 1 79 133.62	9 1 87 122.31	11 1 97 112.10
5 11 13	1 1 79 173.55	3 1 81 160.81	5 1 85 148.53	7 1 91 136.95	9 1 99 126.22	
5 11 15	1 1 93 174.06	3 1 95 162.29	5 1 99 150.90			
5 13 13	1 1 91 173.99	3 1 93 162.10	5 1 97 150.59			
6 6 7	1 1 61 169.61	3 1 65 149.49	5 1 73 131.11	7 1 85 115.06		
6 6 11	1 1 97 171.77					
6 7 7	0 1 67 180.00	2 1 69 160.40	4 1 75 141.88	6 1 85 125.20	8 1 99 110.70	
6 7 8	1 1 75 170.63	3 1 79 152.38	5 1 87 135.45	7 1 99 120.33		
6 7 9	0 1 83 180.00	2 1 85 162.35	4 1 91 145.51			
6 7 10	1 1 93 171.59	3 1 97 155.12				
6 8 9	1 1 91 171.50	3 1 95 154.86				
7 7 8	0 1 81 180.00	2 1 83 162.14	4 1 89 145.11	6 1 99 129.52		
7 7 9	1 1 45 171.45 13 1 87 91.65	3 1 47 154.72	5 1 51 139.02	7 1 57 124.76	9 1 65 112.14	11 1 75 101.15
7 7 10	0 1 99 180.00					
7 7 11	1 1 55 172.27 13 1 97 97.40	3 1 57 157.08	5 1 61 142.66	7 1 67 129.37	9 1 75 117.39	11 1 95 106.75
7 7 13	1 1 67 173.00	3 1 69 159.19	5 1 73 145.97	7 1 79 133.62	9 1 87 122.31	11 1 97 112.10
7 7 15	1 1 81 173.63	3 1 83 161.05	5 1 87 148.91	7 1 93 137.44		
7 7 17	1 1 97 174.18	3 1 99 162.66				
7 8 8	1 1 89 171.40	3 1 93 154.59				
7 8 9	0 1 97 180.00 9 1 73 116.44	2 1 99 163.66 11 1 83 105.73	1 1 53 172.12 13 1 95 96.35	3 1 55 156.66	5 1 59 142.01	7 1 65 128.54
7 9 11	1 1 63 172.78	3 1 65 158.56	5 1 69 144.97	7 1 75 132.32	9 1 83 120.80	11 1 93 110.45
7 9 13	1 1 75 173.38	3 1 77 160.31	5 1 81 147.74	7 1 87 135.92	9 1 95 125.01	
7 9 15	1 1 89 173.92	3 1 91 161.91	5 1 95 150.28			
7 11 11	1 1 73 173.29	3 1 75 160.05	5 1 79 147.33	7 1 85 135.38	9 1 93 124.37	
7 11 13	1 1 85 173.78	3 1 87 161.49	5 1 91 149.61	7 1 97 138.37		
7 11 15	1 1 99 174.24					
7 13 13	1 1 97 174.18	3 1 99 162.66				
9 9 11	1 1 71 173.20	3 1 73 159.78	5 1 77 146.89	7 1 83 134.81	9 1 91 123.71	
9 9 13	1 1 83 173.71	3 1 85 161.27	5 1 89 149.27	7 1 95 137.91		
9 11 11	1 1 81 173.63	3 1 83 161.05	5 1 87 148.91	7 1 93 137.44		
9 11 13						

APPENDIX 3

COMPUTER PROGRAMME

```
      PROGRAM CSLATT(INPUT,OUTPUT)
      DIMENSION NON(4)
      DIMENSION NHART(3,18)
      DIMENSION NCOUNT(300)
CCSLATT PLOTS COINCIDENCE SITE LATTICE PLANES.INPUT DATA ARE
C 1)INDICES OF THE ROTATION AXIS(U,W,V).INDICES MUST BE COPRIMAL
      AND .LE.99.U,V,W ARE NEWU,NEWV,NEWW.
C 2)NO. OF UNIT CELLS CONSIDERED FROM 0,0,0.(BLIM).BLIM-LE.9.5
      PRINT30
 30   FORMAT(*1*)
C READ INPUT DATA.
      READ1,NEWU,NEWV,NEWW,BLIM
 1    FORMAT(3I3,F4.1)
      PRINT31,NEWU,NEWV,NEWW
 31   FORMAT(//X,*INPUT DATA*,5X,*U V W* ,/15X,3(I2,X)//)
C CHECK IF MUST USE 2U,2V,2W
      X=0.0
      Y=0.0
      Z=0.0
      NUM=0
      PRINT55,BLIM
 55   FORMAT(* NO. OF PCC CELLS IS *,F3.1,* IN ALL DIRECTIONS FROM 0,0,0
     *.*,//)
      NSUM=NEWU*NEWU+NEWV*MEWV+NEWW*NEWW
      AU=FLOAT(NEWU)
      AV=FLOAT(NEWV)
      AW=FLOAT(NEWW)
      NTEST=MOD(NSUM,2)
      DO52 I=1,4
 52   NON(I)=99
 51   CALL LATTICE(X,Y,Z,NUM,BLIM)
      IF(NUM.EQ.4)GOTO61
      ANS=2.*AU*X+2.*AV*Y+2.*AW*Z-1.0
      IF(ABS( ANS ).LT.0.005)GOTO60
      GOTO51
 60   IF(NTEST.EQ.0)GOTO62
      DO70 J=1,3
 70   NON(J)=(J-1)*NSUM
      GOTO90
 62   CONTINUE
      DO71 K=1,3
 71   NON(K)=(K-1)*(NSUM/2)
 90   CONTINUE
      AU=2.*AU
      AV=2.*AV
      AW=2.*AW
      PRINT200
 200  FORMAT(* 2U,2V,2W VALUES USED.*,//)
      GOTO64
 61   IF(NTEST.EQ.0)GOTO63
      DO72 L=1,2
 72   NON(L)=NSUM*(L-1)
```

```
      GOTO64
 63   DO73 M=1,3
 73   NON(M)=(NSUM/2)*(M-1)
 64   CONTINUE
C NOW HAVEU,V,W OR 2U,2V,2W AND APPROPRIATE VALUES IF N=P-1.
      DO102 I=1,4
      IF(NON(I).EQ.99)LIM=I-1
 102  CONTINUE
      PRINT101,(NON(I),I=1,LIM),AU,AV,AW
 101  FORMAT(* N=P-1 VALUES ARE *, 316 ,10X,* U,V,W ARE *,3F6.1,//)
C CALCULATE ALL POINTS OF COINCIDENT SITE LATTICE UP TO BLIM FCC CELLS.
C THE ATOM AT THE ORIGIN OF THE FCC LATTICE HAS COORDINATES OF 0,0,0.
      PRINT30
      PRINT601
 601  FORMAT(7X,*COINCIDENT ATOM COORDINATES*,/,X,*REL. TO REF. CRYSTAL*
     *,4X,*CONV. FOR PLOTTING*,5X,*N*)
      KK=0
      TESTZZ=0.0
      CALL GRAPHS(0.,0.,0.,0.,0.,0.,NON(1),0)
      DO80 N=1,4
      X=0.0
      Y=0.0
      Z=0.0
      NUM=0
      IF(NON(N).EQ.99)GOTO100
      ANON=FLOAT(NON(N))
 83   PLANE=AU*X+AV*Y+AW*Z-ANON
      IF(ABS(PLANE).GT.0.005)GOTO81
      KK=KK+1
      NCOUNT(KK)=KK
      IF(NCOUNT.LT.300)GOTO599
      PRINT588
 588  FORMAT(* PROGRAM STOPPED.TOO MANY LATTICE POINTS. REDUCE BLIM.*)
      STOP4
 599  CONTINUE
      XX=X
      YY=Y
      ZZ=Z
      CALL ALATPL(XX,YY,ZZ,AU,AV,AW)
      PRINT82,X,Y,Z,XX,YY,ZZ,NON(N)
 82   FORMAT(X,3F6.1,3X,3F6.1,5X,I4)
      IF(ZZ.GT.TESTZZ+.005)GOTO401
      CALL GRAPHS(XX,YY,X,Y,Z,BLIM,0,2)
      GOTO402
 401  CONTINUE
      TESTZZ=ZZ
      CALL GRAPHS(0.,0.,0.,0.,0.,0.,NON(N),1)
      CALL GRAPHS(XX,YY,X,Y,Z,BLIM,0,2)
 402  CONTINUE
 81   CALL LATTICE(X,Y,Z,NUM,BLIM)
      IF(NUM.GE.4)GOTO80
      GOTO83
 80   CONTINUE
  100 CONTINUE
      CALL GRAPHS(0.,0.,0.,0.,0.,0.,0,3)
      STOP
      END
```

```
      SUBROUTINE LATTICE(U,V,W,NFLAG,ALIM)
C EACH ENTRY TO LATTICE GENERATES NEXT ATOM LOCATION IN A 3D FCC
C STRUCTURE, WHERE ALIM SETS THE NUMBER OF UNIT CELLS CONSIDERED IN EACH
C DIRECTION FROM 0,0,0.
C PRESET NFLAG TO 0 OUTSIDE THE CALLING LOOP IN THE MAIN PROGRAM.
C WHEN NFLAG=4 ALL POINTS HAVE BEEN GENERATED.  USE TEST NFLAG=4 TO
C EXIT CALLING LOOP.
C PRESET U,V,W TO 0,0,0 OUTSIDE CALLING LOOP.
      IF(NFLAG.LE.3)GOTO1
      PRINT9
 9    FORMAT(* PROGRAM STOPPED. NFLAG=4 ESCAPE NOT USED.*)
      STOP1
 1    IF(U.LT.0.0)GOTO2
      U=U+1
      IF(U.LE.ALIM)RETURN
      AU=AMOD(U,1.)
      U=U-ALIM-2.0+2.0*AU
      RETURN
 2    U=U-1
      IF(U.GE.-ALIM)RETURN
      U=U+ALIM+1
      IF(V.LT.0.0)GOTO3
      V=V+1
      IF(V.LE.ALIM)RETURN
      AV=AMOD(V,1.)
      V=V-ALIM-2.+2.*AV
      RETURN
 3    V=V-1
      IF(V.GE.-ALIM)RETURN
      V=V+ALIM+1
      IF(W.LT.0.0)GOTO4
      W=W+1
      IF(W.LE.ALIM)RETURN
      AW=AMOD(W,1.)
      W=W-ALIM-2.+2.*AW
      RETURN
 4    W=W-1
      IF(W.GE.-ALIM)RETURN
      IF(NFLAG.EQ.0)GOTO5
      IF(NFLAG.EQ.1)GOTO6
      IF(NFLAG.EQ.2)GOTO7
      GOTO8
 5    U=0.5
      V=0.5   $  W=0.0
      GOTO8
 6    U=0.5
      V=0.0   $  W=0.5
      GOTO8
 7    U=0.0
      V=0.5   $  W=0.5
 8    NFLAG=NFLAG+1
      RETURN
      END
```

```
      SUBROUTINE ALATPL(RH,RK,RL,CH,CK,CL)
C THE H,K,L COORDINATES OF THE CRYSTAL ARE FED INTO RH,RK,RL.
C THE AXIS ABOUT WHICH THE NEW PLANES WILL BE NORMAL IS FED IN AT
C   CH,CK,CL. THE REVISED COORDINATES ARE OUTPUT AT RH,RK,RL.
      DEN1=SQRT(CL*CL+CH*CH)
      DEN2=SQRT(CH*CH*CK*CK+(CL*CL+CH*CH)*(CL*CL+CH*CH)+CL*CL*CK*CK)
      DEN3=SQRT(CH*CH+CK*CK+CL*CL)
      SH=(CL*RH-CH*RL)/DEN1
    SL=(CH*RH+CK*RK+CL*RL)/DEN3
    RH=SH
    RK=SK
    RL=SL
    RETURN
    END


      SUBROUTINE GRAPHS(DXX,DYY,RX,RY,RZ,CLIM,NOP,NCTRL)
C RX,RY,RZ ARE ORIGINAL 3-D COORDINATES.
C DXX,DYY ARE COORDINATES TRANSFORMED FOR 2-D PLOTTING.
C CLIM IS NUMBER OF UNIT CELLS (FCC) CONSIDERED IN ANY DIRECTION FROM
C    0,0,0.
C NOP IS CURRENT PLANE .
C SET UNUSED ELEMENTS TO 0.0.
C    NCIRL=0  START FIRST GRAPH.
C         =1  START A NEW GRAPH.
C         =2  PLACE DXX,DYY,ON THE GRAPH AND LABEL WITH RX,RY,RZ.
C         =3  END OF GRAPH(S).
      DIMENSION BOTLINE(2)
      IF(NCTRL.EQ.0)GOTO1
      IF(NCTRL.EQ.1)GOTO2
      IF(NCTRL.EQ.2)GOTO3
      IF(NCTRL.EQ.3)GOTO4
      STOP 5
 1    CALL PAUPLOT(18HBLANK PAPER PLEASE,18)
      CALL PAUPLOT(17H0.2 NTB BLACK INK,17)
      CALL PAUPLOT(19HREQUIRED FOR THESIS,19)
      CALL PLOT10
      CALL XLIMIT(35.0)
      GOTO5
 2    CALL PLOT(6.0,-5.,-3)
 5    CALL PLOT(10.,0.,2)
      CALL PLOT(10.,10.,2)
      CALL PLOT(0.,10.,2)
      CALL PLOT(0.,0.,2)
C DRAW IN P=VALUE,TOP L/H CORNER.
      CALL PLOT(0.0,9.4,3)
      CALL PLOT(1.0,9.4,2)
      CALL PLOT(1.0,10.0,2)
      NPP=NOP+1
      CALL NUMBER(0.10,9.6,0.2,NPP,0.0,7H*P=*,I3)
      CALL PLOT(5.,5.,-3)
      CALL SYMBOL(0.,0.,0.1,0,0.0,-1)
      RETURN
```

```
C SCALE INPUT VALUES.
 3     DXX=DXX*5./(CLIM*1.5)
       DYY=DYY*5./(CLIM*1.5)
       BOTLINE(1)=10HXXXXXXXXXX
       BOTLINE(2)=10HXXXXXXXXXX
       XF=1H
       IF(RX.GT.-.005)GOTO10
       XF=1H-
 10    YF=1H
       IF(RY.GT.-.005)GOTO11
       YF=1H-
 11    ZF=1H
       IF(RZ.GT.-.005)GOTO12
       ZF=1H-
 12    COMMA=1H,
       QX=ABS(RX)
       QY=ABS(RY)
       QZ=ABS(RZ)
       ENCODE(6,20,TOPLINE)XF,YF,ZF
 20    FORMAT(3A1)
       ENCODE(11,21,BOTLINE)CX,COMMA,QY,COMMA,QZ
 21    FORMAT(F3.1,2(A1,F3.1))
C PLOT THE POINT.
       CALL PLOT(DXX,DYY,3)
       CALL SYMBOL(DXX,DYY,.10,3,0.0.-1)
C SET LETTERING HEIGHT.
       HI=0.08
C PLOT THE INDICES OF THE POINT.
       CALL SYMBOL(DXX+2.0*HI,DYY-0.5*GI,HI,BOTLINE,0.0,11)
C PLACE NEGATIVE SIGNS, IF NEEDED.
       CALL SYMBOL(DXX+2.0*HI,DYY-0.8*HI,4.*HI,TOPLINE,0.0.3)
       RETURN
 4     CALL PLOT(6.,-5.,-3)
       RETURN
       END
```

BIBLIOGRAPHY

AARON, H.B. and AARONSON, H.I., (1971): Met Trans., 2, 23.

AARONSON, H.I., (1956): 'The Mechanism of Phase Transformations in Metals', The Inst. of Metals, London, p.47.

AARONSON, H.I., (1962): 'Decomposition of Austenite by Diffusional Processes', Interscience, New York, p.387.

AARONSON, H.I., AARON, H.B. and KINSMAN, K.R., (1971): Metallog., 4, 1.

AARONSON, H.I., PLECHTA, M.R., FRANTI, G.W. and RUSSELL, K.C. (1978): Met. Trans. (A), 9, 363.

ACTON, A.F. and BEVIS, M., (1971): Acta Cryst., A27, 175.

ANDREJEVA, A.V. and FIONOVA, L.K., (1978): Phys. Met. Metallog., 44, 141.

ANDREJEVA, A.V., SALNIKOV, G.I. and FIONOVA, L.K., (1978): Phys. Met. Metallog., 26, 1331.

AUST, K.T. and RUTTER, J.W., (1959): Trans. T.M.S. - A.I.M.E., 215, 119 and 820.

BALLUFFI, R.W., GOODHEW, R.J., TAN, T.Y. and WAGNER, W.R., (1975): Journal de Physique, 36, C4-17.

BARBACKI, A. and HONEYCOMBE, R.W.K., (1976): Metallography, 9, 277.

BATTE, A.D. and HONEYCOMBE, R.W.K., (1973): J.I.S.I., 211, 284.

BERRY, F.G. and HONEYCOMBE, R.W.K., (1970): Met. Trans., 1, 3279.

BOLLMANN, W., (1970): 'Crystal Defects and Crystalline Interfaces', Springer, Berlin.

BRANDON, D.G., (1966): Acta Met., 14, 1479.

BRANDON, D.G., RALPH, B., RANGANATHAN, S. and WALD, M.S., (1964): Acta Met., 12, 813.

BUTLER, E.P. and SWANN, P.R., (1976): Acta Met., 24, 343.

CAHN, J.W., PAN, J.D. and BALLUFFI, R.W. (1979): Scripta Met., 13, 503.

CAMPBELL, K. and HONEYCOMBE, R.W.K. (1974): Metal Science, 8, 197.

CHALMERS, B. and GLEITER, H., (1971): Phil. Mag., 23, 1541.

CLARK, W.A.T. and SMITH, D.A., (1978): Phil. Mag., 38, 367.

CLARK, W.A.T. and SMITH, D.A., (1979): J. Mat. Science, 14, 776.

CLEMM, P.J. and FISHER, J.C., (1955): Acta Met., 3, 70.

CLOUGH, S.P., LEE, J.K., BRADLEY, J.R., CARLSON, J.A., LANGE III, W.F., MICHAELS, K.F., SEATON, C., AARONSON, H.I. and RUSSELL, K.C., (1974): Scripta Met., 8, 791.

DAVENPORT, A.T. and HONEYCOMBE, R.W.K., (1971): Proc. Roy. Soc., A322, 191.

DEMIANCZUK, D.W. and AUST, K.T., (1975): Acta Met., 23, 1149.

DICKSON, E.W. and PASHLEY, D.W., (1962): Phil. Mag., 7, 1315.

DIMOU, G. and AUST, K.T., (1974): Acta Met., 22, 27.

DINGLEY, D.J. and POND, R.C., (1979): Acta Met., 27, 667.

DIPPENAAR, R.J., (1970): Ph.D. Thesis, University of Cambridge.

DOIG, P. and EDINGTON, J.W., (1975): Met. Trans., 6A, 943.

EDMONDS, D.V., (1972): J.I.S.I., 210, 363.

EDMONDS, D.V. and HONEYCOMBE, R.W.K., (1973): J.I.S.I., 211, 209.

FOREST, B. and BISCONDI, M., (1978): Metal Science, 12, 202.

FORWOOD, C.T. and CLAREBROUGH, L.M., (1977): Phil. Mag., 36, 1131.

FOURNELLE, R.A. and CLARK, J.B., (1972): Met. Trans., 3, 2757.

FREBEL, M. and SCHENK, J., (1979): Z. Metallk., 70, 230.

FREEMAN, S., (1971): Ph.D. Thesis, University of Cambridge.

GARMONG, G. and RHODES, C.G., (1974): Met. Trans., 5, 2507.

GLEITER, H., (1970a): Acta Met., 18, 117.

GLEITER, H., (1970b): Acta Met., 18, 23.

GLEITER, H., (1971): Phys. Status Sol. (B)., 45, 9.

GLEITER, H. and PUMPHREY, P., (1976): Mat. Sci. and Eng., 25, 159.

GOODHEW, P.J., (1979): Metal Science, 13, 108.

GOODHEW, P.J., TAN, T.Y. and BALLUFFI, R.W., (1978): Acta Met., 26, 557.

GRIMMER, H., BOLLMANN, W. and WARRINGTON, D.H., (1974): Acta Cryst., A30, 197.

HANCOCK. P.C. and LORIMER, G.W., (1970): Societe Francaise de Microscopie Electronique, Grenoble Conference, 187.

HASSON, G., BOOS, J.Y., HERBEUVAL, I., BISCONDI, M. and GOUX, C., (1972): Surface Sci., 31, 115.

HASSON, G. and GOUX, C., (1971): Scripta Met., 5, 889.

HEIMENDAHL, M. von, (1973): Micron, 4, 111.

HEIMENDAHL, M. von., BELL, W. and THOMAS, G., (1964): J. Appl. Phys., 35, 3614.

HERMANN, G., GLEITER, H. and BÄRO, G., (1976): Acta Met., 24, 353.

HILLERT, M. and PURDY, G.R., (1978): Acta Met., 26, 333.

HONEYCOMBE, R.W.K., (1976): Met. Trans., 7A, 915.

HONEYCOMBE, R.W.K., (1979): Scand. J. Metallurgy, 8, 21.

HORNBOGEN, E., (1972): Met. Trans., 3, 2717.

HORNSTRA, J., (1960): Physica, 26, 198.

HOWELL, P.R., BEE, J.V. and HONEYCOMBE, R.W.K., (1979a): Inst. of Metallurgists, 2, Series 3, [illegible]. No 11 Vol 2. pp 11-87

HOWELL, P.R., BEE, J.V. and HONEYCOMBE, R.W.K., (1979b): Met. Trans., 10A, 1213.

HOWELL, P.R., SOUTHWICK, P.D. and HONEYCOMBE, R.W.K., (1979c): J. Microsc., 116, 151.

HOWELL, P.R., FLEET, D.E., WELCH, P.I. and RALPH, B., (1978): Acta Met., 26, 1499.

IMAI, Y. and NAMEKATA, J., (1970: Sci. Rep. of the Research Inst. Tohoku University (A) 21, 260.

ISHIDA, Y., (1972): J. Mater. Sci., 7, 75.

ISHIDA, Y., HASEGAWA, T. and NAGATA, F., (1969): J. Appl. Phys., 40, 2182.

ISHIDA, Y., INOVE, T., YAMAMOTO, T. and MORI, M., (1976): Metal Science, 10, 424.

ISHIDA, Y., MORI, M. and IIDA, F., (1977): Acta Met., 25, 815.

ISHIDA, Y. and SMITH, D.A., (1974): Scripta Met., 8, 293.

JASWON, M.A., (1956): 'Mathematical Crystallography', Longmans, London.

JOHARI, O. and THOMAS, G., (1969): 'The Stereographic Projection and Its Application', Interscience, New York, 96.

JONES, A.R., HOWELL, P.R. and RALPH, B., (1976a): J. Mat. Sci., 11, 1593; (1976b) ibid, 1600.

KEGG, C.R., HORTON, C.A.P. and SILCOCK, J.M., (1973): Phil. Mag., 27, 1041.

KINSMAN, K.R. and AARONSON, H.I., (1974): Metallography, 7, 361.

KINSMAN, K.R., EICHEN, E. and AARONSON, H.I., (1975): Met. Trans., 6A, 303.

KITTL, J.E. and MASSALSKI, T.B., (1967): Acta Met., 15, 161.

KRONBERG, M.L. and WILSON, F.H., (1949): Trans. A.I.M.E., 185, 501.

LAIRD, C. and AARONSON, H.I., (1967): Acta Met., 15, 73.

LAIRD, C. and SANKARAN, R., (1979): J. Microsc., 116, 123.

LANGE, F.F., (1967): Acta Met., 15, 311.

Le COZE, J., RANSON, C. and GOUX, C., (1970a): C.R. Acad. Sc., Paris, C271, 1120.

Le COZE, J. and GOUX, C., (1970b): ibid, C271, 1225.

LEE, J.K. and AARONSON, H.I., (1975): Acta Met., 23, 799, 809.

LIU, Y.C. and AARONSON, H.I., (1968): Acta Met., 16, 1343.

LOBERG, B. and NORDEN, H., (1976): 'Grain Boundary Structure and Properties', Academic Press, London, 10.

LORIMER, G.W., (1975): Journal de Physique, 36, C4-233.

MATTHEWS, J.W., (1962): Phil. Mag., 7, 915.

MURR, L.E., HORYLER, R.J. and LIN, W.N., (1970): Phil. Mag., 22, 511.

NICHOLS, S., (1979): Scripta Met., 13, 263.

PASHLEY, D.W. and STOWELL, M.J., (1963): Phil. Mag., 8, 1605.

PETERMANN, J. and HORNBOGEN, E., (1968): Z. Metallk., 59, 814.

PHILLIPS, V.A., (1972): Acta Met., 20, 1143.

POND, R.C., (1974): Can. Met. Quart., 13, 33.

POND, R.C. and SMITH, D.A., (1974): Can. Met. Quart., 13, 39.

POND, R.C., SMITH, D.A. and VITEK, V., (1976): 'Grain Boundaries', The Inst. of Metallurgists, Series 3, No. 5, p.A19.

POND, R.C., SMITH, D.A. and VITEK, V., (1979): Acta Met., 27, 235.

POND, R.C. and VITEK, V., (1977): Proc. Roy. Soc. Lond. A, 357, 453.

PUMPHREY, P.H., (1973): Scripta Met., 7, 1043.

PUMPHREY, P.H., (1976): 'Grain Boundary Structure and Properties', Academic Press, London, 139.

PUMPHREY, P.H. and BOWKETT, K.M., (1971): Scripta Met., 5, 365.

PURDY, G.R. (1978): Acta Met., 26, 477.

RALPH, B., (1975): Journal de Physique, 36, C4-71.

RANGANATHAN, S., (1966): Acta Cryst., 21, 197.

RANGANATHAN, S., (1969): J. Aust. I. M., 14, 336.

READ, W.T. and SCHOCKLEY, W., (1950): Phys. Rev., 78, 275.

RICKS, R.A., HOWELL, P.R. and HONEYCOMBE, R.W.K., (1979): Met. Trans. 10A, 1049.

ROY, A. and BAUER, C.L., (1975): Acta Met., 23, 957.

RUTTER, J.W. and K.T. AUST., referred to by K.T. Aust. in 'Surfaces and Interfaces, I Chemical and Physical Characteristics', ed. Burke, Reid and Neiss, p.435, Syracuse University Press, (1967).

SASS, S.L., TAN, T.Y. and BALLUFFI, R.W., (1975): Phil. Mag., 31, 559.

SAUTTER, H., GLEITER, H. and BÄRO, G., (1977): Acta Met., 25, 467.

SCHOBER, T. and BALLUFFI, R.W., (1970): Phil. Mag., 21, 109; (1971a) Ibid, 24, 165; (1971b) Phys. Stat. Sol., 44, 115.

SHEWMON, P.G., (1966): 'Recrystallization, Grain Growth and Textures', A.S.M., 165.

SMIDODA, K., GOTTSCHALK, C. and GLEITER, H., (1979): Metal Science, 13, 146.

SMITH, C.S., (1953): Trans. A.S.M., 45, 533.

SMITH, D.A., (1974): Scripta Met., 8, 1197.

SMITH, D.A., VITEK, V. and POND, R.C., (1977): Acta Met., 25, 475.

SUNDQUIST, B.E., (1973): Met. Trans., 4, 1919.

TAN, T.Y., SASS, S.L. and BALLUFFI, R.W., (1975): Phil. Mag., 31, 575.

TU, K.N. and TURNBULL, D., (1967): Acta Met., 15, 1317.

UNWIN, P.N.T. and NICHOLSON, R.B., (1969): Acta Met., 17, 1379.

VAN DER MERWE, J.H., (1974): J. Microsc. 102, 261.

VAUGHAN, D., (1968): Acta Met., 16, 563.

VAUGHAN, D., (1970): Acta Met., 18, 183.

VARIN, R.A., (1979): J. Mat. Sci., 14, 811.

WAGNER, W.R., TAN, T.Y. and BALLUFFI, R.W., (1974): Phil. Mag., 29, 895.

WARRINGTON, D.H. and BUFFALINI, P., (1971): Scripta Met., 5, 771.

WARRINGTON, D.H. and BOON, M., (1975): Acta Met., 23, 599.

WEATHERLY, G.C. and SARGENT, C.M., (1970): Phil. Mag., 22, 1049.

WEINS, M., GLEITER, H. and CHALMERS, B., (1971): J. Appl. Phys., 42, 2639.

WESTENGEN, H. and RYUM, N., (1978): Mat. Sci. and Eng., 34, 227.

WHITE, C.H. and HONEYCOMBE, R.W.K., (1962): J.I.S.I, 200, 457.

WILLIAMS, D.B. and EDINGTON, J.W., (1976): Acta Met., 24, 323.

ZENER, C., (1949): Private Communication to Smith, C.S., Trans. A.I.M.E., 175, 15.